ISSN: 1945-3094 Volume 2, Number 10, October 2010

Scientific Research

Journal of Water Resource and Protection

Editors-in-Chief : Jian Shen Ni-Bin Chang

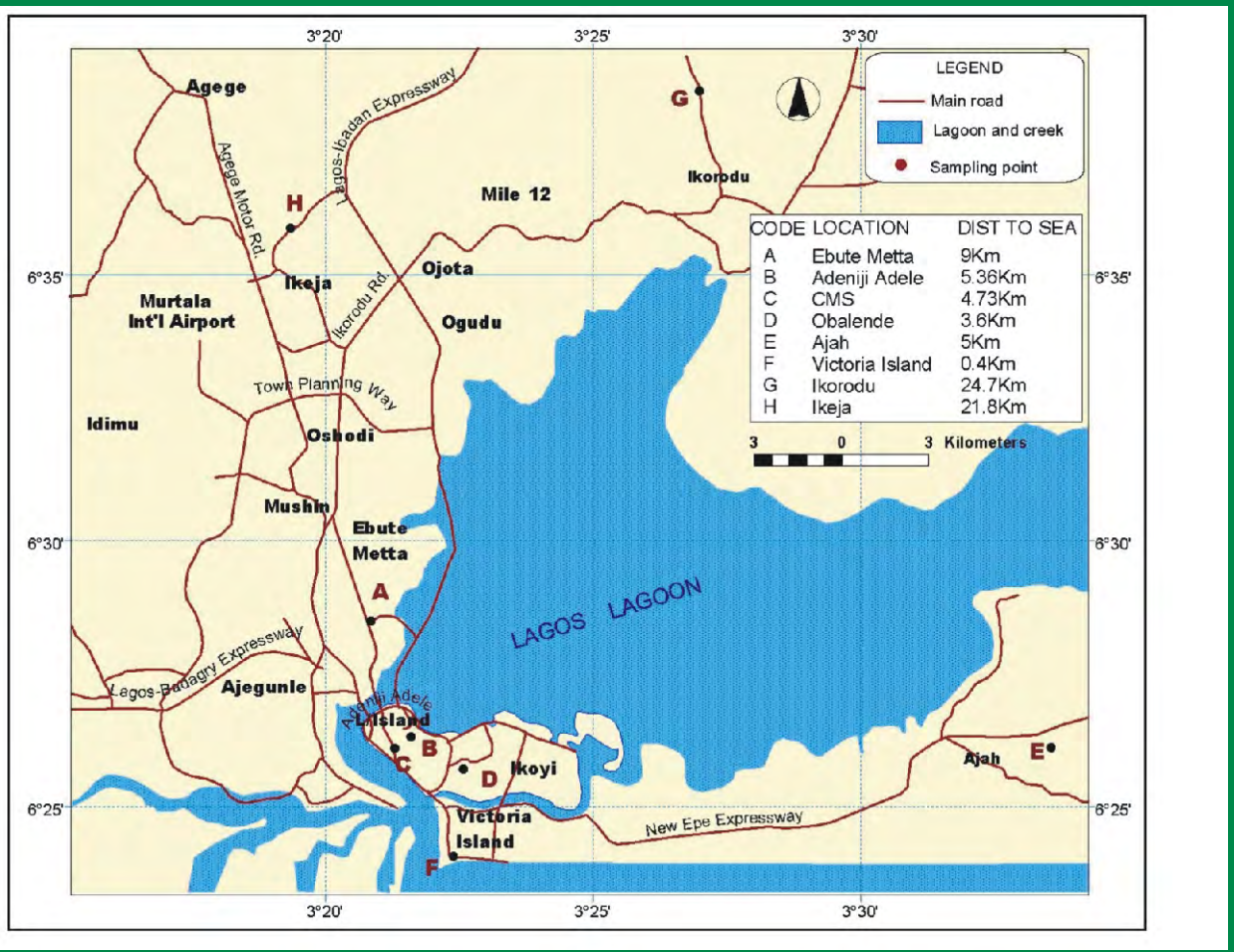

ISSN: 1945-3094

www.scirp.org/journal/jwarp

Journal Editorial Board

ISSN: 1945-3094 (Print) ISSN: 1945-3108 (Online)

http://www.scirp.org/journal/jwarp

Editors-in-Chief

J. Water Resource and Protection, 2010, 2, 849-922
Published Online October 2010 in SciRes (http://www.SciRP.org/journal/jwarp/)

TABLE OF CONTENTS

Volume 2 Number 10 October 2010

Journal of Water Resource and Protection (JWARP)

Journal Information

SUBSCRIPTIONS

The *Journal of Water Resource and Protection* (Online at Scientific Research Publishing, www.SciRP.org) is published monthly by Scientific Research Publishing, Inc., USA.

Subscription rates:

Print: $50 per issue.
To subscribe, please contact Journals Subscriptions Department, E-mail: sub@scirp.org

SERVICES

Advertisements
Advertisement Sales Department, E-mail: service@scirp.org

Reprints (minimum quantity 100 copies)
Reprints Co-ordinator, Scientific Research Publishing, Inc., USA.
E-mail: sub@scirp.org

COPYRIGHT

PRODUCTION INFORMATION

For manuscripts that have been accepted for publication, please contact:
E-mail: jwarp@scirp.org

J. Water Resource and Protection, **2010, 2, 849-853**
doi:10.4236/jwarp.2010.210100 Published Online October 2010 (http://www.SciRP.org/journal/jwarp)

Assessment of Groundwater Quality and Saline Intrusions in Coastal Aquifers of Lagos Metropolis, Nigeria

Adewuyi Gregory Olufemi[1*], Oputu Ogheneochuko Utieyin[2], Opasina Mukaila Adebayo[3]
[1]*Department of Chemistry, University of Ibadan, Ibadan, Nigeria*
[2]*Department of Chemical Sciences, Olabisi Onabanjo University, Ago-Iwoye, Nigeria*
[3]*Oyo State College of Education, Eruwa Campus, Eruwa, Nigeria*
E-mail: *adewuyio@yahoo.co.uk*
Received July 1, 2010; *revised September* 3, 2010; *accepted September* 18, 2010

Abstract

As a result of immense industrialisation and high population growth, groundwater is heavily relied on in Lagos metropolis to serve as an alternative source of water where surface water is seriously polluted. The continued reliance on ground water has resulted in its decline in quantity and quality. In this study, the coastal aquifers of Lagos metropolis were selected for an assessment of its groundwater quality and impact of saline intrusion. Water samples collected along the coastal region were subjected to various physicochemical analyses. Results obtained were compared with permissible values for drinking water stated by Federal Environmental Protection Agency (FEPA) and World Health Organization (WHO). The results revealed that all the water samples were significantly hard (range 522.14–1233.34 mg/L). The salinity was delineated by conductivity measurements. Three samples had specific conductance above the stated limits for fresh water. The samples however met the stipulated limits for drinking water for the other tested parameters.

Keywords: Industrialisation, Groundwater, Physiochemical Analysis, Salinity, Conductivity

1. Introduction

Groundwater has long served as a source of drinking water and it is still very important today. The development of ground water has provided great socio-economic benefits to humanity. Globally, groundwater is estimated to provide about 50% of current drinking water supplies. As groundwater is isolated from the surface, most people take it for granted that groundwater should be relatively pure and free from pollutants. Although most groundwater are still of high quality, at some locations, it is becoming increasingly difficult to maintain the purity of groundwater. One of the major sources of pollution of groundwater is by saltwater intrusions. Others include seepages from underground storage tanks, oil wells, septic tanks, land fills and agricultural leaching.

Saline intrusions into coastal groundwater via aquifer penetration have become a major concern [1] because it is the commonest source of pollution to groundwater. The extent of saltwater intrusions into groundwater is dependent on several natural and anthropogenic factors; the nature of the aquifer and its natural recharge rates being the major natural factors. The anthropogenic factors include excessive groundwater withdrawals [1-6] and lack of sealing of abandoned boreholes and oil wells. Studies have indicated that increased groundwater salinity may be due to clearing of natural forests resuslting in enhanced recharges which leaches salt downwards from salt stored in the unsaturated zone [7] or causes the water to rise dissolving salt as it does so [8]. The pollution of shallow aquifers under cities represents a major treat to sustainability of drinking water supplies in many urban areas throughout the world [4,9]. Frohlich and Urish [10] reported that the deterioration of the freshwater quality due to natural sea water infiltration affects the balanced life of the coastal strip of Rhodes Island. The present study was conducted in Lagos State in South western Nigeria, boarded in the south by the Atlantic ocean, in the north and east by Ogun state and in the west by Republic of Benin. It occupies an area of about 3.577 sq km with a population of about 14 million. 80% of the population resides in the metropolitan Lagos, making the state the most urbanized in Nigeria [11].

The aquifer structure of Lagos state falls in the Benin basin where salt water intrusion into the recent sediments aquifers occurs beneath the fresh water lens [12]. These

intrusions of salt water from the Atlantic ocean have caused untold hardship to habitats of the coastal areas of the state. There is an increasing pressure on the ground water reserves of the state as a result of massive influx of people from other parts of Nigeria to Lagos metropolis (rural to urban migration). Longe *et al.* [13], estimate that about 10 million gallons of water are extracted from the multilayer aquifers areas per day. Most of the bore holes drilled in the areas of Lagos have been abandoned due to salt water intrusions into the aquifer

The federal and state water agencies have initiated several hydrogeological evaluation of its groundwater resources [14,15]. However, the extent of groundwater intrusions and nature of these intrusions still require further investigations [16].

The objective of the present study is to ascertain the groundwater quality along the coastal region of Lagos state and assess the extent of saline intrusions in coastal aquifers of Lagos metropolis. Sampling sites were identified along the coastal line and groundwater samples were collected and subjected to physicochemical analysis.

2. Materials and Methods

2.1. Sampling

Groundwater samples were collected from eight (8) different sites (wells) along the coastal areas of Lagos metropolis. The wells were pumped for ten (10) minutes before samples were collected to ensure representative sampling. Plastic containers used for collection of samples were pre-treated by washing with 0.05 M HCl and then rinsed with distilled water [17]. After collection, sample bottles were tightly covered and transported under 4^{o}C to the laboratory for chemical analysis. The location of sampling sites is shown in **Figure 1**. The global positioning coordinates as well as relief features of the sites are shown in **Table 1**.

Refrigerated samples were allowed to attain room temperature prior to chemical analysis. Fast changing parameters such as pH, temperature and electric conductivity were determined insitu. Temperature was measured using a mercury thermometer (range 0^{o}C to 100^{o}C), pH was measured using a pre-calibrated pH meter. Electrical

Figure 1. Map showing sampling points. Code A-H refers to points on the map.

Table 1. Showing sampling points, GPS coordinates and relative positions from the ocean.

Location	Code	Elevation (ft)	Dist. from ocean (m)	Latitude (°North)	Longitude (°)
Adeniji Adele	AA	52	3600	6.4572	3.3961
Ajah	AJ	57	2470	6.4686	3.5924
CMS	CMS	68	2180	6.4541	3.3902
Ebutte Metta	EBM	77	9000	6.4903	3.3813
Ikeja	IKJ	91	4730	6.6065	3.3482
Ikorodu	IKO	102	5000	6.6411	3.4806
Obalende	OBA	116	5360	6.4489	3.1482
Victoria Island	VIL	23	400	6.4211	3.4806

conductivity (specific conductance) was measured using a Horiba U90 meter with an accuracy of 0.001 µs/cm. Total dissolved solids, total hardness, sulphate, alkalinity and chloride were determined by standard methods [17, 18]. Alkali metals – sodium and potassium was determined by flame absorption spectrophotometry. All reagents used for analysis were prepared from analar grade chemicals. Appropriate reagent blanks were prepared for each analysis. All analysis was done in triplicates.

3. Results and Discussion

The results obtained from the analyses of ground water samples collected revealed that some of the tested parameters fall within the permissible limits stipulated by FEPA (Federal Environmental Protection Agency) [19] and WHO (World Health Organization) [20]. The pH, sulphate SO_4^{2-}, phosphate PO_4^{3-}, hardness due to calcium and alkalinity fall within the accepted values for drinking water as shown by the results in **Table 2** and standards for FEPA and WHO in **Table 3** and **Table 4** respectively.

The total hardness of all the water samples however exceeds the permissible limits stated by the controlling agencies (refer to **Tables 2**, **3** and **4**). The total hardness is a measure of contributions from calcium, magnesium, and other polyvalent cations such as iron, zinc, manganese, aluminium, and strontium. The low contribution of calcium to the total hardness may be suggestive of an absence of calcium bearing mineral from the underlying aquifer. The high values of total hardness may be due to the introduction of polyvalent cations into the groundwater system. All the water samples may be regarded as 'very hard' (hardness > 300 mg/L) according to the classification for hardness [18].

The chloride concentration measured for the samples did not exceed the limit set by WHO and FEPA (250 mg/L). Chloride is not considered harmful to humans, but imparts a salty taste to water above this limit. The high chloride concentration recorded in this study may however cause harm to plants if used for irrigation purposes. Chloride concentrations as high as 70 mg/L have been reported to cause damage to plant tissues [18]. The concentration of alkali metals sodium and potassium varied widely. Sodium concentrations ranged from 46.78 mg/L for Ebutte Metta to 490 mg/L for Victoria Island. Potassium concentrations ranged from 8.67 mg/L for Ebutte Metta to 341.70 for Victoria Island. The correlation R^2 (0.759), for both ions though weak is suggestive of identical sources for both ions.

Conductivity measurement is widely used as substitute for total dissolved solids (TDS) and salinity determinations. Adekunle [19] used resistivity method (inverse of conductivity) to delineate salt water intrusions into fresh water aquifer of Lekki Peninsula, Lagos, Nigeria. The data obtained for conductivity measurements in this study ranged from 126 µs/cm for Ikeja to 1565 µs/cm for Victoria Island. Permissible values for conductivity for drinking water is 1000 µs/cm. Values exceeding this limit are indicative of saline intrusions into the groundwater. Water samples collected from Adeniji Adele (1251.2 µs/cm), CMS (1520.0 µs/cm) and Victoria Island (1565.2 µs/cm) exceed the permissible value and could be under threat of saline pollution. The intrusions gradual intrusion of saline water into the groundwater for Adeniji Adele, CMS and Victoria Island may be attributed to their relative closeness to the Atlantic Ocean and their elevation from sea level. Data on relative elevation and distance from sea level is shown in **Table 1**. The groundwater in Victoria Island is under stress due to pollution from saline waters. Characteristic features of the area include: close proximity to the ocean, low elevation from sea level, poor aquifer structure (belonging to the Benin basin where salt water bearing sand overlie fresh water [12]. Adekunle [19]; Oteri and Atolagbe [12] have previously reported cases of saline intrusions occurring in Lekki Peninsula which is separated from Victoria Island by Falomo River. Obalende which has the highest eleva-

Table 2. Showing mean results of physico-chemical analyses of samples.

Code	pH	$(SO_4)^{2-}$ mg/L	$(PO_4)^{3-}$ mg/L	Ca -Hardness mg/L	Total Hardness mg/L	Cl^- mg/L	Na^+ mg/L	K^+ mg/L	Electric. Cond. µs/cm	TDS mg/L
AA	6.01	34.91	0.01	120.9	1090.25	94.3	232.82	86.67	1251	625.50
AJ	6.38	29.68	ND	89.24	998.56	61.28	156.99	36.01	407	203.51
CMS	6.68	63.4	ND	121.2	1233.34	58.2	483.42	193.2	1520	760.01
EBM	6.76	24.28	0.03	27.98	522.14	22.33	46.78	8.67	130	65.05
IKJ	6.59	32.62	ND	41.73	526.14	19.01	56.15	10.91	126	63.31
IKO	6.45	32.71	ND	47.32	890.53	28.98	91.99	20.46	288	144.13
OBA	5.93	44.07	ND	148.76	1131.46	92.16	311.24	92.88	940	470.00
VIL	6.63	42.13	ND	119.2	926.25	109.5	430.07	341.7	1565	782.51

ND = Not detected

Table 3. Federal Environmental Protection Agency (FEPA) now Federal Ministry of Environment - water quality criteria (FEPA, 1988).

Parameter	permissible criteria (mg/L)	Desirable Criteria mg/L
Colour	75	< 10
Odour	Virtually absent	Virtually absent
Turbidity	25 Turbidity unity	Nil
pH	6.0-8.5	6.0-8.5
Alkalinity $CaCO_3$	30-500	30-500
Cl-	2.5	< 2.5
SO_4^{2-}	250	< 50
TDS	500	500
P	0.01	0.01

Table 4. World Health Organisation (WHO) standards for drinking water (WHO, 1971).

Parameter	Maximum permissible limit
Turbidity	25 turbidity units
pH	6.5-9.2
Total solids	1500 mg/L
Total Hardness	500 mg/L
Hardness-Ca	200 mg/L
Cl^-	600 mg/L
SO_4^{2-}	400 mg/L

Table 5. Assessment of water samples based on the stipulated limits.

Location	pH	SO_4^{2-}	PO_4^{3-}	Hardness-Ca	Cl^-	Total Hard-ness	Electric. Conduc-tivity
AA	+	+	+	+	+	−	−
AJ	+	+	+	+	+	−	+
CMS	+	+	+	+	+	−	−
EBM	+	+	+	+	+	−	+
IKJ	+	+	+	+	+	−	+
IKO	+	+	+	+	+	−	+
OBA	+	+	+	+	+	−	+
VIL	+	+	+	+	+	−	−

+ meets the stipulated permissible limits

− fails to meet the stipulated permissible limits

tion from sea level (**Table 1**) still has high electrical conductivity. This may be attributed to the area's close proximity to the ocean (3.6 Km) as compared to values for the other sites.

4. Conclusions

Conclusively, at present there is no universal system for classification of groundwater systems. Several agencies such as the Rhode Island department of environmental management office of water resource have classified groundwater based on its suitability for drinking with or without pre-treatment. The assessment of groundwater for Lagos state adopted in this study is based on whether the water meets all the requirements as stated by FEPA and WHO. The result from this study revealed that all the water samples analysed were hard and three did not meet the standard for conductivity. The water samples however met the permissible limits for drinking water for SO_4^{2-}, PO_4^{3-}, Cl^-, pH and hardness due to calcium.

5. Acknowledgements

The Authors wish to thank the Department of Chemistry University of Ibadan for providing some of the materials in carrying out the study. Also, the assistance received from Mrs. Ronke Abdulwaheed, Mrs. Fadeke Opeseitan and Pastor Dipo Ayodele during collection and analysis of samples is acknowledged.

6. References

[1] A. T. Batayneh, "Use of Electrical Resistivity Methods for Detecting Subsurface fresh a Saline Water and Delineating their Interfacial Configuration: A Case Study of the Eastern Dead Sea Coastal Aquifers," *Jordan Hydrogeology Journal*, Vol. 14, No. 7, 2006, pp. 1277-1283.

[2] J. O. Oseji and O. Ujuanbi, "Hydrogeophysical Investigation of Groundwater potential in Emu kingdom, Ndokwa land of Delta State, Nigeria," *International Journal of Physical Sciences*, Vol. 4, No. 5, 2009, pp. 275-284.

[3] J. Y. Lee and S. H. Song, "Evaluation of Groundwater Quality in Coastal Areas: Implications for Sustainable Agriculture" *Environmental Geology*, Vol. 52, No. 7, 2007, pp. 1231-1242.

[4] K. Choudhury, D. K. Saha and P. Chakraborty, "Geophysical Study for Saline Water Intrusion in a Coastal Alluvial Terrain," *Journal of Applied Geophysics*, Vol. 46, No. ER4, 2001, pp. 189-200.

[5] R. K. Frohlich, D. W. Urish, J. Fuller and M. O. Reilly, "Use of Geoelectrical Method in Groundwater Pollution Surveys in a Coastal Environment," *Journal of Applied Geophysics*, Vol. 32, No. 2-3, 1994, pp. 139-154.

[6] D. W. Urish and R. K. Frohlich, "Surface Electrical Resistivity in Coastal Groundwater Exploration," *Geoexploration*, Vol. 26, No. 4, 1990, pp. 267-289.

[7] F. W. Leaney, A. L. Herizeg and G. R. Walker, "Salinization of a Fresh Paleo-Groudwater Resource by Enhanced Recharge," *Groundwater*, Vol. 41, No. 1, 2003, pp. 84-90.

[8] P. G. Macumber, "Interaction between Groundwater and Surface Systems in Northern Victoria," Department of Conservation and Environment, Victoria, 1991.

[9] World Health Organization. "Guidelines for Drinking Water Quality," W.H.O., Geneva, 1993, p. 188.

[10] R. K. Frohlich and D. W. Urish, "The use of Geoelectrics and Test Wells for the Assessment of Groundwater Quality of a Coastal Industrial Site," *Journal of Applied Geophysics*, Vol. 50, No. 3, 2002, pp. 261-278.

[11] E. O. Longe and A. Williams, "A Preliminary Study of Medical Waste Management in Lagos Metropolis, Nigeria," *Iranian Journal of Environmental Health, Science and Engineering*, Vol. 3, No. 2, 2006, pp. 133-139.

[12] A. U. Oteri and F. P. Atolagbe, "The second international conference on saltwater Intrusion and Coastal Monitoring, Modelling, and Managenent," Merida, Yucatan, Mexico, 2003.

[13] E. O. Longe, S. Malomo and M. A. Olorunniwo, "Hydrogeology of Lagos Metropolis," *African Journal of Earth Sciences*, Vol. 6, No. 2, 2007, pp. 163-174.

[14] K. Kruger and S. Associates, "Underground Water Resources of the Metropolitan Lagos," Final Report to Lagos State Ministry of Works, Lagos, 1997, p. 170.

[15] Coode Blizard Ltd., Akute Geo-Resource Ltd. and Rofe Kennard & Lapworth, "Hydrogeological Investigation of Lagos State," Final Report, Vol. 1 & 2, 1996.

[16] UNESCO, "World-Wide Hydrogeological Mapping and Assessment Programme (WHYMAP)," 4th World Water Forum, Mexico City, March 2006.

[17] APHA, "Standard methods for the examination of water and wastewater," America Public Health Association, 18th Edition, New York, 1992.

[18] M. Radojevic and V. Bashkin, "Practical Environmental Analysis," The Royal Society of Chemistry, Cambridge, 1999.

[19] FEPA, "Present Water Quality Status in Nigeria," Federal Environmental Protection Agency, Lagos, 1998, pp. 35-41.

[20] World Health Organization, "International Standards for Drinking Water," 2nd Edition. W.H.O., Geneva, 1971.

J. Water Resource and Protection, **2010, 2, 854-859**
doi:10.4236/jwarp.2010.210101 Published Online October 2010 (http://www.SciRP.org/journal/jwarp)

Comparison of the Water Quality between the Surface Microlayer and Subsurface Water in Typical Water Bodies in Sichuan

Jiang Yu[1], Yonghong Shui[2], Waitim Ho[3], Jianquan Liu[4], Xin Yi[1], Hao Wang[1], Fang Zhang[1]

[1]*College of Architecture and Environment, Sichuan University, Chengdu, China*
[2]*Department of Dyeing Chemistry & Environmental Engineering, Chengdu Textile College, Chengdu, China*
[3]*Commission on Environmental Consultation, Macao SAR Government, Macao, China*
[4]*Chengdu Electromechanical College, Chengdu, China*
E-mail: *Yujianggz@163.com*
Received August 7, 2010; *revised August* 24, 2010; *accepted August* 31, 2010

Abstract

Investigation and assessment of water quality status in the surface microlayer (SML) and subsurface water (SSW) in several kinds of typical water bodies in Sichuan were carried out from May to June 2010. The results showed that N, P were enriched to some extent at SML in Xichi pool, Funan River and Longquan reservoir, which made concentrations of the indexes such as total nitrogen (TN), total phosphorus (TP), chemical oxygen demand (COD) of SML be much higher than those of SSW ($P < 0.05$), and the exceeding rates were up to 100%. The contents of TN, TP, COD of SML and SSW in Xichi pool, and Funan River exceeded III even Ⅳ level of water quality standard, while these indexes in Longquan reservoir were lower than Ⅲ or Ⅱ level of water quality standard. Though Chl. *a* mass concentration at SML and SSW in Funan River was prominently lower than those in Xichi pool and Longquan reservoir, according to the eutrophic evaluation standard, the water bodies of SML and SSW in Funan River and Xichi pool were in middle eutrophication, the highest index of eutrophication (E value) was up to 66.78, while there was light entuophic in Longquan reservoir, and there had obvious difference with E value and COD, TP, TN ($P < 0.05$). This research shows that the water quality of Longquan reservoir is generally well. While Funan River is a middle eutrophication, and its pollution is more serious than Xichi pool, the two waters belong to national III even IV level, and SML has the capability of enrichment to the pollutants such as N, P.

Keywords: Surface Microlayer, Eutrophication, Subsurface Water, Funan River, Assessment

1. Introduction

Total water resources in Sichuan Province are rich in years of average rainfall across the province about 488.975 billion cubic meters. However, due to the complex terrain of Sichuan, a large number of domestic sewage, industrial waste and agricultural irrigation water through a variety of different ways into the water body, cause physical and chemical properties of water environment and the spatial distribution of biological communities to change, then to effect the optimization of regional water resources configuration and aquatic ecosystems virtuous circle.

Surface Microlayer (SML) is the interface between air and water. The SML has been generally considered to be enriched, relatively to subsurface water (SSW), with various chemical and microbiological components. Compared to SSW, the SML normally contains relatively high amounts of nutrients, organic carbon, phytoplankton and bacteria [1-3]. Numerous substances, especially those with low water solubility and a high lipid/water partitioning coefficient such as polycyclic aromatic hydrocarbons [4] and polychlorinated biphenyls [5], exhibit a strong interfacial affinity. Therefore, SML biota may be exposed to higher levels of pollutants than organisms residing below the underlying water. Properties of the SML influence the flux of gases across the air–water interface [6,7]. Air–water gas exchange may also be affected by chemical and biological processes of contaminants during transport through the SML.

At present, most national and abroad researchers focus on the study that the concentration, distribution, transformation and enrichment of the heavy metal, organic compound, and nutrient salt have effects on the biology of SML in sea. It is seldom to report the relevant features of pollution of SML in rivers, lakes and reservoirs. In this article, it is the first time to do an investigation and assessment on the water quality status of SML and SSW in three kinds of typical water bodies in Sichuan Province, in order to explore the physicochemical characteristic changes in fresh water, and provide a strong theory basis for environmental protection of water bodies in Sichuan Province.

2. Materials and Methods

2.1. Sampling Points and Water Sampling

Three kinds of typical water bodies selected in Sichuan Province included man-made lake (Xichi pool), Longquan reservoir and Funan River in this investigation; each type of water set two representative samples. Sampling time was from May to June 2010. Water samplings were collected from SML and subsurface water at the two points respectively.

SML samples were collected using a glass plate technique of Harvey and Burzell [8]. During sampling, a glass plate (30 cm × 40 cm) was dipped vertically through the water surface and then drawn up at a constant velocity. The water film adhering to the glass plate was wiped off into a sample bottle with a silicone wipe blade. The thickness of the sample obtained with this device was 50–80 μm.

SSW samples were collected with a glass bottle from a depth of 20–50 cm.

2.2. Determination of Water Physicochemical Index

Chlorophyll *a*, was determined using a UV/Vis spectrometry of Crank [9]. Nutrient determinations were made according to the standard methods [10]. COD (COD_{Mn}) was determined by improved Permanganate Method. Water body eutrophic situation was evaluated by comprehensive nutrition state index method [11].

The enrichment of SML in three types of water bodies was analyzed according to enrichment factor. Enrichment factor (EF) in the micolayer is defined as follows:

$$EF = C_M/C_s$$

where C_M is the concentration of any substance in the microlayer, and C_s is its concentration in the subsurface water. An EF value > 1.0 was termed an enrichment, while a value < 1.0 was designated a depletion.

2.3. Statistical Analyse

Statistical analyses were done with the software SPSS at the level of significance at $P < 0.05$. All data were reported as means ±S.D.

3. Results

3.1. Comparison of Physicochemical Characteristics in Typical Water Bodies

3.1.1. COD

The monitoring results of COD of SML and SSW at different sampling sites in Xichi pool, Funan River and Longquan reservoir were shown in **Figure 1**. From **Figure 1**, COD contents of SML at all sampling points were higher than those of SSW. According to Environmental

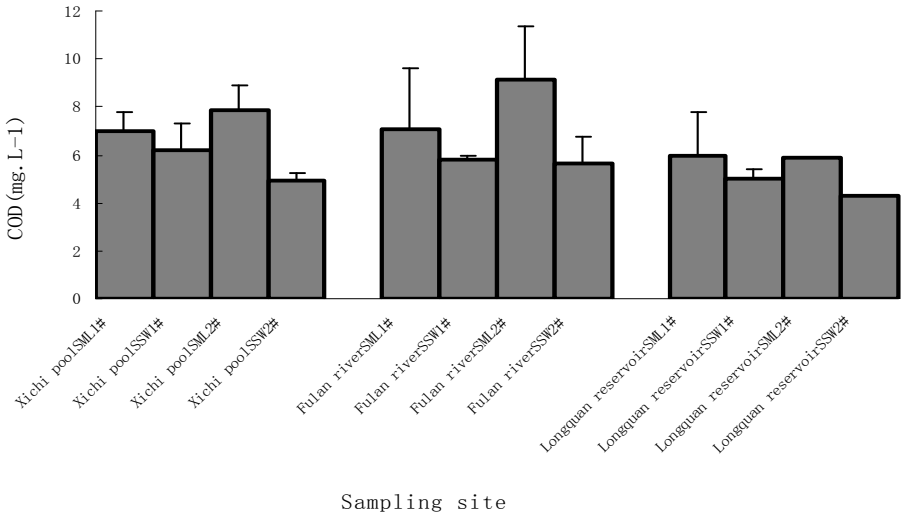

Figure 1. COD contents of SML and SSW at different sampling sites in Xichi pool, Funan River and Longquan reservoir.

Quality Standard for Surface Water (GB 3838-2002), COD contents of SML in Xichi pool and Funan River exceeded III level of water standard, and the exceeding rates were 100%. COD contents of SML and SSW in Longquan reservoir were lower than III level of water standard, which showed the water quality well in general.

3.1.2. TP

TP mass concentrations of SML and SSW at different sampling sites in Xichi pool, Funan River and Longquan reservoir were shown in **Figure 2**. From **Figure 2**, there was no obvious difference between TP mass concentrations of SML and that of SSW in Funan River（$P > 0.05$）, but TP mass concentrations of the two layers exceeded III level of water standard with the exceeding rates up to 100%, and higher than those of other two water bodies（$P < 0.05$）. TP mass concentration ranges of SML and SSW in Longquan reservoir were 0.096 ~ 0.105, 0.049 ~ 0.084 mg/L, respectively, there was no remarkable difference ($P > 0.05$).

3.1.3. TN

TN mass concentrations of SML and SSW in Xichi pool, Funan River and Longquan reservoir exceeded III, Ⅳand Ⅲ level of water standard, respectively, and the exceeding rates were up to 100%. Among three kinds of water bodies, the TN mass concentrations of SML were higher than those of SSW, except for 1 # sampling site in Funan River, there was no obvious difference between different layers at other sampling sties (**Figure 3**).

3.1.4. Chl.*a*

Chl.*a* mass concentrations of SML and SSW in Xichi pool and Longquan reservoir were much higher than those of Funan River (**Figure 4**). Chl.*a* mass concentrations of two layers in Funan River were low, and there was no significant difference（$P > 0.05$）. But Chl.*a* mass concentrations of SSW in Xichi pool exceeded those of SML ($P < 0.05$), with an increase by 90.48, 55.59%, respectively, compared with the SML; the same monitoring results were shown in Longquan reservoir, but there was no obvious difference between the two layers ($P > 0.05$).

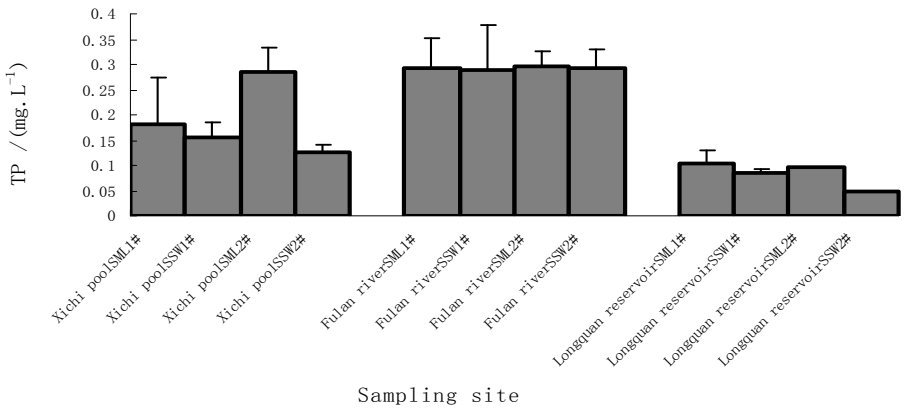

Figure 2. TP contents of SML and SSW at different sampling sites in Xichi pool, Funan River and Longquan reservoir.

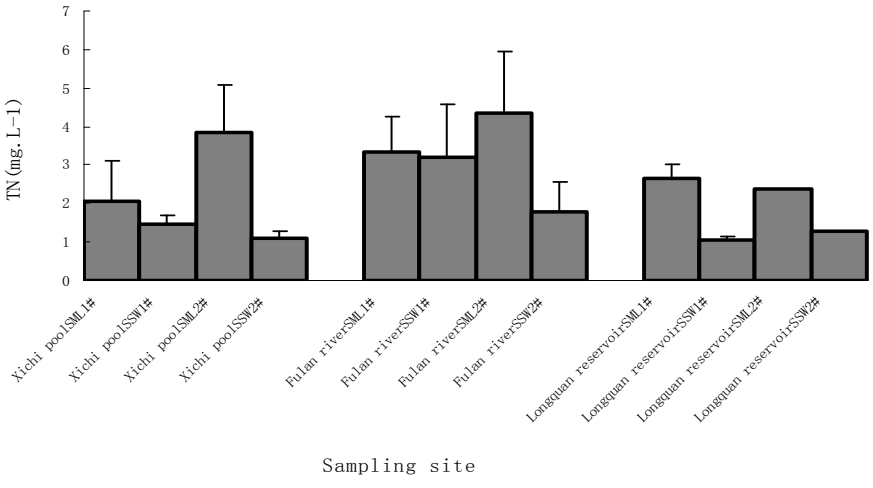

Figure 3. TN contents of SML and SSW at different sampling sites in Xichi pool, Funan River and Longquan reservoir.

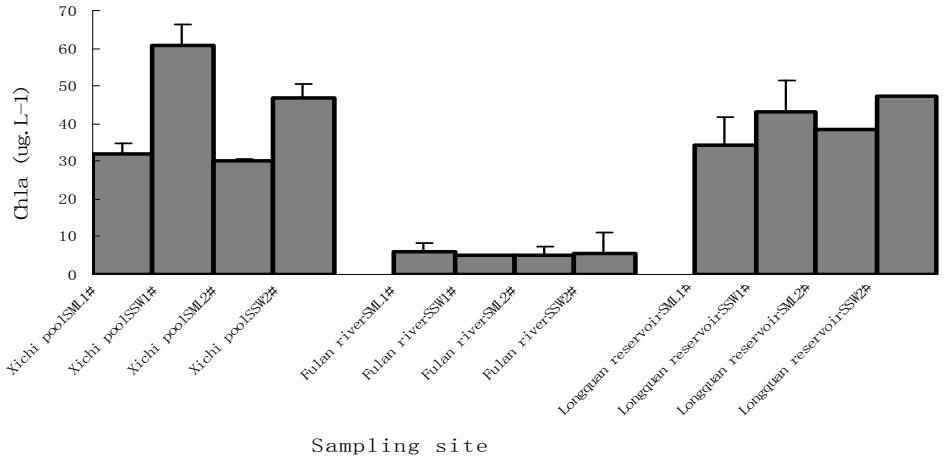

Figure 4. Chl.*a* contents of SML and SSW at different sampling sites in Xichi pool, Funan River and Longquan reservoir.

2.2. Enrichment of SML to N, P and Chl. *a*

From **Table 1**, it was obvious that N, P were enriched to some extent at SML in Xichi pool, Funan River and Longquan reservoir, with enrichment rates all reaching 100%. The enrichment of SML to TN, TP was remarkable at 2# sampling point in Xichi pool, the EF_N, EF_P was 2.28, 3.51, respectively. However, the enrichment of SML to Chl. *a* in Funan River was low, the $EF_{Chl.\,a}$ was only 16.67%.

2.3. Assessment of Water Body Eutrophication

The eutrophic indexes (E value) of SML at three types of water samples were higher than those of SSW. The two layers in Funan River were middle eutrophication, and the SML in Xichi pool showed the same, and 50% of SSW was light eutrophication. 75% of SML and SSW in Longquan reservoir presented light eutrophic situation, which showed the water quality in Longquan reservoir was better than Xichi pool and Funan River (**Table 2**). By analyzing the correlation between E value and COD, TN, TP, Chl. *a* (**Table 3**), the results showed that there was a significant positive correlation between E and COD, TN, TP, and while there had a negative correlation between E and Chl. *a*, which indicated that water body eutrophication of SML might be limited by nitrogen and phosphorus.

3. Discussion

Many studies indicate that the microlayer is generally enriched with various organisms and chemical substances and considered to exhibit distinct physical, chemical and biological properties due to the accumulation of surface-active material within this thin layer [12-14]. Peng *et al*. [15] observed that BOD and COD average enrichment factor of sea and air interface SML was 3.00 and 3.28, respectively in Daya Bay. Our investigation shows that SML of different kinds of fresh water bodies can enrich to N and P. Pollution of SML is becoming more serious due to SML enriching to many pollutants. The study also shows that COD, TN, TP of SML in Xichi pool and Funan River is obviously higher than the ones of SSW, and the water quality exceeds III and IV level standard.

Eutrophication is an excess of organic substances and N, P nutrient, which will bring algae bloom. It is certain that algae quantity is too much with little types, and the algae variety index decreases, dissolved oxygen of lake upper layer is too high and the one of lower layer is too low, and the water quality is getting steadily worse. As we can know from **Figure 1** to **Figure 3**, most of TN, TP, COD of SML and SSW in Xichi pool and Funan River exceed the level in comparison with national III level of water standard, which indicates that pollution for matters containing nitrogen, phosphorus is severe and the water quality is getting worse. According to the eutrophic evaluation criteria, SML and SSW at sampling points are in a eutrophic level, especially in Funan River. It is known from **Table 3**, there is a significant difference between E of SML and COD, TP and TN in three types of water bodies ($p < 0.05$), which can indicates that eutrophication is mainly restricted by nitrogen and phosphorus in three types of water bodies.

Moreover, this investigation indicates that Chl. *a* mass concentration at SML and SSW in Funan River are prominently lower than those in Xichi pool and Longquan reservoir. The reason might be that large runoff volume of Funan River, muddy river water, fast flow velocity, flow erosion and dilution in the high flow period (May to June) which decreases the cell number of plankton, and further causes Chl. *a*, a comprehensive index of biomass of phytoplankton in water, to decrease.

Table 1. Enrichment factor of SML to P, N, Chl. *a* in three kinds of typical water bodies.

Index	Xichi pool		Funan River		Longquan reservoir	
	1#	2#	1#	2#	1#	2#
TP	1.16	2.28	1.01	1.02	1.25	1.96
TN	1.42	3.51	1.04	2.41	2.49	1.88
Chla	0.52	0.64	1.15	0.88	0.79	0.81

Table 2. Eutrophic status of SML and SSW in three kinds of typical water bodiese.

Layer Pollution	Xichi pool		Funan River		Longquan reservoir	
	1#	2#	1#	2#	1#	2#
SML E-value	63.71	66.78	63.52	65.54	60.31	59.48
Eutrophic Level	M	M	M	M	M	L
SSW E-value	62.81	58.37	61.95	60.22	56.06	53.96
Eutrophic Level	M	L	M	M	L	L

Remarks: M to be moderation; L to be light.

Table 3. The relationship of E value and COD, TN, TP and Chl. *a* of SML.

Index	Regression Equation	p
COD	$y = 2.002x + 48.906$, $R^2 = 0.7508$, n=12	<0.05
TN	$y = 1.3572x^2 - 6.3862x + 69.077$, $R^2 = 0.5631$, n=12	<0.05
TP	$y = 27.12x + 57.537$, $R^2 = 0.8078$, n=12	<0.05
Chl. *a*	$y = -0.0239x^2 + 0.8705x + 60.604$, $R^2 = 0.73$,n=12	<0.05

However, much higher TN, TP, COD contents in Funan River still make E value increase and result in these waters to be eutrophic.

4. Acknowledgements

The project is supported by Youth Research Fund of Sichuan University (2009SCU11055), Key Laboratory of Aquatic Eutrophication and Control of Harmful Algal Blooms of Guangdong Higher Education Institutes. Special thanks are due to Dr. Liu Qing (Jinan University, in China) and Dr. Liu (Aalborg University, in Denmark) for the experimental study and very valuable comments and on the manuscript.

5. References

[1] G. P. Yang, W. W. Jing and Z. Q. Kang, "Spatial Variations of Dimethylsulfide and Dimethylsulf on Propionate in the Surface Microlayer and in the Subsurface Waters of the South China Sea during Springtime," *Marine Environmental Research*, Vol. 165, 2008, pp. 85-97.

[2] U. Munster, E. Heikkinen and J. Knulst, "Nutrient Composition, Microbial Biomass and Activity at the Air–Water Interface of Small Boreal Forest," *Hydrobiologia*, Vol. 363, No. 1-3, 1998, pp. 261-270.

[3] C. Guitart, N. Garciaflor and J. M. Bayona, "Occurrence and Fate of Polycyclic Aromatic Hydrocarbons in the Coastal Surface Microlayer," *Marine Pollution Bulletin*, Vol. 54, No. 2, 2007, pp. 186-194.

[4] J. R. Kucklick and T. F. Bidleman, "Organic Contaminants in Winyah Bay, South Carolina 1. Pesticides and Polycyclic Aromatic-Hydrocarbons in Subsurface and Microlayer Waters," *Marine Environmental Research*, Vol. 37, 1994, pp. 63-78.

[5] A. M. A. Abd-Allah, "Organochlorine Contaminants in Microlayer and Subsurface Water of Alexandria Coast, Egypt," *Journal of AOAC International*, Vol. 82, No. 2, 1999, pp. 391-398.

[6] J. Chi, G. L. Huang, X. Lu, *et al*., "DEHP Enrichment in the Surface Microlayer of a Small Eutrophic Lake," *Water Research*, Vol. 37, No. 19, 2003, pp. 4657-4662.

[7] M. X. Pan, Z. B. Zhang and A. D. Wang, "Biological and Chemical Studies of Sea-Surface Microlayer at Daya Bay Ⅱ. (B) Diurnal Variations of Biological and Chemical Characteristics," *Tropic Oceanology*, Vol. 19, No. 2, 2000, pp. 57-63.

[8] J. T. Harvey and L. A. Burzell, "A Simple Microlayer Method for Small Samples," *Limnology Oceanology*, Vol. 17, No. 1, 1972, pp. 156-157.

[9] J. Crank, "The Mathematics of Diffusion," 2nd Edition, Oxford University Press, London, 1975.

[10] National Environmental Protection Bureau, "Analytical Methods for the Examination of Water and Wastewater," 2nd Edition, Environmental Science Press, Beijing, 1997.

[11] X. C. Jin, H. L. Li and Q. Y. Tu, "Eutrophication of Lakes in China," Chinese Environmental Science Publication, Beijing, 1990, pp. 121-133.

[12] B. P. Deng and Y. F. Yang, "Comparative Studies on Water Quality and Community Structure of Zooplankton between the Sea Surface Microlayer and the Subsurface Microlayer in Mar-Culture Areas in Dapeng Cove," *Journal of Jinan University* (*Natural Science*), Vol. 30,

No. 3, 2009, pp. 101-105 (in Chinese with English abstract).

[13] J. Yu, Y. F. Yang and C. C. Yang, "Study on the Eutrophic Status and the Genetic Toxicity of Water Body in Certain Sections of the Pearl River and Several Artificial Lake," *Journal of Chongqing University* (*Natural Science Edition*), Vol. 30, No. 9, 2007, pp. 139-143 (in Chinese with English abstract).

[14] O. Wurl and J. P Obbard, "A Review of Pollutants in the Sea Surface Microlayer (SML): A Unique Habitat for Marine Organisms," *Marine Pollution Bulletin*, Vol. 48, No. 11-12, 2004, pp. 1016-1030.

[15] Y. H. Peng, Z. D. Wang, M. X. Pan, *et al*., "Studies on BOD and COD of Sea Surface Microlayer (MSL) and Subsurface Layer (SSL) water in Day Bay," *Transactions of Oceanology and Limnology*, Vol. 4, 2000, pp. 13-19.

J. Water Resource and Protection, **2010, 2, 860-863**
doi:10.4236/jwarp.2010.210102 Published Online October 2010 (http://www.SciRP.org/journal/jwarp)

Interpretation of Water Quality Parameters for Villages of Sanganer Tehsil, by Using Multivariate Statistical Analysis

Manish Kumar, Yashbir Singh
Department of Statistics, University of Rajasthan, Jaipur, India
E-mail: {*singh.yshbir, manishkr*29}*@gmail.com*
Received July 30, 2010; *revised August* 20, 2010; *accepted August* 28, 2010

Abstract

In this study, the factor analysis techniques is applied to water quality data sets obtained from the Sanganer Tehsil, Jaipur District, Rajasthan (India). The data obtained were standardized and subjected to principal components analysis (PCA) extraction to simplifying its interpretation and to define the parameters responsible for the main variability in water quality for Sanganer Tehsil in Jaipur District. The PCA analysis resulted in two factors explaining more than 94.5% of the total variation in water quality data set. The first factor indicates the variation in water quality is due to anthropogenic sources and second factor shows variation in water quality due to organic sources that are taking place in the system. Finally the results of PCA reflect a good look on the water quality monitoring and interpretation of the surface water.

Keywords: Factor Analysis, Principal Component Analysis, Drinking Water, Fluoride

1. Introduction

Quality of water is an important factor in development and use of ground water as resources. Due to pressure of human activity, urbanization and industrialization, the groundwater sources are degraded gradually; therefore pure, safe, healthy and odorless drinking water is a matter of deep concern. There are many pollutants in groundwater due to seepages viz. organic and inorganic pollutants, heavy metals, pesticides, fluorides etc. The quality of water is identified in terms of its physical, chemical and biological parameters [1]. The particular problem in the case of water quality monitoring is the complexity associated with analyzing the large number of measured variables [2]. The data sets contain rich information about the behavior of the water resources. The classification, modelling and interpretation of monitoring data are the most important steps in the assessment of water quality.

The application of different multivariate statistical techniques such as Cluster Analysis (CA) and Principal Component Analysis (PCA) helps in the interpretation of complex water quality data matrix. These techniques have been applied by many researchers to characterize and evaluate groundwater and surface water quality. In the present study, a water quality data matrix, obtained from 50 villages of Sanagner Tehsil, Jaipur District, Rajasthan, has been subjected to different multivariate statistical techniques such as Factor analysis and Principal Component Analysis (PCA).

2. Materials and Methods

In Rajasthan (a state of India), all 32 districts are affected with high fluoride concentration in groundwater and among these Jaipur ranks second. Sanganer, the Tehsil of Jaipur District, is attached with the main city of Jaipur. It lies between 26° 49’ to 26° 51’ N latitude and 75° 46’ to 75° 51’ E longitude. It covers an area of 635.5 sq. km. There are different sources of drinking water viz., hand pumps, tube wells, open wells, PHED supply etc.

Samples of drinking water were collected in clean polyethylene bottles from different sources viz. hand pumps, open wells, tube wells and PHED supply from villages of study area [3]. Using Multivariate statistical technique we analyzed the data for different parameters as pH, F^-, EC, TDS, Ca, Mg, TH, Cl^-, CO_3^{-2}, HCO_3^-, Alkalinity, Na^+, K^+ and NO_3^-.

3. Results and Discussion

Data were analyzed and result presented in **Table 1**.

Table 1. Summary statistics of the parameters and villages% fall in permissible limit.

		Summary			Villages (%)		
Parameters	Permissible	Mean	Minimum	Maximum	Below	Optimum	Higher
PH	6.9-9.2	8.37	8.0	9.0	-	100%	-
F-	1-1.5 ppm	1.10	0.2	5.4	42%	48%	10%
EC	300 μ mho s/cm	1,985.10	483.0	9,570.0	-	-	100%
TDS	500-1500 mg/l	1,059.54	242.0	4,650.0	12%	72%	16%
Ca-H	75-200 mg/l	38.18	4.0	172.0	86%	14%	-
Mg-H	30-150 mg/l	36.28	2.0	132.0	50%	50%	-
TH	100-500 mg/l	236.66	90.0	700.0	6%	88%	6%
Cl-	200-600 mg/l	217.68	42.0	2,173.0	82%	8%	10%
Alkalinity	200 mg/l	634.38	49.0	1,460.0	2%	-	98%
Na+	50-60 mg/l	387.46	39.0	1,000.0	2%	-	98%
K+	20 mg/l	3.03	0.8	10.6	100%	-	-
NO_3	40-50 mg/l	47.70	2.0	202.0	64%	10%	26%

Table 2. Correlation matrix of parameters.

	pH	F-	EC									
pH	1.00											
F-	0.88	1.00										
EC	−0.64	−0.48	1.00									
TDS	−0.66	−0.50	1.00	1.00								
Ca-H	−0.65	−0.50	0.96	0.97	1.00							
Mg-H	−0.73	−0.57	0.93	0.95	0.98	1.00						
TH	−0.69	−0.53	0.91	0.94	0.98	0.99	1.00					
Cl-	−0.50	−0.35	0.97	0.95	0.92	0.87	0.85	1.00				
TA	−0.77	−0.58	0.85	0.87	0.88	0.90	0.91	0.76	1.00			
Na+	−0.82	−0.65	0.84	0.87	0.90	0.94	0.93	0.74	0.93	1.00		
K+	−0.67	−0.53	0.94	0.96	0.97	0.96	0.97	0.89	0.89	0.91	1.00	
NO3	−0.65	−0.49	0.92	0.95	0.97	0.98	0.99	0.87	0.89	0.93	0.98	1.00

Table 3. Eigenvalues of the correlation matrix.

	Eigenvalue	Difference	Proportion	Cumulative
1	10.174	9.006	0.848	0.848
2	1.167	0.862	0.097	0.945
3	0.305	0.155	0.025	0.971
4	0.150	0.074	0.013	0.983
5	0.076	0.029	0.006	0.989
6	0.047	0.009	0.004	0.993
7	0.038	0.018	0.003	0.996
8	0.020	0.009	0.002	0.998
9	0.011	0.003	0.001	0.999
10	0.008	0.004	0.001	0.999
11	0.004	0.003	0.000	1.000
12	0.001		-	1.000

Analysis revealed that pH of all water samples are within range. pH showed positive correlation with fluoride and negative correlation with other parameters (**Table 2**). 10% of villages of the study area are affected with high concentration of fluoride; whereas 42% villages had lower F-. Only 48% of the villages are under optimum limit of fluoride.

EC was reported higher than the permissible limit for all the villages. TDS was found to be within limit in 72% of villages, whereas 16% villages showed TDS higher than limit. Ca-H (Calcium hardness) and Mg-H (Magnesium hardness) combined to form total hardness. 14% villages showed Ca-H within limit, whereas 86% are below the limit. Mg-H reported 50% below the limit and 50% within the limit. Total hardness was higher in 6%

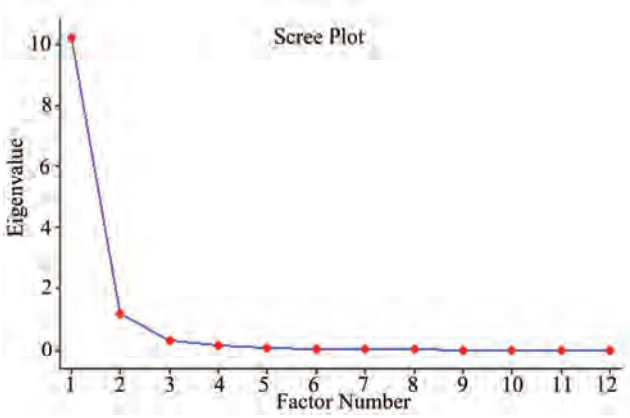

Figure 1. Scree plot of the eigenvalues.

villages; below than limit in 6% villages whereas 88% samples contained TH within optimum limit (**Table 2**). In this study, hardness showed negative correlation with F- and pH (**Table 2**).

Chloride (Cl) varied from 42 to 2173 mg/l. The chloride content was higher than permissible limit (200-600 mg/l) in 10% villages and lower in 82% villages. Only 8% villages were within optimum limit (**Table 1**). High content of chloride gives salty taste to water. Carbonate (CO3-2) and bicarbonate (HCO3-) together make total alkalinity. Alkalinity was higher than permissible limit *i.e*., (200 mg/l) in 98% villages, only 2% villages contain alkalinity below than limit (**Table 1**). Alkalinity showed positive correlation with EC, TDS, Cl, TH, NO3-, Na+ and K+ (**Table 2**). High values of alkalinity give undesirable taste to water. Almost all the villages (98%) contain higher concentration of sodium (Na+). Potassium (K+) content of water samples varied from 0.782 to 10.557 mg/l and all the water samples (100%) contain K+ content lower than permissible limit, *i.e.*, 20 mg/l (**Table 1**). Nitrate (NO3-) content was lower than permissible limit (40-50 mg/l) in 64% villages; 10% villages are within limit and 26% villages have NO3- concentration higher than limit. Higher concentration of NO3- in water causes a disease called "Methaemoglobinaemia" or known as "Blue-baby Syndrome". It is particularly infant disease up to 6 months of child.

Factor analysis was applied to data obtained from 50 villages and factors extracted by the centroid method, rotated by Varimax rotation [4]. Calculated eigenvalues, percent total variance, factor loading and cumulative variance are given in **Table 3**.

The factor analysis generated two significant factors shown by scree plot (**Figure 1**) which explain 94.5% of the variation in the data set. Factor 1 explained 84.7% of the variance and Factor 2 explained 9.7% of the variance.

The following factors were indicated considering the hydro-chemical aspects of the water.

Table 3. Rotated factor pattern, rotation method = varimax.

	Factor 1	Factor 2
CL-	0.942	-0.132
Ca-H	0.934	-0.330
TDS	0.933	-0.321
EC	0.930	-0.291
NO3	0.919	-0.347
K+	0.912	-0.367
TH	0.898	-0.395
mg-H	0.883	-0.436
TA	0.777	-0.522
Na+	0.760	-0.591
F-	-0.190	0.941
pH	-0.390	0.892

- Factor 1 includes EC, TDS, Calcium hardness (Ca-H), Magnesium hardness (mg-H), Total hardness (TH), Chloride (CL^-), Alkalinity, Sodium (Na^+), Potassium (K^+) and Nitrate (NO_3), which originate from anthropogenic causes like industrial and agricultural pollution in surface water. So we named this factor as '*anthropogenic origin'*.
- Factor 2 includes pH which comes from natural sources. Fluorides are due to industrial waste but also due to geological sources so we named this factor as 'Organic origin'.

4. Conclusions

The data indicate that the groundwater of Sanganer Tehsil is highly deteriorated as it is polluted with high amount of fluoride, nitrate and alkalinity. Most of the water quality parameters are above the permissible limit. PCA of water quality data for Sanganer Tehsil shows that the main variation in water quality of the Sanganer Tehsil of Jaipur city is due to anthropogenic sources and organic sources.

5. References

[1] A. Sargaonkar and V. Deshpande, "Development of an Overall Index of Pollution for Surface Water Based on a General Classification Scheme in Indian Context," *Environmental Monitoring and Assessment*, Vol. 89, No. 1, 2003, pp. 43-67.

[2] K. Saffran, "Canadian Water Quality Guidelines for the Protection of Aquatic Life," *CCME Water Quality Index* 1.0: *User's Manual*, Excerpt from Publication No. 1299, 2001.

[3] J. D. Sharma, P. Sharma, P. Jain and D. Sohu, "Chemical Analysis of Drinking Water of Sanganer Tehsil, Jaipur District," *International journal of Environmental Science and Technology*, Vol. 2, No. 4, 2005, pp. 373-379.

[4] S. Ahmed, M. Hussain and W. Abderrahman, "Using Multivariate Factor Analysis to Assess Surface/Logged Water Quality and Source of Contamination at a Large Irrigation Project at Al-Fadhli, Eastern Province, Saudi Arabia," *Bulletin of Engineering Geology and the Environment*, Vol. 64, 2005, pp. 315-232.

J. Water Resource and Protection, **2010, 2, 864-871**
doi:10.4236/jwarp.2010.210103 Published Online October 2010 (http://www.SciRP.org/journal/jwarp)

Hydrochemical Analysis of Groundwater in the Lower Pra Basin of Ghana

E. K. Ahialey[1,2], Y. Serfoh-Armah[2,3], B. K. Kortatsi[4]
[1]*Department of Chemistry, National Nuclear Research Institute, Ghana Atomic Energy Commission, Legon, Ghana*
[2] *Department of Nuclear Sciences and Applications, Graduate School of Nuclear and Allied Sciences, University of Ghana, Accra, Ghana*
[3]*Ghana Atomic Energy Commission, Accra, Ghana*
[4]*Water Research Institute, Council for Scientific and Industrial Research, Accra, Ghana*
E-mail: *rsma*19*@yahoo,com*
Received June 17, 2010; *revised July* 8, 2010; *accepted July* 15, 2010

Abstract

Investigating into the quality of groundwater in the lower Pra basin using physico-chemical parameters have been carried out. Samples were collected from thirty one (31) water points. All major ions were determined using standard methods. The results show that approximately 97% of the water sampled has TDS values less than 1000 mg/l. Chemical parameters are influenced primarily by silicate weathering, ion exchange processes and sea aerosol spray. Sodium ion (Na^+) concentration is generally high compared to other cations and bi-carbonate (HCO_3^-) is the most abundant anion. Approximately 90% of the samples have iron concentrations greater than the W.H.O. limit for drinking water. Aluminium showed relatively higher concentration than other trace metals. The maximum and minimum concentrations recorded for cadmium Cd are 0.005 mg/l and 0.013 mg/l respectively. Concentrations of lead (Pb) zinc (Zn) were below detection limit. The groundwater in the basin is generally Na-Cl in character. Minor water types such as Ca-Mg-HCO_3, Na-Mg-Ca-HCO_3 and Na-Cl-SO_4 were also delineated.

Keywords: Lower Pra Basin, Ghana, Groundwater, Hydrochemistry

1. Introduction

In the last decade, there has been an increase in the exploitation of groundwater for water supply needs of many small communities in Africa including Ghana. Groundwater is not only feasible, but also the most cost effective source of potable water for scattered and remote communities. In Ghana, about 68 per cent of the population lives in rural communities. Until the last decade, groundwater contamination was not a priority concern for water resource managers in Ghana but potential for groundwater contamination is now acknowledged widely [1]. Groundwater has become an important source of potable water for most communities in the lower Pra basin since the mining activities within the Pra Basin has rendered most surface waters polluted and the cost of water treatment highly prohibitive. However, groundwater in hard rock areas and mostly in mining areas as the lower Pra Basin is known to be susceptible to quality problems that may have serious connotation on human health [2]. Secondly the mining activities in the areas generate acid mine drainage (low pH waters) that can leach trace metals in dangerous proportions into the groundwater system rendering it dangerous for human consumption. Despite the susceptibility of groundwater in the area to pollution, only scanty chemical data exist on groundwater. Accordingly, the present quality of many groundwater systems is largely unknown and the baseline chemical data on which changes, in present and future water quality, can be based is unavailable. The necessity, therefore, to generate baseline data cannot be overemphasized. It is equally imperative to know natural processes or phenomena that govern the chemical composition of the groundwater or the anthropogenic factors that presently affect it. The objectives of this research are to investigate the quality of groundwater in the lower Pra basin; characterize the groundwater and to delineate the relevant water-rock interaction and anthropogenic factors

that control water quality in the study area and acquire a database for further research and monitory of groundwater quality in the basin. Season is from September to October [3]. Temperatures are almost the same as in the south-west equatorial region (26°C in August and 30°C between March and April). Monthly relative humidity is higher in the rainy seasons than during the rest of the year. The highest average monthly humidity does not exceed 75% and the lowest is about 60% [3]. The vegetation is Coastal scrub and grassland. The study area is within the coastal plain. The land is not flat but rather undulating. Various types of rock are found here, but the most widespread are the granites which also form most of the hills. The coastline is different from that of the south-east coastal plains and forms a series of bays and headlands, and is cliffed in numerous places [3]. The Upper Birimian Series consists of great thickness of basaltic and andesitic lavas, beds of agglomerate, tuff and tuffaceous sediments [4].

2. Materials and Methods

Samples were collected from thirty one (31) water points (boreholes and hand-dug wells). Sampling protocols described by Claasen [5] and Barcelona *et al.* [6] were strictly followed during sample collection: the sampling bottles were conditioned by washing with detergent, then with ten percent (10%) nitric acid, and finally rinsing several times with distilled water. This was carried out to ensure that the sample bottles were free from contamination, which could affect the concentrations of various ions in the groundwater samples. At the sampling points, the boreholes were pumped for five minutes to purge the aquifer of stagnant water so as to acquire fresh samples for analysis. Samples were collected in duplicate, and samples earmarked for metal analysis were acidified to a pH less than 2 after filtration using reagent grade nitric acid. Samples for anion analysis were without preservation because addition of acids could lead to a reaction with the carbonates in the water sample. Samples for cation analysis were filtered on site through 0.45 µm filters on acetate cellulose into 250 ml bottles and immediately acidified to a pH less than 2 by addition of Merck TH Ultra pure nitric acid. Samples for anion analysis were collected into 600 cm^3 polyethylene bottles without preservation. All samples were stored in an ice-chest and transported to the Ghana Atomic Energy Commission chemistry laboratory, stored at temperature less than four degrees Celsius (4°C) and analysed in ten days. The physical parameters and major ions were determined using standard methods [7]. Zinc (Zn), cadmium (Cd) and lead (Pb) were analysed using digestion, followed by atomic absorption spectrometry using the AA240FS Fast Sequential Atomic Absorption Spectrometer [8-10]. Aluminum (Al), Iron (Fe), Calcium (Ca), magnesium (Mg), manganese (Mn) were analysed by Neutron Activation Analysis (NAA) using the GHARR-1 at a neutron flux of 1×10^{11} ncm^2s^1 [11-13]. **Figure 1** shows the location and geological map of the study area.

3. Results and Discussion

3.1. Hydrochemistry

The results were analysed statistically and the summary, which include minimum and maximum values; mean and median, as well as standard deviation has been presented in **Table 1** below. The actual results will be put in the appendix. The groundwater pH is generally low, in the range of 5.29 and 7.91 with mean and median values of 6.47 and 6.42 respectively. The pH values, however, fall within the natural water pH range of 4.5 to 9.0 [14]. The mean and median values of the electrical conductivity (EC) are 675.3 µs/cm and 416 µs/cm respectively. The range is a minimum of 51 µs/cm to a maximum of 4060 µs/cm. The standard deviation with respect to the mean is 938.8 µs/cm. The difference may reflect the wide variation in activities and processes prevailing in the surface and subsurface [15]. The order of the relative abundances of cations and anions as measured in the basin are: $Na^+ > Ca^{2+} > Mg^{2+} > K^+$ and $HCO_3^- > Cl^- > SO_4^{2-} > NO_3^- > PO_4^{3-}$, respectively. Sodium is, by far the most abundant cation. A high percentage of the TDS is contributed by Na^+ Cl^-, and SO_4^{2-} Conductivity is also most influenced by Na^+, Cl^- and SO_4^{2-} as depicted in **Table 2** by the Pearson correlation which shows the extent of correlation between and among major ions, TDS and conductivity. Phosphate concentrations are, in general, very low as compared to NO_3^- and SO_4^{2-}.

3.2. Sources of Major Ions

Figure 2 shows the relationship between Na^+ and Cl^-, for the deduction of the origin of salinity in the basin. Approximately 74% of the water samples have $Na^+/(Na^+ + Cl^-)$ ratio within the range of 0.5 ± 0.1 or plot along or close to 1:1 line of the Na^+ vrs. Cl^- gragh, implying that sea aerosol spray or halite dissolution is partially responsible for Na^+ and Cl^- in the groundwater. However, halite is not known to be associated with the geology of the sampling area (Cape Coast granitoid complex, Discove granotide complex and Upper Birimian). This leaves sea aerosol spray as the most likely source of Na^+ and Cl^-. A very small percentage of the samples plot below and away from the 1:1 line, which indicate that reverse ion exchange might be a minor process controlling the chemical evolution of the basin.

If ion exchange is the controlling factor of groundwa-

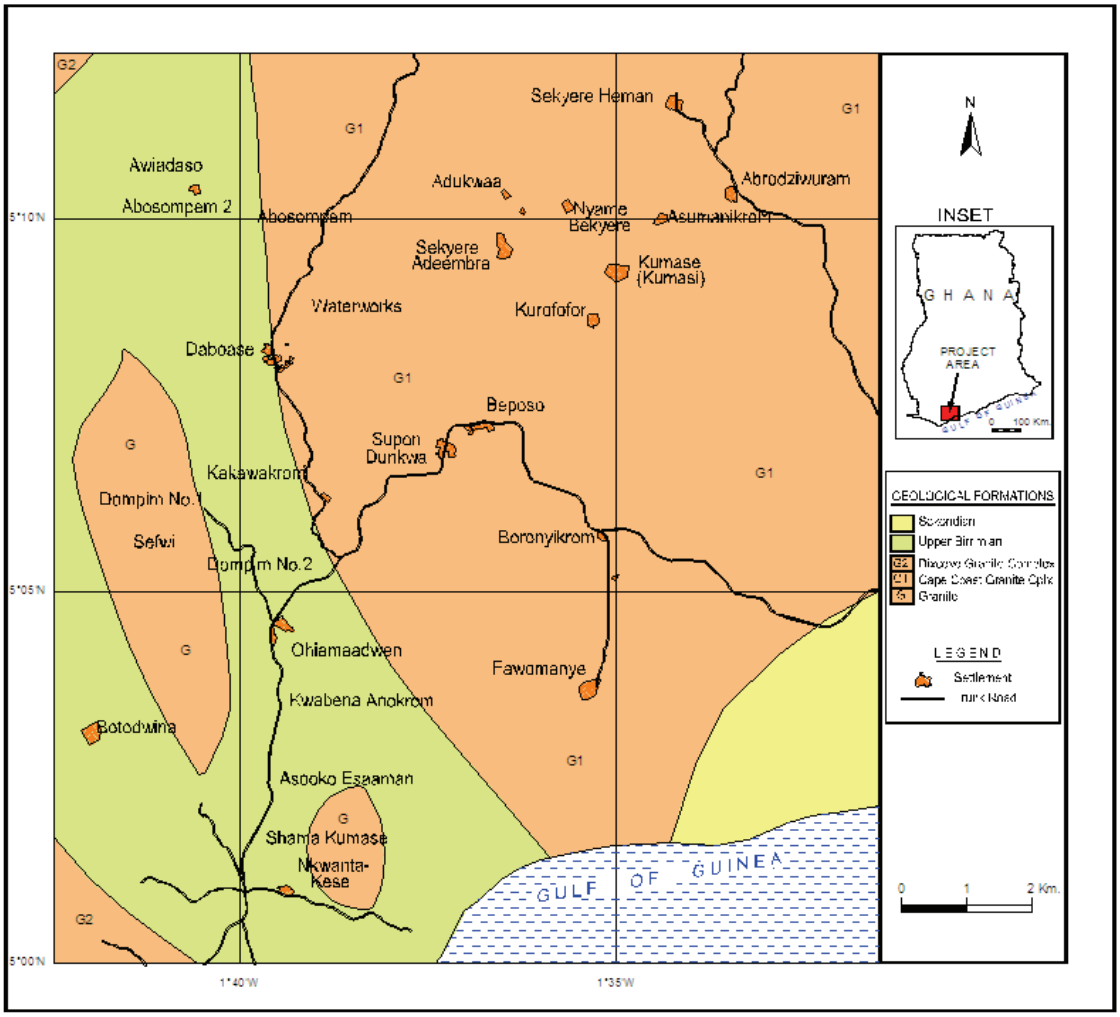

Figure 1. Location and geological map of the study area.

Table 1. Statistical summary of physical and chemical parameters.

Parameter	Unit	Min.	Max.	Mean	Median	Std. Dev.	WHO (2004) Guideline limit
Temp.	(°C)	25.20	29.80	27.87	28.00	1.52	
pH	pH units)	5.29	7.91	6.47	6.42	0.67	6.5-8.5
Cond.	(µs/cm)	51.00	4060	675.27	416.00	938.79	
Sal.	(ppm)	0.00	2.11	0.27	0.11	0.51	
TDS	(mg/l)	146.00	2030	507.83	394.50	425.29	
Hardness	(mg/l)	55.89	165.09	104.87	101.88	32.19	
Ca^{2+}	(mg/l)	5.98	29.50	17.92	17.93	6.39	
Mg^{2+}	(mg/l)	2.86	25.38	15.34	15.69	5.20	
Na^{+}	(mg/l)	22.60	697.50	132.80	77.90	155.40	200
K^{+}	(mg/l)	3.10	52.00	15.30	13.90	11.40	
HCO_3^{-}	(mg/l)	43.90	300.80	139.30	130.20	63.90	
Cl^{-}	(mg/l)	10.60	715.10	130.10	93.90	158.60	250
SO_4^{2-}	(mg/l)	18.10	266.90	83.60	68.40	63.30	250
NO_3^{-}	(mg/l)	0.09	9.03	2.79	2.16	2.594	50
PO_4^{3-}	(mg/l)	0.02	0.19	0.07	0.07	0.05	
Fe	(mg/l)	0.16	0.78	0.42	0.14	0.30	0.3
Mn	(mg/l)	0.003	0.08	0.02	0.01	0.02	0.5
Cd	(mg/l)	0.005	0.01	0.01	0.01	0.002	0.003
Al	(mg/l)	2.522	9.264	5.005	4.583	1.722	0.2

Table 2. Pearson correlation of major ions, TDS and conductivitye.

	Ca^{2+}	Mg^{2+}	Na^{+}	K^{+}	HCO_3^{-}	Cl^{-}	SO_4^{2+}	TDS	Cond.
Ca^{2+}	1								
Mg^{2+}	.427*	1							
Na^{+}	.052	.031	1						
K^{+}	.177	.099	.707**	1					
HCO_3^{-}	.264	.068	.273	.129	1				
Cl^{-}	.111	.112	.969**	.745**	.162	1			
SO_4^{2-}	.058	.149	.811**	.697**	.183	.757**	1		
TDS	.138	.099	**.986****	.762**	.329	**.970****	**.830****	1	
Cond.	.090	.156	**.954****	.774**	.277	**.956****	**.798****	.966**	1

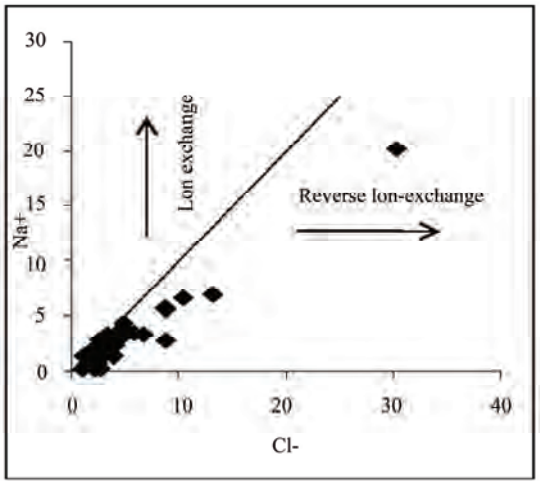

Figure 2. Na^{+} and Cl^{-} relationship.

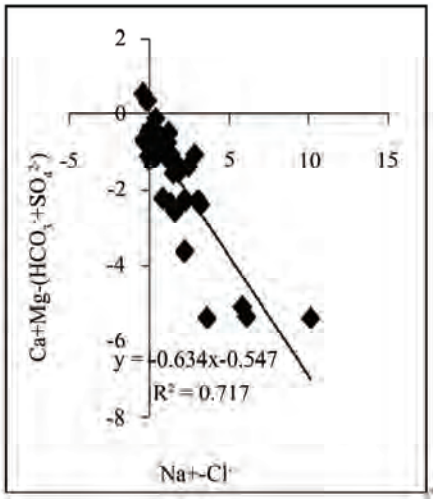

Figure 3. Relationship between Na-Cl and Ca+Mg−(HCO_3 +SO_4).

ter composition, a plot of Na-Cl against Ca+Mg−(HCO_3 +SO_4) will have a negative slope of unity [16]. **Figure 3** shows a plot with a slope of −0.634, indicating some level of ion exchange. Also, approximately 6.5% of samples plot above the 1:1 line.

This percentage represents samples with $Na^{+}/(Na^{+} + Cl^{-})$ ratio greater than 0.5 and suggest that apart from sea aerosol spray, silicate dissolution could also be a source of sodium. The dissolution of albitic feldspars ($NaAlSi_3O_8$), which is present in the Cape Coast granite complex, could be the origin of excess Na^{+} ions.

The functional sources of dissolved ions can also be broadly assessed by plotting a graph of Na^{+}: $(Na^{+} + Ca^{2+})$ as a function of TDS [17]. The data points of the area on the Gibbs' diagram in **Figure 4** suggest chemical weathering of rock-forming minerals and evaporation.

Figure 5 shows the relationship between Ca + Mg (meq/l) and HCO_3 + SO_4 (meq/l). A 1:1 relationship could give an indication of gypsum, anhydrite, calcite and dolomite as the predominant processes controlling solution composition and groundwater falling below the 1:1 signifies ion exchange which involves the depletion of Ca + Mg as compared to HCO_3 + SO_4 [18]. A high per-

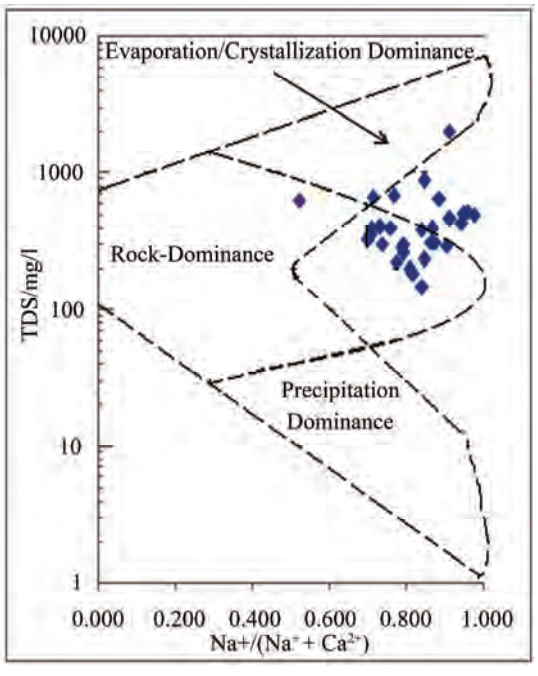

Figure 4. Mechanism governing groundwater chemistry.

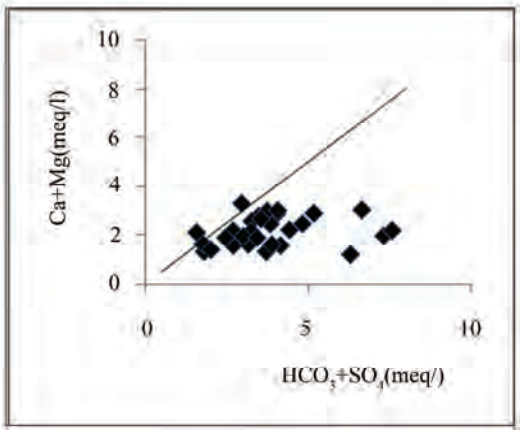

Figure 5. Relationship between Ca + Mg (meq/l) and HCO_3 + SO_4.

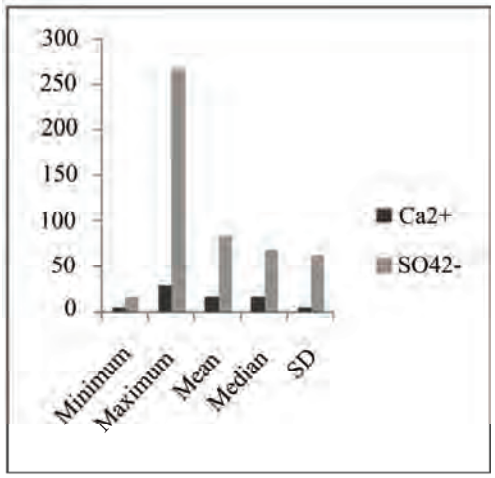

Figure 6. A bar chart: comparing Ca^{2+} and SO_4^{2-}.

centage of the groundwater samples in the basin fall below 1:1 dissolution line: this further proves that there is some level of ion exchange. The plot also depicts deficiency of Ca + Mg relative to HCO_3 + SO_4. Therefore, Na^+ must balance the excess HCO_3 + SO_4. Sulphate in the groundwater is derived principally from the evaporate minerals gypsum (hydrous calcium sulphate = $CaSO_4{\cdot}2H_2O$), and the anhydride ($CaSO_4$). It may also come from oxidation of pyrite, which is an iron sulfide mineral. The groundwater may also contain other minerals like $MgSO_4{\cdot}7H_2O$ (Epsom salt) and $Na_2SO_4{\cdot}10H_2O$ (Glauber's salt).

From the Pearson correlation, there is a fairly high correlation between calcium ions and the sulphate. Also, from the data obtained, there was lower concentration of calcium ions compared to sulphate ions ($Ca^{2+} < SO_4^{2-}$) (**Figure 6**) which is an indication of oxidation of pyrite or calcium removal as a result of calcite ($CaCO_3$) precipitation.

The nitrate concentrations obtained in the sampling area are very low. This is because the samples were taken from predominantly rural areas and the nitrate concentrations could not have been affected by urban wastewater and industrial activities. Sewages generated from domestic and industrial activities and septic tanks are also remote sources of NO_3^- in the area. The NO_3^- could originate from ammonium and NO_3^- fertilizers and aerobic decomposition of organic matter in the soils. All the groundwater in the basin had nitrate concentrations far below the WHO maximum acceptable value. The minimum and maximum concentrations are 0.089 mg/l and 9.028 mg/l respectively, far below 50 mg/l (WHO value). This is an indication of minimal application of ammonium and NO_3^- fertilizers in the basin. Other anthropogenic activities are not likely sources of nitrate in the basin.

3.3. Trace Elements

3.3.1. Aluminium (Al^{3+})

The minimum, maximum, mean, median concentrations, as well as the standard deviation and WHO acceptable limit for drinking water has been depicted in the **Table 1**. All samples clearly had concentrations higher than the acceptable limit. The lower Pra Basin contains potassium feldspars ($KAlSi_3O_8$), albitic feldspars ($NaAlSi_3O_8$) and plagioclase ($CaAl_2Si_2O_8$). The relatively high concentration of Al could be a result of the dissolution of these salts.

3.3.2. Iron (Fe)

A minimum of 0.16 mg/l and a maximum of 0.776 mg/l were recorded (**Table 1**). Approximately 90% of the water has concentration greater than 0.3 mg/l, the WHO standard for iron in drinking water. Igneous rocks minerals whose iron content is relatively high include the pyroxenes, the amphiboles, biotite magnetite and especially the nesosilicate olivine [19]. The Lower Pra Basin has the biotite, which might be the sources of high iron concentrations in the basin.

3.3.3. Manganese

Manganese occurs in rocks mainly as manganese and manganeferrous oxides, particularly in areas underlain by Birimian rocks [4]. Reaction between these oxides and the mildly acidic groundwater results in the production of manganous ion (Mn^{2+}). The manganese concentration measured varies from 0.003 mg/l to 0.078 mg/l. All the measured concentration values are lower than 0.5 mg/l, which is the WHO 1993 permissible limit for potable water [20]. A high concentration of manganese is undesirable impurity in water owing to a tendency to deposit black oxide stains but this was not observed. Manganese

usually occurs with iron as redox couple, where the Mn^{2+} is reduced to Mn and the iron II (Fe^{2+}) is oxidized to iron III (Fe^{3+}).

3.3.4. Cadmium

Cadmium naturally occurs as accessory element in zinc ore (sphalerite, ZnS) (largest industrial source), CdS; $CdCO_3$ (rare). Anthropogenic sources are industrial wastes (batteries; electroplating; pigment manufacture; video/fluorescenttubes, Galvanized pipes, Roadside soils (vehicle use) [21]. The maximum and minimum concentrations of cadmium measured in the lower Pra basin are 0.013 mg/l and 0.005 mg/l respectively. The zinc (Zn) concentrations were below detection limit (0.0010) which implies Cd could not have occurred as an accessory element of zinc ore, sphalerite. The other natural sources (rare) could have contributed to the concentration of cadmium in the basin. The cadmium concentrations are above the WHO limit of 0.003 mg/l (WHO, 1993).

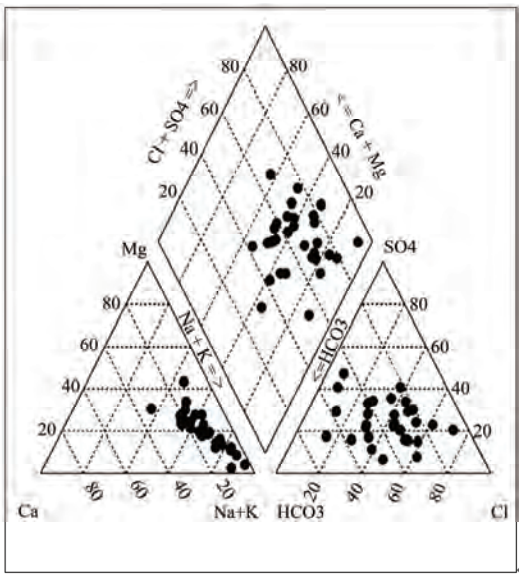

Figure 7. Trilinear Piper diagram.

3.4. Hydrochemical Facies

Hydrochemical facies are generally distinct zones that cation and anion concentrations are described within defined composition categories [22]. The chemical composition of groundwater from the lower Pra Basin is presented in **Figure 7**. A high percentage of samples clustered in the Na-Cl dominant section. Therefore, from the analysis of the chemical plot in the triangular field of the Trilinear Piper, Na-Cl water is the major water type. Minor water types identified are Na-Mg-Ca-HCO_3, Ca-Mg-HCO_3, and Na-Cl-SO_4.

4. Conclusions

The hydrochemical analysis of groundwater in the lower Pra basin revealed that the water is mildly acidic to basic (5.29-7.91). The physico-chemical parameters suggest that the groundwater in the lower Pra basin is generally good for domestic use. Approximately 97% of the water sampled has TDS values less than 1000 mg/l, this falls within fresh water recommended value which is between 0 and 1000 mg/l. Chemical parameter (ions in the water) is influenced primarily by silicate weathering, ion exchange processes and sea aerosol spray. Sodium ion (Na^+) concentration is generally high compared to other cations. Bicarbonate (HCO_3^-) is the most abundant anion with a total concentration of 4251.04 mg/l, followed closely by chloride ions. Aluminium showed relatively high concentrations; all the water sampled has Al concentration greater than 0.2 mg/l, which is the W.H.O. maximum acceptable limit for drinking water. The minimum and maximum iron concentrations are 0.161 mg/l and 0.776 mg/l respectively. Approximately 90% of the samples have iron concentrations greater than the W.H.O. limit for drinking water which is 0.3 mg/l. Considerable concentrations were recorded for manganese (0.003 mg/l to 0.078 mg/l). These are, however, lower levels compared with the W.H.O. guideline limit of 0.5 mg/l. The maximum and minimum concentrations recorded for cadmium (Cd) are 0.005 mg/l and 0.013 mg/l respectively. Concentrations of lead (Pb) zinc (Zn) were below detection limit of the AA240FS Fast Sequential Atomic Absorption Spectrometer used. The ground waters in the basin are generally NaCl waters. Minor water types such as Ca-Mg-HCO_3, Na-Mg-Ca-HCO_3 and Na- Cl-SO_4 were also delineated.

5. References

[1] A. A. Duah, "Groundwater Contamination in Ghana, Yongxin Xu and Brent Usher," Taylor and Francis Group, London, 2007, pp. 57-64.

[2] L. P. Smedly, W. M. Edmunds, J. M. West, S. J. Gardner and K. B. Pelig-ba, "Vulnerability of Shallow Groundwater Quality Due to Natural Geochemical Environment. Health Problems related to Groundwater in the Obuasi and Bolgatanga Areas, Ghana," Report prepared for ODA under the ODA/BGS Technology Development and Research Programme, Project 92/5, 1995.

[3] G. Benneh and B. K. Dickson, "A New Geography of Ghana," Pearson Education Limited, England, 2004, pp. 24-27.

[4] G. O. Kesse, "Rocks and Minerals of Ghana," 1985, pp. 25-26.

[5] H. C. Claasen, "Guidelines and Techniques for Obtaining Water Samples that Accurately Represent the Water

Quality of an Aquifer," U.S. Geological Survey Open File Report 82-1024, 1982.

[6] M. Barcelona, J. B. Gibb, J. A. Helfrich and E. E. Garske, "Practical Guide for Groundwater Sampling," Illinois State Water Survey ISWS, Contract Report 374, 1985.

[7] APHA, "Standard Method for the Examination of Water and Wastewater," 20th Edition, American Public Health Association, Washington D.C., 1998.

[8] J. A. C. Broekaert, "Analytical Atomic Spectrometry with Flames and Plasmas," 3th Edition, Wiley-VCH, Weinheim, 1998.

[9] M. B. Sperling and B. Welz, "Atomic Absorption Spectrometry, " Wiley-VCH, Weinheim, 1999.

[10] D. D. Sood, A. V. R. Reddy and N. Ramamoorthy, "Fundamentals of Radiochemistry," 2004.

[11] A. Chatt, N. Desilva, J. Holzbecher, D. C. Stuart, R. E. Tout and D. E. Ryan, "Cyclic Neutron Activation Analysis of Biological and Metallurgical Samples," Truce Analysis Research Centre, Department of Chemistry, Dalhousie University, Halifax, 1980.

[12] A. Chatt, J. Desilva, D. C. Holzbecher, R. E. Stuart, R. E. Tout and D. E. Ryan, "Cyclic Neutron Activation Ana- lysis of Biological and Metallurgical Samples," Canadian Journal of Chemistry, Vol. 59, No. 5, 1981, pp. 1660-1664.

[13] K. Vetter, "Neutron Activation Analysis with HPGe Detectors," NE 104A Experiment 6, University of California, Brekeley, 2008, pp. 1-6.

[14] D. Langmuir, "Aqueous Environmental Geochemisty," 2nd Edition, Prentice Hall, Upper Saddle River, New Jersey, 1997.

[15] U. M. Amadi and P. A. Amadi, "Saltwater Migration in the Coastal Aquifers of Southern Nigeria," Journal of Mining and Geology, Vol. 26, No. 1, 1990, pp. 35-44.

[16] R. S. Fisher, F. W. Mullican, "Hydrochemical Evolution of Sodium-Sulphate and Sodium-Chloride Groundwater beneath the Northern Chihuahuan Desert, Transpecos, Texas, U.S.A.," *Hydrogeology Journal*, Vol. 5, No. 2, 1997, pp. 14-16.

[17] R. J. Gibbs, "Mechanisms Controlling World Water Chemistry," *Science*, Vol. 170, No. 3962, 1970, pp. 1088-1090.

[18] W. Mclean and J. Jankowski, "Groundwater Quality and Sustainability in an Alluvial Aquifer, Australia," In: Sililo *et al.*, Eds., *Proceedings of XXX IAH Congress on Groundwater*: *Past Achievements and Future Challenges*, A. A. Balkema, Rotterdam, Brookfield, Cape Town South Africa 26 November-1 December 2000.

[19] J. D. Hem, "Study and Interpretation of Chemical Characteristics of Natural Water," 3rd Edition, USGS Water-Supply Paper, 1992.

[20] World Health Organization (WHO), "Guidelines for Drinking Water Quality, Revision of the 1984 Guidelines," Final Task Group Meeting, Geneva, 1993.

[21] D. W. Bolton, "Cadmium in Groundwater and Sediment Samples in the Aquia Aquifer," *Groundwater Symposium*, Maryland Geological Survey, 2006.

[22] D. U. Ophori and J. Toth, "Patterns of Groundwater Chemistry, Ross Creek Basin, Alberta, Canada," *Groundwater*, Vol. 27, 1989, pp. 20-26.

Appendix: Measured Parameters

NO	CODE	Ca^{2+}/ mg/l	Mg^{2+}/ mg/l	Na^{+}/ mg/l	K^{+}/ mg/l	HCO_3^{-}/mg/l	Cl^{-}/mg/l	SO_4^{2-}/mg/l	NO_3^{-}/mg/l	PO_4^{3-}/mg/l	TEMP. (^{O}C)	pH (pH unit)	Cond. (µs/cm)	Sal. (ppm)	TDS (mg/l)	Hard. (mg/l)	Fe/ mg/l	Mn/ mg/l	Cd/ mg/l	Al/ mg/l
1	SF	13.63	15.75	301.7	25.0	184.00	247.50	206.9	9.028	0.0729	29.7	6.85	1919.0	0.93	956.0	98.89	0.161	0.078	0.008	2.522
2	KWAB	9.46	10.39	152.7	3.7	139.08	120.60	31.2	7.809	< 0.0010	29.8	6.61	328.0	0.08	164.0	66.41	0.294	0.005	0.009	3.063
3	OHIA	10.89	12.62	110.2	6.8	131.70	155.90	25.4	4.028	0.061	29.6	5.89	529.0	0.19	265.0	79.16	0.374	0.066	0.006	3.093
4	NK	18.19	15.64	697.5	52.0	103.48	715.10	266.9	0.359	0.0491	29.8	6.17	4060.0	2.11	2030.0	109.83	0.345	0.069	0.010	3.957
5	BOAT	15.54	10.98	83.1	22.8	95.20	121.20	126.5	4.622	< 0.0010	29.5	5.60	601.0	0.23	301.0	84.02	0.321	0.036	0.011	4.014
6	KUM	12.79	18.99	338	20.0	87.84	237.40	46.5	4.172	0.0508	29.3	6.29	1270.0	0.59	635.0	110.14	0.353	0.039	0.010	3.541
7	KAKO	6.78	10.36	60.9	19.4	117.12	103.20	195.3	3.309	< 0.0010	29.6	7.51	560.0	0.20	277.0	59.59	0.300	0.017	0.008	3.401
8	PRA.DAB	13.42	8.05	22.1	8.9	96.16	24.50	33.8	1.151	0.06105	25.2	7.91	123.5	0.00	61.6	66.66	0.564	0.007	0.006	5.202
9	WW	14.38	10.52	60.0	4.2	83.62	25.20	40.7	0.809	0.0339	25.5	6.48	222.0	0.03	111.2	79.23	0.476	0.012	0.007	7.513
10	ABOS	13.89	11.53	139.0	5.0	43.92	100.60	49.6	0.431	< 0.0010	25.3	6.01	51.0	0.00	25.9	82.16	0.401	0.008	0.006	6.427
11	ABOS2	13.43	18.46	15.0	3.2	69.28	34.30	57.3	0.539	< 0.0010	25.6	5.29	60.3.0	0.00	30.6	109.55	0.370	0.007	0.006	6.961
12	AWI	18.16	12.02	48.8	26.4	87.84	15.10	24.6	0.971	0.1017	25.8	6.72	229.0	0.03	114.2	94.84	0.380	0.009	0.010	6.569
13	SUP1	24.26	25.38	85.6	15.6	51.24	119.80	12.7	4.424	< 0.0010	26.4	5.68	469.0	0.16	235.0	165.09	0.346	0.052	0.011	5.840
14	SUP2	16.03	26.72	89.9	13.9	58.56	87.30	25.8	3.165	0.0729	26.6	5.88	500.0	0.17	250.0	150.06	0.349	0.048	0.011	4.100
15	BB	22.06	12.31	23.9	7.2	58.56	25.40	28.8	0.953	0.1102	26.7	7.18	112.2	0.00	56.0	105.78	0.530	0.007	0.010	6.150
16	BEB	25.91	21.22	30.8	3.2	300.80	125.10	82.7	4.982	< 0.0010	26.5	6.65	1266.0	0.58	632.0	152.08	0.437	0.038	0.012	4.178
17	SAD	17.65	18.02	22.4	6.6	165.88	20.90	63.4	0.395	< 0.0010	26.9	6.00	121.2	0.00	61.0	118.28	0.338	0.008	0.009	4.248
18	SAC	24.1	16.72	58.0	16.8	175.68	100.70	18.1	0.971	0.0169	27.4	6.99	572.0	0.21	286.0	129.03	0.284	0.004	0.005	4.575
19	ADU	13.89	21.55	91.0	3.1	183.00	20.30	19.6	0.179	0.0848	27.8	6.30	309.0	0.07	154.4	123.43	0.472	0.014	0.012	3.896
20	NYAM	26.66	20.15	41.0	9.0	73.20	14.80	21.7	0.341	< 0.0010	27.7	6.07	161.6	0.00	80.9	149.55	0.492	0.007	0.013	4.828
21	KSI	16.65	22.40	54.5	17.3	56.90	27.60	19.7	1.528	< 0.0010	27.9	5.61	257.0	0.05	128.7	133.82	0.387	0.012	0.008	8.427
22	ASUM	20.82	23.71	201.3	15.0	212.28	116.90	78.8	0.413	< 0.0010	27.9	7.00	664.0	0.01	90.3	149.63	0.537	0.013	0.011	4.590
23	SH	11.52	12.64	38.3	14.0	131.76	12.90	82.4	1.438	< 0.0010	28.2	5.86	180.1	0.01	90.3	80.82	0.470	0.008	0.009	4.168
24	SHP	0.136	13.49	22.6	7.3	80.52	10.80	32.3	1.061	0.0915	28.5	7.26	112.2	0.00	55.9	55.89	0.634	0.010	0.010	5.162
25	AB	14.37	13.84	90.8	10.4	109.80	73.30	38.8	0.719	0.0491	28.5	6.38	416.0	0.13	208.0	92.88	0.776	0.016	0.009	9.264
26	KOF	18.99	14.70	47.0	10.1	161.04	73.00	28.8	0.179	0.022	28.3	6.85	416.0	0.13	208.0	107.95	0.511	0.010	0.007	4.952
27	FW	26.28	20.60	232.0	12.0	139.08	204.60	60.8	0.089	0.0983	28.1	6.21	1164.0	0.53	581.0	150.45	0.492	0.012	0.008	5.858
28	BK	19.58	2.86	180.4	9.0	95.16	101.10	36.9	0.215	0.1967	28.6	6.10	499.0	0.17	249.0	60.67	0.456	0.013	0.008	5.354
29	ASO	12.83	11.87	119.3	23.0	87.84	55.40	49.6	3.723	< 0.0010	28.9	6.82	578.0	0.21	288.0	80.92	0.444	0.009	0.011	3.751
30	DOM	13.3	15.73	58.7	7.0	65.88	12.34	68.5	3.340	< 0.0010	29.5	6.77	317.0	0.008	158.3	97.99	0.304	0.003	0.007	4.130
31	DOMR	17.95	12.14	22.9	5.1	102.48	10.64	83.6	2.970	0.0373	29.7	7.29	105.7	0.00	52.7	94.81	0.428	0.010	0.007	3.6535

J. Water Resource and Protection, **2010, 2, 872-879**
doi:10.4236/jwarp.2010.210104 Published Online October 2010 (http://www.SciRP.org/journal/jwarp)

Micro-Droplet Flux in Forest and its Contribution to Interception Loss of Rainfall – Theoretical Study and Field Experiment

Michio Hashino[1], Huaxia Yao[2]*, Takao Tamura[1]
[1]*Department of Civil Engineering, University of Tokushima, Tokushima, Japan*
[2]*Dorset Environmental Science Centre, Ontario Ministry of the Environment, Dorset, Ontario, Canada*
E-mail: *huaxia.yao@ontario.ca*
Received July 16, 2010; *revised August* 9, 2010; *accepted August* 17, 2010

Abstract

A new approach to explain forest interception was proposed by introducing micro-droplets of crushed raindrops during rainfall. The aerodynamic diffusion and transfer of both vapour and micro-droplets from canopy to upper air were described and calculated, and proposed formulas applied to eight rainfall events at the Okunoi Experimental Station, Tokushima, Japan. Contributions from droplet transfer were 0.9-58.2 times of contributions from vapour transfer, taking a majority portion in total interception loss. Accounting only the vapour transfer or evaporation loss as estimated by Penman equation was not able to account for actual interception loss. The micro-droplet flux component took major portion in the two heavily rained events, and completely made up the interception as happened in October 2004. The droplet flux could accommodate a high interception rate, even when the air was nearly vapour-saturated and vapour flux was zero. This approach provided a new explanation to extraordinarily high interception rates.

Keywords: Rainfall Interception, Micro-Droplet Transfer, Vapour Flux, Forest Canopy, Aerodynamic Diffusion

1. Introduction

Traditional theories and estimation methods of rainfall interception and its evaporation were based on a dominating conception: raindrops fell on leaves and branches of vegetation, some of raindrops were caught or intercepted by the leaves and branches, and intercepted raindrops were vaporized and transported outward during rainfall periods and after the periods. Three major methodologies as summarized by Chow *et al.* [1] have been developed to describe the interception evaporation process and estimate interception-evaporation rates: aerodynamic methods such as Thornthwaite-Holzman equation, energy balance methods, and combined methods such as Penman equation. They performed well for many geographical regions and various types of vegetations in the world. However, at some locations (especially humid tropical forests, maritime areas, or islands experiencing frequent storms or typhoons), none of the three methods could give satisfactory estimations.

One main reason for the failure would be that only vapour flux was considered in these methods, while other forms of water in the air – floating or suspended water droplets, or micro-droplets created by the canopy during rainfall interception – have not been paid much attention. Apart from the raindrops captured by the canopy, some raindrops were crushed into tiny/micro droplets looking like mist or fog droplets. These micro-droplets have much smaller sizes than raindrops and can float in the air, and can be aerodynamically transported from inside canopy to outside. During rainfall events, the air near ground or around forest was easily saturated with water vapour, and the micro-droplets appeared. This portion of micro-droplets and their vertical flux were a loss to the rainfall (they did not fall down onto ground as throughfall), and should be a component of interception loss. If that portion took a substantial proportion in the total interception loss, an underestimation of interception loss could occur as explained later. Therefore, the role of micro-droplet flux in interception loss needs to be noted for the situations of tropical forests, maritime areas, and islands.

So far no specific studies have been conducted to address the flux of micro-droplets and its connection to interception process. A few field studies have partially touched the topic. The fogwater droplets and their vertical movement were confirmed by field measurements [2,3], reminding a possible contribution from the micro-droplets. The phenomenon of extraordinarily high interception rates (higher than the Penman-Monteith equation rate) was partially explained by different perspectives: an extra energy coming from horizontal transfers (from dry locations to raining locations, or from warmer oceans to cooler forests) might lead to the high evaporation rate [4,5], the aerodynamic resistance of the canopy could be very low to force a high evaporation rate [5,6], the interception rate was related to rainfall rate and exceeded the net radiation [7], or the wind gusts and splashed droplets might enhance evaporation rates [8,9]. But neither of these studies or suggestions has given a thorough explanation for the phenomenon.

Therefore, we tried and suggested a new approach by introducing the existence and transport of micro-droplets. In our scheme for interpretation of interception loss of rainfall, the interception flux is composed of two flux components: vapour flux and micro-droplets flux. The vapour flux has its source from the liquid water on canopy surface and raindrops within the canopy; liquid water is vaporized first because of radiation or heat and the vapour is transported in the air. The micro-droplets are not gaseous vapour, not created by vapouration but by rain crushing on leaves and branches; the droplets do not fall down, they are transported by aerodynamic diffusion and winds. Not neglecting the droplets, an aerodynamic transfer estimation method was proposed and applied to both the vapour and droplets in the air within and above the canopy to calculate interception evaporation process, and each of the two flux components were calculated. The new method was presented in this article, and a case study was provided to demonstrate its applicability (capable to explain the extraordinarily high interception loss).

2. Experimental Station and Data

The Okunoi Forest Experimental Station (latitude 34° 01', longitude 134° 12') is located at Yamakawa Town, Yoshinokawa City, Tokushima Prefecture, Japan (**Figure 1**), where the annual precipitation and annual averaged air temperature are 1600 mm and 15°C respectively.

A meteorological observation tower was set up at the elevation of 230 m, with a height of 26 meters. Meteorological observations were conducted at three different heights along the tower. A set of meteorological factors (temperature, humidity, wind speed, wind direction, sunshine duration, and net radiation) were measured at the height of 18.2 m, temperature and humidity were measured at the height 1.5 m and 25.8 m.

Figure 1. Location of experimental station.

Measurements of canopy's interception of rainfall were made for two typical trees: a Hinoki cypress (*Chamaecyparis obtusa*, a conifer in cypress family and native to Japan) and a Sugi cypress (*Cryptomeria japonica*, a conifer in cypress family and endemic to Japan), using similar methods as described by Chang [10]. The gross rainfall was measured at an open spot close to the station with standard rain gauges. The representative Hinoki and Sugi trees were both 17 m high.

Automatic recording of meteorological variables was started in 1999 at the meteorological tower, and hourly, daily and annual data were collected for the station. Interception measurements were conducted in 2003 and 2004, providing hourly data of throughfall, stemflow and interception loss.

3. Methods

Vertical transfer flux of vapour and micro-droplets by turbulent air diffusion were described by the Fick law of aerodynamics as follows.

$$\rho_w E = -\rho_a K_w (dq/dz) \quad (1)$$

where, ρ_w was the density of liquid water, E the rate of interception loss (volumetric water loss per unit time per unit area), $\rho_w E$ the vertical flux of interception, ρ_a the density of moist air, K_w the coefficient of turbulent air diffusion, q the specific humidity of water vapour and droplets in the air at a giving height z.

Momentum flux of turbulent air mass was expressed as

$$\tau = \rho_a K_m (du/dz) \quad (2)$$

where τ was the friction stress at height z, K_m the diffusion coefficient for the momentum (usually equal to the turbulent air diffusion coefficient K_w), and u the wind velocity at height z.

Vertical profiles of wind velocity and specific humidity, and an illustrative scheme of transfer fluxes of va-

pour and droplets were illustrated in **Figure 2**. The tree canopy had a height of *h*, produced a roughness height of z_0 at which the wind velocity was zero, gave a canopy's displacement height of *d* at which a zero heat flux existed. The z_1 and z_2 were two heights (may be the meteorological measurement heights), and their corresponding wind velocity and specific humidity were u_1, u_2 and q_1, q_2 respectively. Note that any height as *z*, z_1 or z_2 was the height measured against the position of displacement height, or it was a residual height of actual height from the ground minus the displacement.

Applying (1) and (2) to the heights z_0 and z_1 respectively and combining the results together, gave the following equation.

$$\rho_w E = -\tau K_w / K_m \cdot (q_1 - q_0) / (u_1 - u_0) \quad (3)$$

Wind velocity distribution in vertical was well described by a logarithm formula:

$$u = u_* / \kappa \cdot \ln(z / z_0) \quad (4)$$

Here u_* was the frictional velocity of air, κ the Von Karman constant (0.4). Applying (4) to the height z_1 provided an estimation of frictional velocity,

$$u_* = \kappa u_1 / \ln(z_1 / z_0) \quad (5)$$

The friction stress was expressed as a relationship of frictional velocity,

$$\tau = \rho_a (u_*)^2 \quad (6)$$

In (3) let the u_0 being zero and K_m being equal to K_w, and substitute it for (6), an estimation formula for the rate of interception loss *E* was obtained.

$$E = \kappa^2 \rho_a / \rho_w \cdot u_1 (q_0 - q_1) / \ln(z_1 / z_0) \quad (7)$$

This equation of interception rate had a similar shape as traditional ones. However, here the specific humidity included both water vapour and droplets. The vapour pressure or its humidity component could be measured in field or calculated with empirical formulas, while the droplet pressure or its humidity component were not measured at present and had to be estimated.

Vapour pressure e_v was related to its specific humidity q_v as

$$q_v = 0.622 e_v / p \quad (8)$$

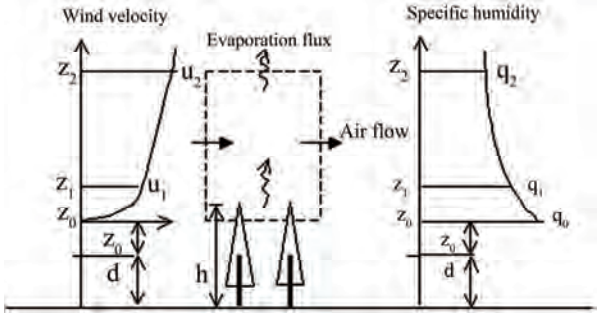

Figure 2. Scheme of evaporation flux and profiles of wind velocity, specific humidity.

where *p* was air pressure. It was assumed that the combined pressure *e* of water vapour and droplets in the air was similarly related to their specific humidity *q*: $q = 0.622e/p$. A new equation of interception rate in terms of pressure was obtained by inserting the $q \sim e$ relation into (7).

$$E = 0.622 \cdot \kappa^2 \rho_a / \rho_w \cdot u_1 (e_0 - e_1) / p / \ln(z_1 / z_0) \quad (9)$$

Since u_1 was known from wind observation, and all other parameters except e_0 and e_1 were known too, (9) was written as

$$E = A u_1 (e_0 - e_1) \quad (10)$$

in which *A* was a constant for a given canopy. For example, for the Sugi tree, $h = 17$ m, $z_0 = 0.07$ h or 1.19 m, $d = 0.78$ h [11] or 13.26 m, $z_1 = 4.94$ m. Other constant parameters in (9) or (10) took values as $p = 1{,}013$ hPa, $\rho_a = 1.19$ kg/m^3, $\rho_w = 997$ kg/m^3. By using the units of *E*, u_1, e_o and e_1 in mm/hr, m/s, and hPa respectively, a value for *A* was determined as 0.20835.

An effort was made to separate pressure *e* into two compartments – the vapour pressure e_v and droplet pressure e_m, so that e_v could be described by existing knowledge and e_m could be estimated in some way. For the height z_0, the separation was expressed as

$$e_0 = e_{0v} + e_{0m} = e_{sat} + e_{0m} = e_{sat} + f_m \cdot e_{sat} \quad (11)$$

$$f_m = e_{0m} / e_{0v} = e_{0m} / e_{sat} \quad (12)$$

where e_{sat} was the saturated vapour pressure and was determined solely by air temperature at the site. It was acceptable that the vapour pressure e_{0v} would be equal to or very close to the saturated vapour pressure, when it was raining and floating droplets existed in and around canopy. In order to estimate the droplet pressure, e_{0m} was supposed to be proportional to e_{0v} as appeared in (12). Whenever the ratio f_m was determined, the droplet pressure and flux could be estimated.

Similarly the separation was used for the height z_1 that was usually a meteorology observation height and close to the top of canopy, resulting in $e_1 = e_{1v} + e_{1m} = e_{1v} + f_m \cdot e_{1v}$. By substituting this e_1 expression and (11) for (10), a calculation formula for vapour and droplet flux was established as:

$$E = A u_1 (e_{sat} - e_{1v}) + f_m A u_1 (e_{sat} - e_{1v}) \quad \text{or}$$

$$E = E_v + E_m = E_v + f_m E_v \quad (13)$$

where E_v and E_m were water vapour flux and droplet flux respectively. The integrated vapour and droplet flux *E* was a sum of vapour flux and droplet flux.

It was difficult to determine the separation ratio f_m for any given time as it varied with time. It was not practical to derive a ratio value by using (13) and observing vapour and droplet pressures for any time in a rainfall process. Therefore, an approximate method of determining the ratio f_m was proposed. A rainfall-interception event or process (with time scale of some hours to a few

days) was divided into many segments timely with each segment being a time unit such as an hour. From the starting hour till a time point in the process, the cumulative interception amount I was the sum of cumulative loss via vapour flux and cumulative loss via droplet flux, *i.e.*,

$$I = S_c + I_v + I_m = S_c + \sum_{i=1}^{n} E_v(i) + \sum_{i=1}^{n} E_m(i) = S_c + \sum_{i=1}^{n} E_v(i) + \sum_{i=1}^{n} f_m E_v(i) \quad (14)$$

where I_v was the interception loss via vapour transfer, I_m was the loss via droplet transfer, S_c was the storage of water held by canopy, and i was the number of time segments. The S_c possessed a small portion in total interception loss when the rainfall was large enough, and could be negligible. For instance if there was a rainfall of 50 mm, the loss would be 10 mm via interception, while the water on canopy was 1 mm.

If the average value of f_m over a time period (from segment 1 to n) was named as f_{ma}, Equation (14) became (15).

$$I = \sum_{i=1}^{n} E_v(i) + f_{ma} \sum_{i=1}^{n} E_v(i) \quad (15)$$

Now the average ratio for the cumulative time period at a time point was estimated by following formula. And that average ratio was an approximate estimation of f_m at a time point during rainfall.

$$f_{ma} = (I - \sum_{i=1}^{n} E_v) / (\sum_{i=1}^{n} E_v) = (I - I_v) / I_v \quad (16)$$

A calculation process for a rainfall event looked like this: starting from the first time segment, getting interception loss and vapour flux during the segment using observed data, obtaining a ratio value for the first segment with (16), obtaining the droplet flux loss with (14); then going to the second segment, getting cumulative interception loss and vapour flux loss for the two segments, obtaining a ratio (average) and a droplet loss; and so on continued until the end of rainfall. The processes of cumulative interception, vapour flux and droplet flux were calculated, and separate vapour flux loss and droplet flux loss for a rain event were thus obtained.

The rainfall events whose rainfall amount was more than 50 mm were considered, because the canopy water storage in (14) could be neglected for these events. Eight such events were chosen from collected data in year 2004. The date of events, duration D, total rainfall amount R, observed interception amount I of the Sugi cypress tree at the Okunoi Experimental Station, mean temperature T for a event, mean wind speed u and mean relative humidity $Rh1$ as observed at height 18 m, and mean humidity $Rh2$ as observed at height 26 m were listed in **Table 1**.

The rain events occurring in May through October had rainfall durations of 14 to 74 hours, rainfall amounts of 56 to 425 mm, interception loss of 7.7 to 51.7 mm, air temperatures of 14.6 to 24.2^{o}C, wind speeds of 0.2 to 1.4 m/s, and relative humidity of 97.6 to 99.7% at the height 18 m which was just on top of canopy. Humidity in the canopy was very high for all events. However, the humidity at height of 26 m was 86.6 to 96.0%, a little bit lower.

Another typical method of estimating evaporative loss from intercepted water was the Penman method as follows,

$$E_P = \frac{\Delta}{\Delta + \gamma} R_n + \frac{\gamma}{\Delta + \gamma} f(u) \cdot (e_{sat} - e_v) \quad (17)$$

where E_P was the Penman's evaporation rate from canopy surface (water vapour flux from captured water), γ the psychrometric constant, equal to 0.66 mbar/^{0}C, Δ the slope of the saturation-vapour-pressure versus temperature curve (mbar/^{0}C), $f(u) = 0.26(1 + 0.537u)$, (mm $\cdot$hr$^{-1}\cdot$mbar^{-1}), u the wind velocity (m/s), e_{sat} and e_v are the saturation and actual values of vapour pressure.

4. Results

4.1. Existence of Droplet Transfer and its Separation from Total Interception

Interception loss of each event (**Figure 3**) was strongly proportional to total rainfall. A traditional aerodynamic method estimating interception took only vapour flux into consideration, *i.e.*, the I_v component in Equation (14). Obviously I_v was much less than observed interception I. In other words, an important interception component, the droplet transfer, did exist in these rain events and could not be ignored. The difference $I - I_v$ was the droplet transfer and had values of 7.1 to 70.0 mm, possessing a percentage of 48 to 98 % in total interception amount.

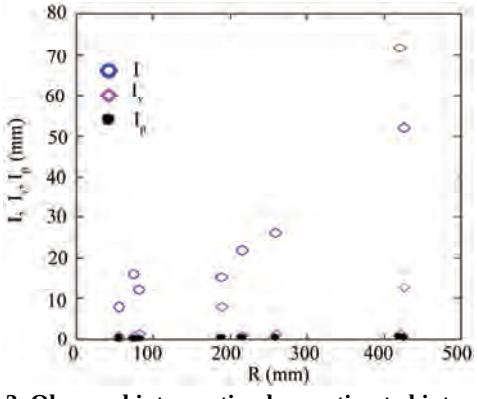

Figure 3. Observed interception loss, estimated interception by aerodynamic method or Penman method, corresponding to total rainfall of eight events.

Table 1. Interceptions of Sugi tree and meteorological conditions of rain events (2004).

No	Month	Day	D (hr)	R (mm)	I (mm)	T (^{0}C)	u (m/s)	Rh1 (%)	Rh2 (%)
1	5	19	38	56.0	7.7	14.6	0.2	98.8	97.0
2	6	11	14	83.0	12.0	19.2	0.5	99.4	95.5
3	7	30	74	425.0	51.7	22.6	0.7	97.6	93.4
4	8	17	15	75.5	16.0	24.2	0.4	98.5	95.6
5	8	29	27	189.5	15.2	24.1	1.4	98.1	86.6
6	9	6	36	259.5	26.0	22.8	0.6	99.7	94.9
7	9	28	28	215.5	21.7	20.7	0.5	99.7	96.0
8	10	19	43	420.5	71.6	16.3	0.5	99.7	95.6

Estimated interception I_P with the Penman equation was compared with observed I in the figure. I_P was too less than I to give a reasonable estimation. The underestimation of aerodynamic method (I_v) or Penman method (I_P) against observed interception loss was explained like this: during the hours or days of rainfall events, water vapour in and around canopy was saturated or near saturation, and vapour diffusion could hardly proceed to transfer the moisture which was lost via interception process; the low level of net radiation was not able to vapourize water on wet canopy and maintain the interception rate, and vapour transfer did not contribute much to interception. On the other hand, the floating droplets created by raindrop crushing provided water source for interception loss, and this part of water transfer became the major part in interception for these events.

The average ratio f_{ma} of droplet pressure to vapour pressure for an event, or the average ratio of total droplet transfer to vapour transfer in the event, was calculated with (16). The ratio varied between 0.9 and 58.2 (**Figure 4**) among the eight events depending on individual condition of each event. It did not imply that a bigger rainfall gave a bigger ratio value.

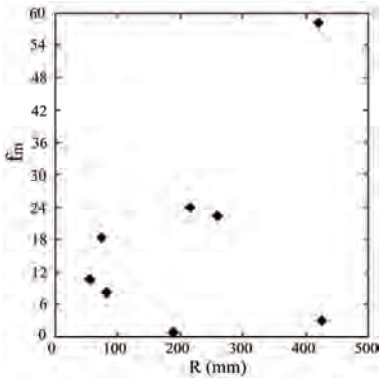

Figure 4. Average separation ratio and total rainfall.

4.2. Detailed Processes in Two Different Events and their Comparison

In the above section, total interception losses of eight rainfall events were displayed and explained. Hourly process of interception in an event was discussed by using two events that have different meteorological conditions and interception features, and their difference was explained. There were two events with extraordinary heavy rainfall: one occurred on July 30-31-August 1, the other occurred on October 19-20-21. Name them as Event A and B. Both A and B had rainfall over 400 mm, but A had higher temperature, greater wind speed, smaller humidity, smaller rain intensity, longer rain duration, and less interception loss, compared to B. The meteorological condition and hourly interception rate were displayed in **Figure 5**.

Among the meteorological factors, rainfall intensity played the most important role in shaping interception rates. Although the higher temperature, lower humidity and larger wind speed condition in Event A would have caused more interception than Event B would do, the weaker rain intensity of A determined that its total interception loss was 51.7 mm, less than the total loss 71.6 mm of B which had stronger intensity, even A has a longer duration (74 hours versus 43 hours). The interception amount which happened around the peak rainfall rate was keen in determining the total loss. A clear proportional relationship between interception rate and rain intensity was seen in **Figure 6**, especially for Event B.

Interception process or the changes with time was described in terms of cumulative features. Cumulative interception $\sum i$ (*i.e.*, accumulated interception by the 10th hour was $i1 + i2 + \ldots\ldots + i10$), and cumulative rainfall amount $\sum r$, were displayed in **Figure 7** for Event A and B, starting from the first hour and ending at the last hour. Cumulative vapour transfer $\sum i_v$ estimated with aerodynamic Equation (10) and cumulative interception estimation $\sum i_p$ estimated with Penman equation were also showed in the figure. For Event A, vapour component $\sum i_v$ dominated the cumulative interception for the initial hours, and then lose its domination, and the droplet component ($\sum i - \sum i_v$) dominated the cumulative interception. Estimation by Penman method $\sum i_p$ was almost zero.

For Event B, cumulative vapour transfer did not appear, and the entire interception process was controlled

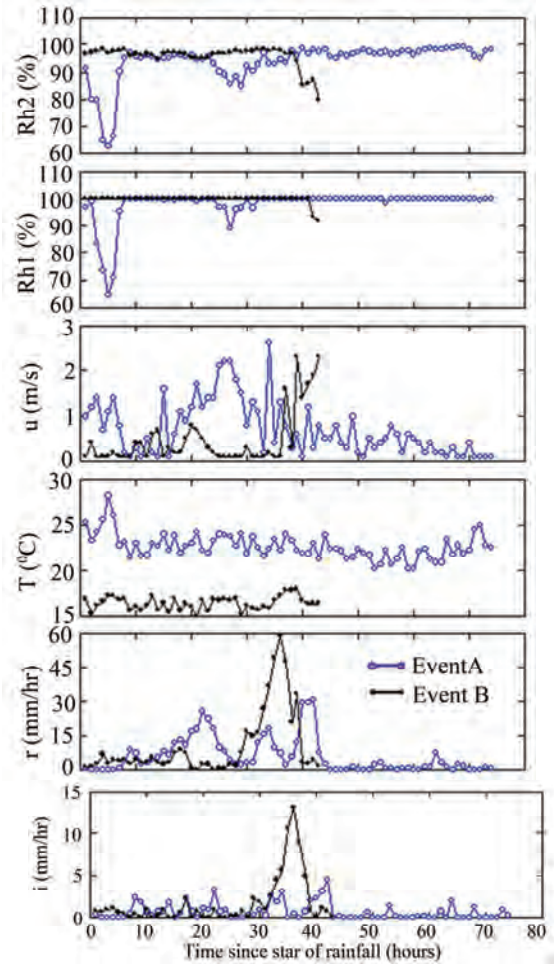

Figure 5. Meteorological conditions and interception rates for Events A and B (*r* – rainfall intensity, *T* – temperature, *u* – wind speed, *Rh1* – relative humidity at height 1, *Ph2* – relative humidity at height 2, *i* – interception rate as observed).

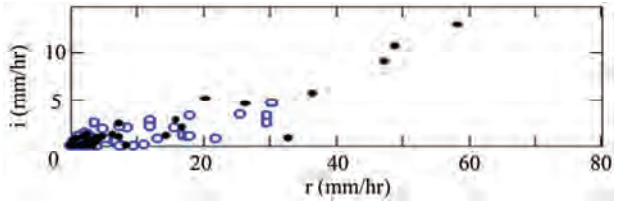

Figure 6. Relationship of interception rate *i* and rainfall intensity *r* (circles for Event A, solid dots for Event B).

by droplet transfer component.

The ratio of cumulative droplet transfer ($\sum i$ - $\sum i_v$) to cumulative vapour transfer $\sum i_v$ was named as f_{mc}, and showed in **Figure 8**. For Event A, it fluctuated at first, and then increased with cumulative rainfall (or with time) and reached over 3. This meant that droplet component possessed more and more contribution in the cumulative interception. The ratio for Event B was not seen in the

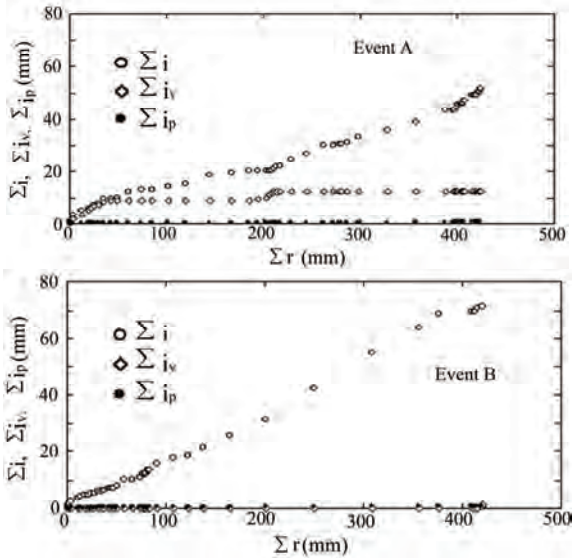

Figure 7. Cumulative interception during Event A or B, respectively from observation, aerodynamic method and Penman method.

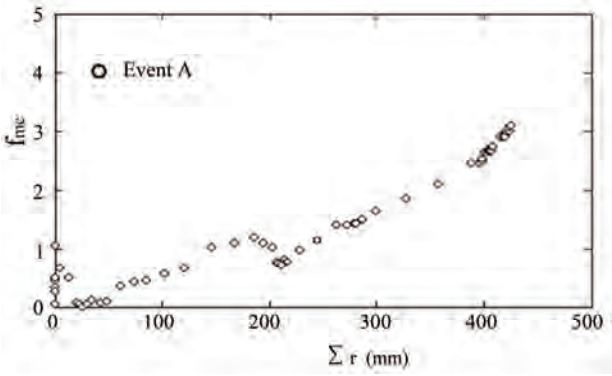

Figure 8. Ratio of droplet flux to vapour component.

figure as the value was too big – the cumulative vapour component was close to zero.

To explain the importance of droplet transfer component more clearly, a ratio of cumulative droplet transfer ($\sum i$ - $\sum i_v$) to cumulative interception $\sum i$ was plotted in **Figure 9**. For Event A the ratio changed between 0.0 and 0.8 and increased with cumulative rainfall. Droplet component possessed more than 50% in most of the duration. For Event B, the ratio did not change and took the highest value 1.0, or there was only droplet component in the interception for that case.

5. Discussion

The behavior and relative importance of the two components vary with climate condition, rainfall type and size, canopy structure and so on. It is reasonable that vapour

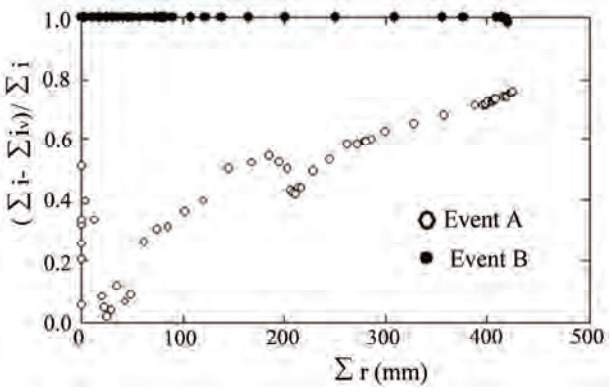

Figure 9. Ratio of droplet flux component to cumulative interception.

transfer is the main part of interception loss in areas of temperate/cold regions where there are often drizzle rains – they do not show a good chance to produce droplets, and the canopy is easily wetted. The droplet transfer component may be the main part of interception in other areas such as tropical rainforests or humid islands where there are more storms with heavy rainfall and larger raindrops.

Droplet transfer, advected heat/energy provision from nearby environment, and upward wind may together contribute to the reported and questioned high interception rates, or some of the three mechanisms contribute more substantially. For example, to take droplet transfer into consideration would help to explain the questions and contradictions indicated by Dykes, Schellekens *et al.*, Zimmermann *et al*., Hashino *et al.*, Murakami, and Vernimmen *et al*.

Hall's investigation [12] at tropical tree canopies showed that predicted interception loss was relatively insensitive to raindrop size, while some others' results indicated the sensitivity. The interception calculation he used was based on a mechanism of canopy wetting, and therefore raindrop size was not as important as canopy characteristics in determining the loss. If we also think of the existence of micro-droplets and their contribution to interception loss, the size of raindrops may need to be considered, because the volume of micro-droplets are related to raindrops.

Toba and Ohta [13] compared two Siberian forest sites and five Japanese forest sites with regards to interception loss. At the Siberian sites, net radiation was always larger than latent heat flux consumed by interception, therefore the energy supply met the interception evaporation usage. The Japanese sites often showed opposite pattern: latent heat flux exceeded net radiation and gave high interception rates. They noted that air temperature at upper levels were higher than that at lower levels, and thought that the sensible heat flux was directed downward to support the evaporation from wet canopies. We would like to say that micro-droplets are another reason for the exceedance of interception rate over net radiation. In the temperate and humid Japanese sites, heavy and frequent rains produce micro-droplets that are not negligible for interception loss, while in the cold Siberian sites, micro-droplet transfer is not so important.

6. Conclusions

The aerodynamic diffusion and transfer of both vapour and micro-droplets from canopy zone to upper air were described and calculated in a new perspective, and proposed formulas were applied to eight rainfall events at the Okunoi Experimental Station. Contributions from droplet transfer were 0.9-58.2 times of contributions from vapour transfer, taking a majority portion in total interception loss of the rain events. Taking only the vapour transfer or evaporation loss estimated by Penman equation was not able to account for the actual interception loss at some tropical forests and maritime areas, because the important portion as droplet flux were ignored.

Micro-droplets flux component took major portion in the two heavily rained events, and even completely made up the interception as happened in October 2004. It was an important finding that droplet flux could accommodate a high interception rate, even when the air was nearly vapour-saturated and vapour flux was zero. This proposed approach was tried to answer the difficult question on significantly high interception rates.

The separation ratio f_m or f_{mc} was estimated using observed interception data in our study. An effective method to determine the ratio and then to derive interception process without using the observed data has not been established because of limited information and research source. Detailed experiments on droplets size, their pressure or liquid water content, and droplets flux have not been conducted at our study site. This problem or challenge should be targeted in future studies.

7. References

[1] V. T. Chow, D. R. Maidment and L. W. Mays, "Applied Hydrology," McGraw-Hill Book Company, New York, 1988.

[2] R. Burkard, W. Eugster, T. Wrzesinsky and O. Klemm, "Vertical Divergence of Fogwater Fluxes above a Spruce Forest," *Atmospheric Research*, Vol. 64, No. 1, 2002, pp. 133-145.

[3] G. M. Lovett, "Rates and Mechanisms of Cloud Water Deposition to a Subalpine Balsam Fir Forest," *Atmospheric Environment*, Vol. 18, No. 9, 1984, pp. 361-371.

[4] A. P. Dykes, "Rainfall Interception from a Lowland

Tropical Rainforest in Brunei," *Journal of Hydrology*, Vol. 200, No. 1, 1997, pp. 260-279.

[5] J. Schellekens, F. N. Scatena, L. A. Bruijnzeel and A. J. Wickel, "Modelling Rainfall Interception by a Lowland Tropical Rain Forest in Northeastern Puerto Rico," *Journal of Hydrology*, Vol. 225, No. 3, 1999, pp. 168-184.

[6] L. Zimmermann, C. Fruhauf and C. Bernhofer, "The Role of Interception in the Water Budget of Spruce Stands in the Eastern Ore Mountains/Germany," *Physics and Chemistry of the Earth* (*B*), Vol. 24, No. 7, 1999, pp. 809-812.

[7] M. Hashino, H. Yao and H. Yoshida, "Studies and Evaluations on Interception Processes during Rainfall Based on a Tank Model," *Journal of Hydrology*, Vol. 255, No. 1, 2002, pp. 1-11.

[8] S. Murakami, "A Proposal for a New Forest Canopy Interception Mechanism: Splash Droplet Evaporation," *Journal of Hydrology*, Vol. 319, No. 1-4, 2005, pp. 72-82.

[9] R. R. E. Vernimmen, L. A. Bruijnzeel, A. Romdoni and J. Proctor, "Rainfall Interception in Three Contrasting Lowland Rain Forest Types in Central Kalimantan, Indonesia," *Journal of Hydrology*, Vol. 340, No. 3-4, 2007, pp. 217-232.

[10] M. Chang, "Forest Hydrology: An Introduction to Water and Forests," CRC Press LLC, Boca Raton, 2006.

[11] Y. Tsukamoto, "Forest Hydrology (in Japanese)," Buneido Press, Tokyo, 1992.

[12] R. Hall, "Interception Loss as a Function of Rainfall and Forest Types: Stochastic Modelling for Tropical Canopies Revisited," *Journal of Hydrology*, Vol. 280, No. 1-4, 2003, pp. 1-12.

[13] T. Toba and T. Ohta, "An Observational Study of the Factors that Influence Interception Loss in Boreal and Temperate Forests," *Journal of Hydrology*, Vol. 313, No. 3-4, 2005, pp. 208-220.

J. Water Resource and Protection, **2010, 2, 880-887**
doi:10.4236/jwarp.2010.210105 Published Online October 2010 (http://www.SciRP.org/journal/jwarp)

Development of Flood Forecasting System Using Statistical and ANN Techniques in the Downstream Catchment of Mahanadi Basin, India

Anil Kumar Kar[1], Anil Kumar Lohani[2], Narendra Kumar Goel[1], Gopal Prasad Roy[3]
[1]*Department of Hydrology, Indian Institute of Technology, Roorkee, India*
[2]*National Institute of Hydrology, Roorkee, India*
[3]*Department of Water Resources, Government of Orissa, Bhubaneswar, India*
E-mail: *aklnih@gmail.com, lohani@nih.ernet.in*
Received May 6, 2010; *revised July* 27, 2010; *accepted August* 12, 2010

Abstract

The floods in river Mahanadi delta are due to either dam release of Hirakud or due to contribution of intercepted catchment between Hirakud dam and delta. It is seen from post-Hirakud periods (1958) that out of 19 floods 14 are due to intercepted catchment contribution. The existing flood forecasting systems are mostly for upstream catchment, forecasting the inflow to reservoir, whereas the downstream catchment is devoid of a sound flood forecasting system. Therefore, in this study an attempt has been made to develop a workable forecasting system for downstream catchment. Instead of taking the flow time series concurrent flood peaks of 12 years of base and forecasting stations with its corresponding travel time are considered for analysis. Both statistical method and ANN based approach are considered for finding the peak to reach at delta head with its corresponding travel time. The travel time has been finalized adopting clustering techniques, there by differentiating high, medium and low peaks. The method is simple and it does not take into consideration the rainfall and other factors in the intercepted catchment. A comparison between both methods are tested and it is found that the ANN methods are better beyond the calibration range over statistical method and the efficiency of either methods reduces as the prediction reach is extended. However, it is able to give the peak discharge at delta head before 24 hour to 37 hour for high to low peaks.

Keywords: Flood Forecasting, Mahanadi Basin, Hirakud Dam, Statistical Method, ANN Architecture, Clustering

1. Introduction

Flood is a regular phenomenon in the delta of Mahanadi basin. The discharge of the intercepted catchment of below Hirakud dam has contributed largely to the flood at delta. The delta is highly fertile and thickly populated with population density 400-450 persons per sq.km. The drainage capacity of deltaic rivers is 25500 m^3/s only. Any discharge above this can create a flood like situation.

Establishment of a workable flood forecasting method for the downstream catchment of Mahanadi basin is always under scanner. A lot of hydro-meteorological information is needed for establishment of a model. The dam at upstream is operated by a rule curve. The intercepted catchment is very big around 40000 sq.km. In order to establish a Rainfall-Runoff model, rainfall data of all station is highly essential. For further strengthening of model evaporation, soil moisture, temperature, dam release etc. are needed. Sometimes all information is not available on real time basis making it difficult for establishment of a physical based model. In that case statistical methods are more useful.

The statistical methods are generally graphical or in the form of mathematical relationship, developed with the help of historical data, using statistical analysis. These include simple gauge to gauge relationships, gauge to gauge relationship with additional parameters and rainfall-peak stage relationship. These relationships can be easily developed and are most commonly used in India as well as other countries of the world [1]. Spok-

kerreff [2] has mentioned about application of statistical model till 1995 on river Rhine.

Consequently, there is need for models capable of efficiently forecasting water levels and discharge rates. In this regard application of ANN is more effective. Earlier the works of Bruen and Yang [3], Campolo *et al.* [4,5], Coulibaly *et al*. [6], Dawson and Wilby [7], Imrie *et al.* [8], Lekkas *et al.* [9], Lohani [10], Minns and Hall [11], Muhamad and Hassan [12], Mukerji *et al.* [13], Solomantine and Xue [14], Solomantine and Price [15], Zealand *et al.* [16] emphasized the application of artificial neural networks over other methods. In flood forecasting both the peak and travel time has equal significance. The travel time is also of great importance in prediction of the stage. It varies with stages and channel condition. Travel time generally reduces when water approaches the top of the bank. As the river overflows flooding over the flood plain the travel time may begin to increase again due to the relatively rough surfaces lying in the overbank stages. In order to give justification for different types of peaks with respect to travel time clustering method is adopted in this study. Earlier, Zhang and Hall [17] have applied clustering methods in regional flood frequency analysis and Xiongrui *et al.* [18] in establishing rainfall-runoff relationships. In view of the above an attempt has been made in this study to apply both statistical method and ANN based approach for forecasting the peak discharge and travel time in the downstream reach of the Mahanadi River.

2. Study Area

The Mahanadi basin lies between 80^0-30` to $86^0$-50` of East Longitude and 19^0-20` to $23^0$-35` of North Latitude. The river Mahanadi is an interstate river. The catchment area of the basin is 141569 sq. km. The major part of this catchment lies in Chhatisgarh (75136 sq. km.) (**Figure 1**). As this part is the upstream part, 143 channels in this zone generally feeds the Hirakud reservoir having a catchment of 83400 sq.km. The downstream catchment has three main tributaries like Jeera, Ong and Tel with catchments 2383, 5128 and 25045 sq.km. respectively. So the contributions from the Tel catchment always remain predominant. Even the flood of 2008 is mainly due to the contribution of this tributary. It has produced a peak discharge of 33762 cumecs during 2008. So establishment of a flood forecasting model below the joining of these tributaries reduces the ambiguity. The river Tel joins at Patharla to the main river Mahanadi and our base station Khairmal is at downstream of Patharla station. The other tributaries Ong and Jeera join also at the upstream of base station (Khairmal). The whole river from Khairmal is taken as one unit ignoring the contribution of further small tributaries. A schematic presentation shows the distance and travel time from Hirakud to Mundali presently being used for the official purposes of Department of Water Resources, Government of Orissa [19].

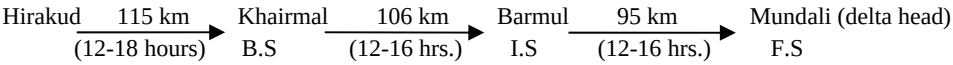

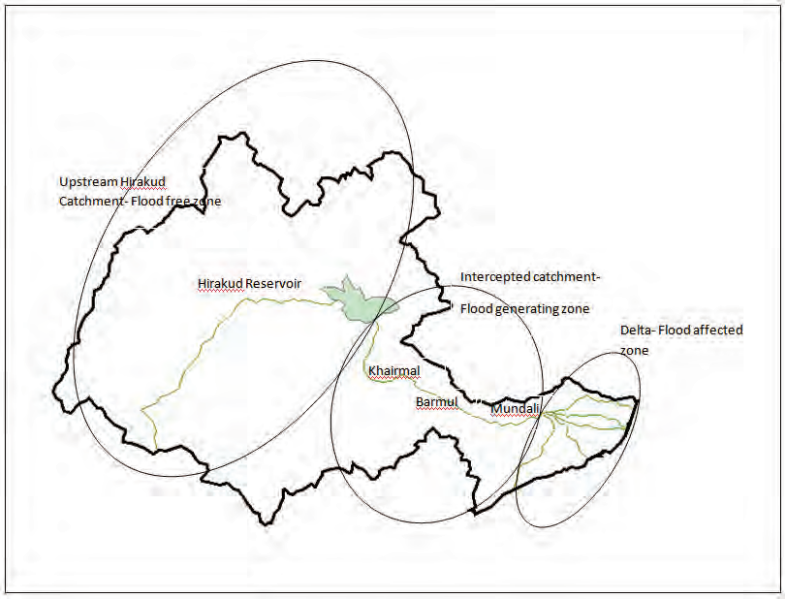

Figure 1. Showing catchment details with different zones of Mahanadi basin.

In our study the station at Khairmal is taken as the base station (B.S) which is 115 km away and with an average lead time of 12-16 hour for Hirakud release to reach here. Barmul is the intermediate station (I.S) and Mundali is the forecasting station (F.S) just upstream of Cuttack city.

3. Data Availability

Adequate data is needed for the formulation of the forecasting services. The development of the river forecasting procedure requires historical hydrological data and for the preparation of operational forecasts sufficient current information is required. Discharge data of (3 hourly) is available at base, intermediate and forecasting station for a period of 1996-2007. Discharge of 2830 cumecs and above at forecasting stations are considered as peaks and its corresponding peaks at intermediate and base station are collected with their related travel times after drawing the corresponding time series. Out of this 80 peaks are considered for our analysis, taking 60 peaks for calibration and 20 peaks for testing of models. Generally, it can be said that it is necessary to have a minimum of 10 years of basic hydraulic data, available to develop adequate river forecasting procedures, the primary requirement being that the period of record should contain a representative range of peak flows [20].

4. Methodology

The selection of an appropriate flood forecasting model depends on the availability of the data, output desired etc. On the basis of the analytical approach for the development of flood forecasting method can be classified as:

1) Methods based on statistical approach.

2) Methods based on mechanism of formation and propagation of floods.

4.1. Statistical Approach

Finding correlation between stage and discharges between upstream and downstream gauging stations is one of the simplest methods. This gives better result when there is less influence of tributaries joining the main stream in between or the intercepted catchment is not influenced by heavy rainfall.

4.2. ANN Approach

There are many ANN architectures and algorithms developed. Out of them most common are Multi layer feed forward, Hoppfield networks, Radial basis function network, Recurrent network, Self organization feature maps, Counter propagation networks. Selection of a particular network is application oriented. However, the multi layer feed forward networks are most commonly used for hydrological applications [7].

Generally four distinct steps applied to any ANN – based solution including flood forecasting problems. First of all data transformation is the initial step. The input always varies in a larger range. So in order to lessen the range the data is put in logarithmic scale. Then normalization and scaling is done. Data sets with many variations make training difficult. In order to prevent it the data are usually scaled using statistical, min-max, sigmoidal or principal component transformations [21]. Also the absolute input values are scaled to avoid asymptotic issues [22].

The second step is the fixing the network architecture in which for a particular problem the number of hidden layers, neurons in each layer and the connectivity between neurons are set. Many experimental results say that one hidden layer may be enough for most forecasting problems [6,17]. The studies of Cybenko [23], Hornik *et al*. [24] revealed that a single hidden layer is sufficient for ANNs to approximate any non-linear transfer function. The number of neurons in each layer depends upon the problem being studied. Less number of neurons in hidden layer will make the network with less degree of freedom for learning and more number of neurons will lead towards more time and over fitting [25]. Validation set error is often used to determine the optimal number of hidden neurons for a given study.

In the third step is the finalization of a learning algorithm for training the network. The parameters are finalized for the training data set to be applicable for any kind of testing data. ANN architecture is considered to be trained when the difference between ANN output and observed output is very small.

Finally the validation step is applied to get the performance of the network. The optimal number of hidden neurons and training iterations can also be determined through validation. The selection of acceptable model is finalized on the basis of RMSE, R^2 and efficiency.

4.3. Clustering Approach

As the data set varies in a wide range, it requires some distinction and in particular when different peaks are available for the same travel time. In order to make proper justice for different peaks with respective travel time, it requires clustering. Both *K*-mean and Fuzzy C-mean clustering methods are attempted.

4.3.1. K-Mean

This method was developed by MacQueen [26]. It is best described as a partitioning method. It partitions the data into *K* mutually exclusive clusters and returns a vector of

indices indicating to which of the *K*-clusters it has assigned each observation. The algorithm to clusters *N* objects based on attributes into *K* partitions where $K < N$. The optimization function

$$V = \sum_{i=1}^{k} \sum_{x_j \in S_i} \left(x_j - \mu_i \right)^2 \quad (1)$$

It tries to achieve minimum intra cluster variance or the squared error function. Where there are *K* clusters $S_i = 1,2\ldots\ldots K$, and V_i is the centroid or mean point of all the points $X_j \in S_i$. [27].

4.3.2. Fuzzy C-Mean (FC)

In this method the affinity of a site to undergo either two or more clusters are visualized. Earlier developed by Dunn [28] and improved by Bezdeck [29] is basically used for pattern recognition. Here the data are bound to each cluster by means of a membership function which represents the Fuzzy behavior of this algorithm. It shows how to group data points that populate some multidimensional space into a specific number of different clusters. The objective function

$$Jm = \sum_{i=1}^{N} \sum_{j=1}^{C} u_{ij}^{m} \left\| x_i - c_j \right\|^2, \quad 1 \le m \le \infty \quad (2)$$

$m =$ any real number, u_{ij} = degree of membership of x_i in cluster j, x_i = *ith* of *d*-dimensional measured data, c_j = *d*-dimension center of cluster.

Similarly, different ANN architectures are attempted over the discharge and corresponding travel times. The calibration and validation data sets remain same for both the methodology. The same methodology is also adopted for finding the travel time. But in order to further distinguish *K*-mean and Fuzzy C mean clustering methods are adopted to find a better answer for travel time of different peaks.

5. Results and Discussion

First of all statistical approach is applied into calibration dataset (60 nos.). The relationships between the discharges between Khairmal-Barmul, Barmul-Mundali, Khairmal-Mundali and Khairmal-Barmul-Mundali are developed. These relationships are put on the testing data sets (20 nos.) and the results are recorded in **Table 1**.

Where, Q_M = discharge at Mundali (Forecasting Station), Q_B = discharge at Barmul (Intermediate Station) and Q_K = discharge at Khairmal (Base Station).

The same dataset is again put into ANN architecture using MATLAB codes. The trial has been taken with a 3-layer feed forward network. Different combinations of feed forward network with changing transfer function, number of neurons and epochs varying at an increment of 50 are trailed. The combinations which are mostly as per performance criteria fixed are noted. The Cascade feed forward network has been most successful for Khairmal-Barmul and Khairmal-Barmul-Mundali and other two cases are with Feed forward network. Numbers of neurons in input and output layers are mentioned in column (2) of **Table 2**. In all cases 'tansig' neurons are used in first layer, 'purelin' in second layer and 'trainbr' remains the training function. Both 'tansig' and 'purelin' are better compatible with feed forward networks. Again the two layer sigmoid/linear network can represent any

Table 1. Relationship between discharges using simple statistical method (peak to peak).

Between stations	Equation	RMSE(m^3/s)		R^2		Efficiency	
		Training	Testing	Training	Testing	Training	Testing
Khairmal-Barmul	$Q_B = 1.122*Q_K - 289.4$	2382.62	1287.4	0.94	0.974	0.952	0.9678
Barmul-Mundali	$Q_M = 1.009*Q_B + 678.17$	1740.26	1275.16	0.968	0.989	0.948	0.9735
Khairmal-Mundali	$Q_M = 1.144Q_K + 225.04$	2623.76	1769	0.929	0.9826	0.929	0.9490
Khairmal-Barmul-Mundali	$Q_M = 0.84197Q_B + 0.1996Q_K + 468.72$	1705.85	1272.12	0.970	0.990	0.934	0.9736

Table 2. Relationship between discharges using ANN architecture.

Between stations	ANN architecture	Epochs	RMSE(m^3/s)		R^2		Efficiency	
			Training	Testing	Training	Testing	Training	Testing
(1)	(2)	(3)	(4)	(5)	(6)	(7)	(8)	(9)
Khairmal-Barmul	CFF 1,7,1	3000	2249.1	1132.2	0.9720	0.9891	0.9446	0.9752
Barmul-Mundali	FF 1,7,1	3000	1681.5	1251.9	0.9852	0.9962	0.9705	0.9745
Khairmal-Mundali	FF 1,5,1	2000	2441.5	1741.7	0.9684	0.9789	0.9375	0.9506
Khairmal-Barmul-Mundali	CFF 2,15,1	4000	1697	1324.1	0.9850	0.9922	0.9700	0.9714

functional relationship between inputs and outputs if the sigmoid layer has enough neurons [30]. The 'trainbr' function updates the weight and bias values as per Levenberg-Marquardt optimization. It minimizes the combination of squared errors and weights and then determines the correct combination so as to produce a network that generalizes well as per Bayesian regularization process. It reduces the difficulty of determining the optimum network architecture also over fitting of training dataset is prevented, whereas in other networks generalization and early stopping is required for reducing over fitting. The performance functions are set as RMSE, R^2 and efficiency. The details of the network applied for different combinations are shown in **Table 2**.

The plots of the statistical method and ANN network over the testing value of 20 numbers of observation as obtained from MATLAB is also produced in **Figures 2(a)** to **(d)** respectively.

For travel time the corresponding discharge and travel times between the stations are trailed with the same calibration and testing data range applying both Statistical (**Table 3**) and ANN architectures (**Table 4**). The ANN is also applied in the same way with many numbers of trials.

It has been revealed that none of the case has a good efficiency, RMSE and R^2. All the relations are ended with a poor correlation. The lack of correlation does not imply lack of association. Because 'r' measures only linear association, a strict curvilinear relationship would not necessarily be reflected in a high 'r' value. Conversely, correlation between two variables does not guarantee that they are causatively connected [31].

However, to have a better answer for efficiency and RMSE values clustering methods are adopted for the discharge value at base station and its corresponding travel time for the calibration dataset. At least 4 clusters are attempted applying K-mean and Fuzzy c-mean method using the same MATLAB code. The datasets are divided into 4 clusters and their varying ranges are recorded. For each range the average travel time has been calculated. In both methods low peak (2660-8256 m^3/s) has large travel time (37.77 hours) to reach at delta head where as high peaks has taken nearly 25 hours to reach at delta head. As each peak is categorized the respective travel time for different discharge values are fixed. However when the result is put over the test dataset K-mean clustering has given 80% efficiency with RMSE value of 2.5 hour (**Table 5**). One value of testing dataset has been removed because it seems that it has some re cording errors. So travel time test series has been carried out with 19 numbers of data.

A plot (**Figure 3**) has been drawn with observed test-

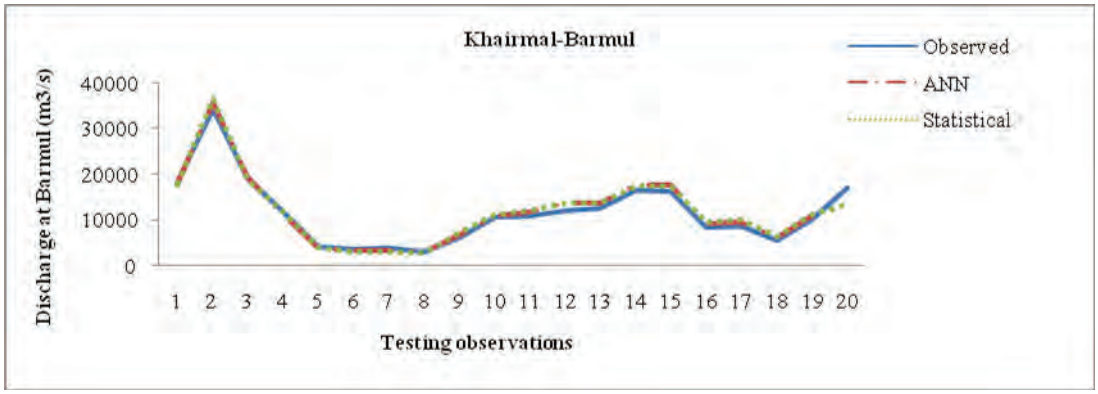

(a)

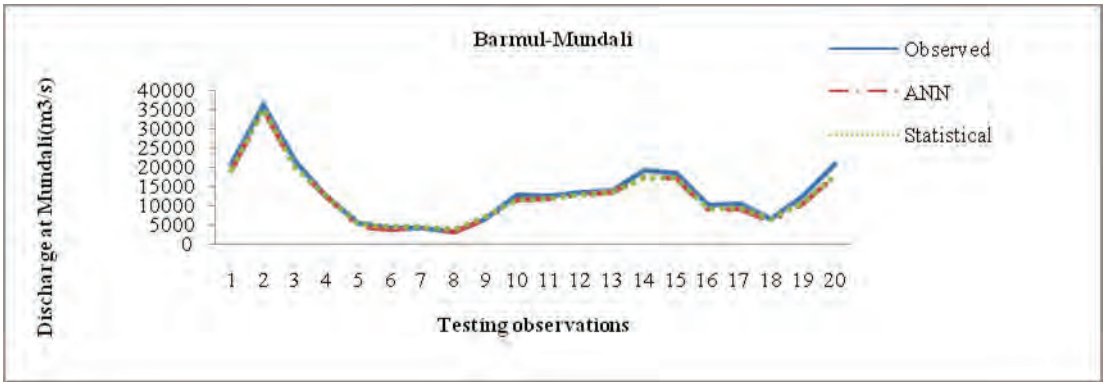

(b)

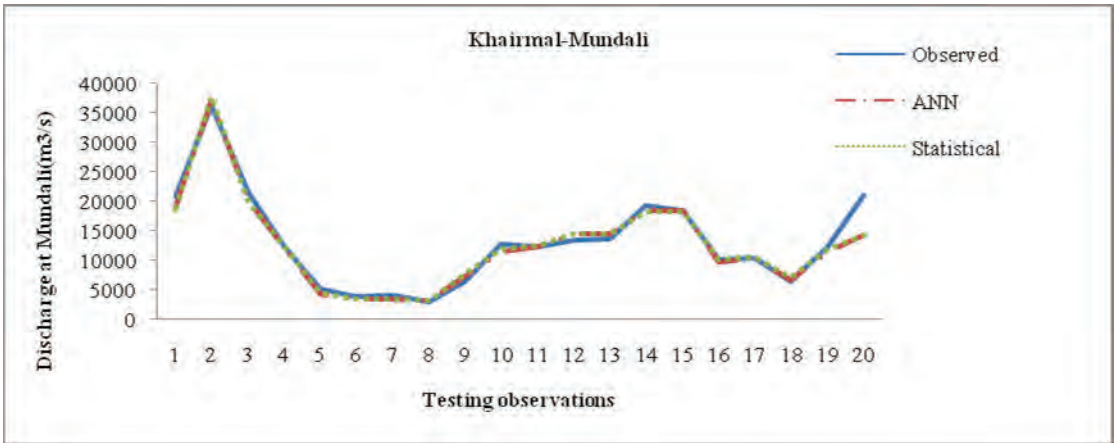

(c)

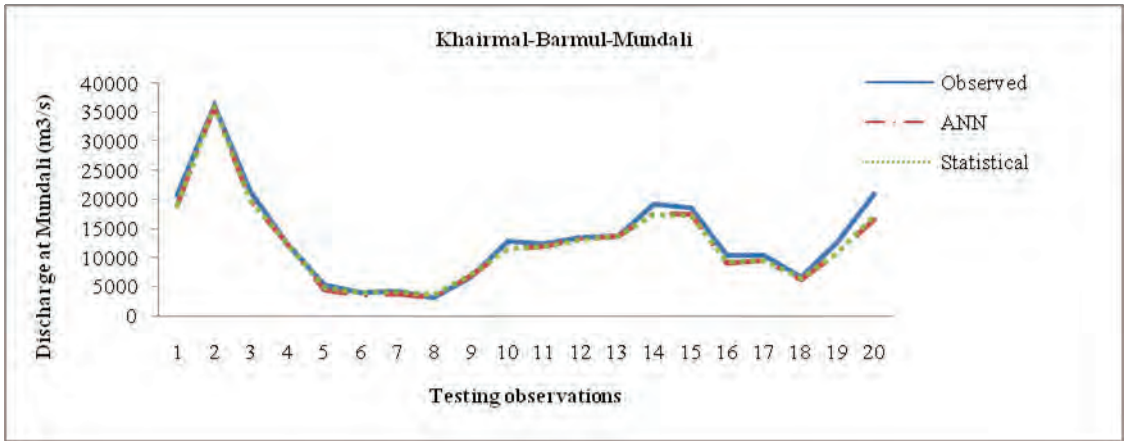

(d)

Figure 2. (a) Comparison between observed and computed discharge (Khairmal-Barmul); (b) Comparison between observed and computed discharge (Barmul-Mundali); (c) Comparison between observed and computed discharge (Khairmal-Mundali); (d) Comparison between observed and computed discharge (Khairmal-Barmul-Mundali).

Table 3. Relationship between discharges and travel time using simple statistical method.

Between stations	Equation	RMSE(hours)		R^2		Efficiency	
		Training	Testing	Training	Testing	Training	Testing
Khairmal-Barmul	$T_B = 270.7*(Q_K)^{-0.32}$	3.42	2.93	0.409	0.261	0.465	0.2973
Barmul-Mundali	$T_M = 64.96*(Q_B)^{-0.15}$	4.34	2.14	0.134	0.607	0.1366	0.507
Khairmal-Mundali	$T_M = 239.1*(Q_K)^{-0.22}$	5.67	3.95	0.394	0.568	0.4191	0.508

where, T_M = time (hour) to peak at Mundali, T_B = time (hour) to peak at Barmul.

Table 4. Relationship between discharges and travel time using ANN.

Between stations	Equation	RMSE (hours)		R^2		Efficiency	
		Training	Testing	Training	Testing	Training	Testing
Khairmal- Barmul	CFF,15,1 (2000)	3.449	2.998	0.6826	0.6259	0.4546	0.2634
Barmul- Mundali	CFF,10,1 (3000)	4.350	2.173	0.3933	0.7961	0.1352	0.4906
Khairmal-Mundali	FF,15,1 (2000)	5.683	3.043	0.6506	0.8306	0.4170	0.6965

Table 5. Peak values with corresponding travel time obtained by using different clusteringmethods

K-mean				Fuzzy-C-Mean			
Discharge range (m^3/s)	Travel time (hours)	Testing RMSE (hours)	Testing Efficiency	Discharge range (m^3/s)	Travel time (hours)	Testing RMSE (hours)	Testing Efficiency
2660-8256	37.77			2660-8256	37.77		
10329-15508	30.53			10329-6300	30		
16102-22810	26.06	2.52	0.8011	16499-5470	27.07	4.27	0.4003
25470-36300	25			28102-6300	25.2		

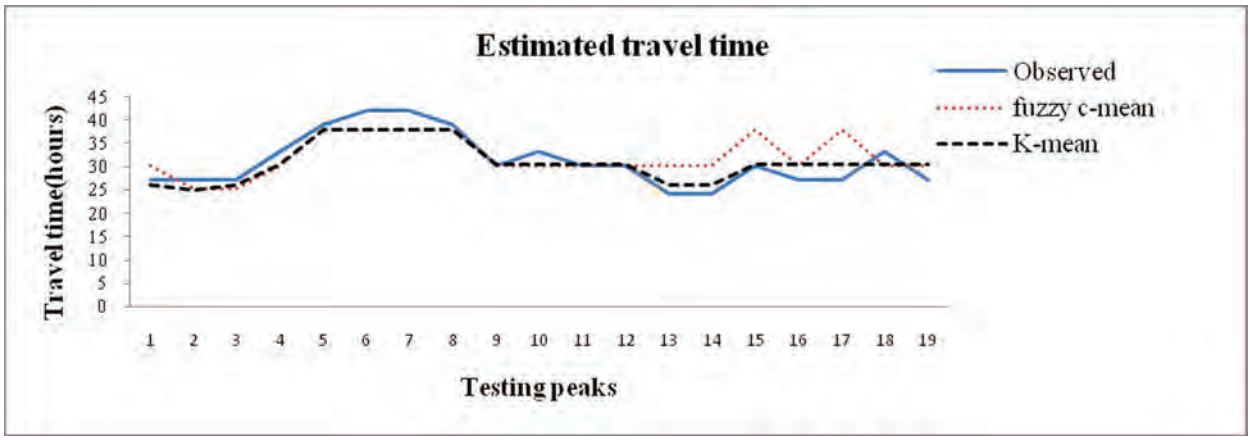

Figure 3. Plot between testing travel time and estimated by different clustering methods.

ing values and validation result of different clustering values. The plot shows the result of K-mean clustering is almost close with that of observed, whereas result of Fuzzy C mean for some low peak values. For high peaks both K-mean and Fuzzy have same results. As K-mean has able to model both high and low peaks with an efficiency of 80.1%,which is higher than Fuzzy C-mean methods, the discharge range values and its corresponding travel time fixed by this method may be taken as the forecast travel time between base station and forecasted station. The travel time has not calculated for other intermediate stations as our concentration is with the peak at base station and travel time of at least 24 hour.

6. Conclusions

Both statistical and ANN methods are applied for downstream Hirakud catchment between stations Khairmal, Barmul and Mundali. The forecasting obtained by both the methods is encouraging. Although the ANN method has a better performance, the existence of statistical method cannot be denied as far as discharge measurement is considered. However, the adoption of clustering method in order to find travel time with respect to different peaks is another finding. The best result for travel time is for Khairmal-Mundali reach (efficiency = 80.11% and RMSE = 2.55 hour). As the data recording is of 3 hour interval this kind of result is still encouraging. The travel time between base and forecasting stations varies between 24-37 hour. By applying clustering method justice has been made for different magnitude of peaks. The results are handy to operate. The moment one gets the discharge at Khairmal (Base Station), he can immediately calculate the discharge to be obtained at Mundali (Forecasting Station) with its corresponding travel time. The result at Mundali (Forecasting Station) with respect to Khairmal (Base Station) basing on the ANN network is best for taking the flood forecasting effectively because in taking Khairmal-Barmul and Barmul-Mundali efficiency is above 97% and RMSE value is 500 m^3/s less than Khairmal-Mundali but lead time of only 12 hours remains after Barmul. So considering the factor of higher lead time for more relief measures we are making a tradeoff with efficiency. Thus calculating peak discharge and travel time at Mundali on the basis of Khairmal discharge and time of occurrence will be a best workable method for practicing hydrologists and field engineers. Still the results are running with the limitation of data insufficiency, large recording intervals, non-consideration of influence of other climatic variation.

7. References

[1] Central Water Commission of India, "Manual on Flood Forecasting," 1980.

[2] E. Spokkereff, "Flood Forecasting for the River Rhine in the Netherlands," *Proceeding of the Symposium the Extreme of Extremes*: *Extraordinary Floods*, Reykjavic, Ireland, July 2000, pp. 347-352.

[3] M. Bruen and J. Yang, "Functional Networks in Real-Time Flood Forecasting - A Novel Application," *Journal of Advances in Water Resources*, Vol. 28, No. 9, 2005, pp. 899-909.

[4] M. Campolo, P. Andreeussi and A. Soldati, "River Flood Forecasting with a Neural Network Model," *Water Resources Research*, Vol. 35, No. 4, 1999, pp. 1191-1197.

[5] M. Campolo, A. Soldati and P. Andreeussi, "Artificial Neural Network Approach to Flood Forecasting in the River Arno," *Hydrological Sciences Journal*, Vol. 48, No. 4, 2003, pp. 381-398.

[6] P. Coulibaly, F. Anctil and B. Bobee, "Daily Reservoir Forecasting Using Artificial Neural Network with Stopped Training Approach," *Journal of Hydrology*, Vol. 230, No. 3-4, 2000, pp. 244-257.

[7] C. W. Dawson and R. L. Wilby, "Hydrological Modeling Using ANN," *Progress in Physical Geography*, Vol. 25, No. 1, 2001, pp. 80-108.

[8] C. E. Imrie, S. Durucan and A. Korre, "River Flow Prediction Using Artificial Neural Network: Generalization beyond the Calibration Range," *Journal of Hydrology*, Vol. 233, No. 1-4, 2000, pp. 138-153.

[9] D. F. Lekkas, C. Onof, M. J. Lee and E. A. Baltas, "Application of Neural Networks for Flood Forecasting," *Global Nest*: *The International Journal*, Vol. 6, No. 3, 2004, pp. 205-211.

[10] A. K. Lohani, "ANN and Fuzzy Logic in Hydrological Modeling and Flow Forecasting," Ph.D Dissertation, Indian Institute of Technology, Roorkee, 2007.

[11] A. W. Minns and M. J. Hall, "Artificial Neural Networks as Rainfall-Runoff Models," *Hydrological Sciences Journal*, Vol. 41, No. 3, 1996, pp. 399-417

[12] J. R. Muhamad and J. N. Hassan, "Khabur River Flow Modeling Using Artificial Neural Network," *Al_Rafidain Engineering*, Vol. 13, No. 2, 2005, pp. 33-42.

[13] A. Mukerjee, C. Chatterji, N. Singh and N. S. Raghuvanshi, "Flood Forecasting Using ANN, Neuro-Fuzzy and Neuro-GA Models," *Journal of Hydrologic Engineering*, Vol. 14, No. 6, 2009, pp. 647-652.

[14] D. P. Solomatine and Y. Xue, "M5 Model Trees and Neural Networks: Application to Flood Forecasting in the Upper Reach of The Huai River in China," *Journal of Hydrologic Engineering*, Vol. 9, No. 6, 2004, pp. 491-501.

[15] D. P. Solomatine and R. K. Price, "Innovative Approaches to Flood Forecasting Using Data Driven and Hybrid Modeling," 6*th International Conference on Hydroinformatics – Liong*, World Scientific Publishing Company, New Jersey, 2004.

[16] C. M. Zealand, D. H. Burn and S. P. Simonovic, "Short Term Streamflow Forecasting Using Artificial Neural Network," *Journal of Hydrology*, Vol. 21, No. 4, 1999, pp. 32-48.

[17] J. Zhang and M. J. Hall, "Regional Flood Frequency Analysis for the Gan-Ming River Basin in China," *Journal of Hydrology*, Vol. 296, No. 1-4, 2004, pp. 98-117.

[18] Y. Xiongrui, X. Jun and Z. Xiang, "Flood Forecasting by Coupling Clustering Methods and Artificial Neural Networks," *Proceeding of Symposium HS* 3006, IUGG, Perugia, 2007.

[19] Water Resources Department, Government of Orissa, "Time of Flow in Mahanadi River between Hirakud & Mundali," 2009. http://www.dowrorissa.gov.in/Flood/DailyFloodBulletin.html

[20] S. N. Ghosh, "Flood Control and Drainage Engineering," A. A. Balkema Publishers, Rotterdam, 1997.

[21] K. L. Priddy and P. E. Keller, "Artificial Neural Networks, an Introduction," SPIE Press, Bellingham, 2005.

[22] S. Haykin, "Neural Networks," Macmillan College Publishing Company, Macmillan, 1994.

[23] G. Cybenko, "Approximation by Superposition of a Sigmoidal Function," *Journal of Mathematics Control Signal System*, Vol. 2, No. 4, 1989, pp. 303-314.

[24] K. Hornick, M. Stinchcombe and H. White, "Multilayer Feed forward Networks are Universal Approximators," *Neural Networks*, Vol. 2, No. 5, 1989, pp. 359-366.

[25] N. Karunanithi, W. J. Granny, D. Whitely and K. Bovee, "Neural Networks for River Flow Prediction," *Journal of Computing in Civil Engineering*, Vol. 8, No. 2, 1994, pp. 201-220.

[26] J. B. MacQueen, "Some Methods for Classification of Multivariate Observation," *Proceeding of* 5*th Berkely Symposium on Probability and Statistics*, University of California Press, Berkely, 1967, pp. 281-297.

[27] K-Means Algorithm, 2009. http://biocomp.bioen.uiuc.edu/oscar/tools/kmeans.html

[28] J. C. Dunn, "A Fuzzy Relative of the ISODATA Process and its Use in Detecting Compact Well-Separated Clusters," *Journal of Cybernetics*, Vol. 3, No. 3, 1973, pp. 32-57.

[29] J. C. Bezdeck, "Pattern Recognition with Fuzzy Objective Function Algorithm," Plenum Press, New York, 1967.

[30] Neural Network Toolbox, Matlab, 2004.

[31] World Meteorological Organization (WMO), "Guide for Hydrological Practices," Geneva, 1994.

J. Water Resource and Protection, **2010, 2, 888-897**
doi:10.4236/jwarp.2010.210106 Published Online October 2010 (http://www.SciRP.org/journal/jwarp)

Thermodynamic and Dynamic of Chromium Biosorption by Pectic and Lignocellulocic Biowastes

Sebastián Bellú[1], Luis Sala[1*], Juan González[1], Silvia García[1], María Frascaroli[1], Patricia Blanes[1], Jousy García[1], Juan Salas Peregrin[2], Ana Atria[3], Julio Ferrón[4], Masafumi Harada[5], Cong Cong[6], Yasuhiro Niwa[6]

[1]*Instituto de Química Rosario, CONICET. Universidad Nacional de Rosario, Rosario, Argentine*
[2]*Departamento de Química Inorgánica, Facultad de Ciencias, Universidad de Granada, Granada, Spain*
[3]*Facultad de Ciencias Químicas y Farmacéuticas, Universidad de Chile, Santiago, Chile*
[4]*Instituto de Desarrollo Tecnológico para la Industria Química, CONICET. Universidad Nacional del Litoral, Santa Fe, Argentine*
[5]*Faculty of Human Life and Environment, Nara Women's University, Nara, Japan*
[6]*Photon Factory, High Energy Accelerator Research Organization* (*KEK*), *Tsukuba, Japan*
E-mail: {*sala, gonzalez*}*@iquir-conicet.gov.ar*
Received July 12, 2010; *revised August* 10, 2010; *accepted August* 18, 2010

Abstract

Orange peel (OP) and rice husk (RH) were tested as low-cost biosorbents for Cr(III) removal from aqueous solutions. Dynamics of the biosorption process indicated that intraparticle mass transfer represents the rate-limiting step in the system that attained equilibrium at 120 min. While the OP sorbent material was capable of taking up 39.11 mg Cr(III)/g at the optimum pH 4.4, RH immobilized 3.20 mg Cr(III)/g at the optimum pH 3.0. The fitting of different sorption isotherms models resulted in the best fit with the Langmuir isotherm model. The mean free energy of the metal sorption process was in the range of 8-16 kJ/M. Abiotic Cr(VI) reduction was observed at various contact times and Cr-laden biomass was characterized by XPS, XAFS and EPR spectroscopy. These instrumental analyses confirmed that Cr(VI) removed from the solution was reduced and bound to the biomass as Cr(III). Results indicated that OP and RH materials are efficient biosorbents for eliminating Chromium from aqueous solutions.

Keywords: Chromium, Adsorption, Orange Peel, Rice Husk

1. Introduction

Chromium and its compounds are widely employed in industry [1] and Cr(III) is used as a tanning agent, resulting in severe groundwater contamination around tanneries [2,3]. Oxidation of polyuronic acids and pectin by hipervalent Chromium showed the presence of Cr(V), Cr(IV) and Cr(III)-saccharide complexes, with Cr(III)-pectin as an insoluble compound in the reaction media [4,5]. Following the treatment of Cr(VI) solution ($[Cr(VI)]_0$ = 0.0176 M) with 1.0 g of D-polygalacturonic acid, only 10% of the total Cr (Cr_T = Cr(III) + Cr(VI)) remained in solution [5].

Different metal removal methods (ion exchange, chemical reduction and precipitation, reverse osmosis, phytoremediation, bioremediation, etc.) have been tested for detoxification of Chromium-laden wastewaters in the recent years. However, these methods have high operating costs and problems in the disposal of the residual metal sludges. Biosorption techniques could use inexpensive sorbent materials as a feasible alternative for Chromium removal that features high efficiency, low operating costs with no adverse effects on the environment [6]. In recent years, several types of agricultural wastes such as sugarcane bagasse, grainless stalk of corn, etc. [7,8] have been applied with the aim of removing Chromium from wastewaters.

In this work, we study the behavior of biomaterials with different proportions of polyuronic acids when contacted with Chromium-containing wastewater. The study focused on easily obtainable waste materials such as orange peels (OP) and rice hulk (RH) which contain high proportions of pectin and lignin, respectively. XPS, XAS and EPR techniques were used to determine the oxida-

tion state of Chromium in the sorbent material, leading to establishing the mechanism of Chromium uptake/removal by OP and RH.

2. Experimental Section

2.1. Materials

The following analytical-grade reagents were used without purification: $K_2Cr_2O_7$, K_2CrO_4, $Cr(NO_3)_3{\cdot}9H_2O$, Cr_2O_3, Na_2CO_3, $K_2S_2O_8$, $AgNO_3$, 1,5-diphenylcarbazide (DPC), and diphenylpicrylhydrazyl (dpph) (Sigma Grade). Na-$[CrO(V)(ehba)_2]{\cdot}H_2O$ was synthesized [9].

OP was obtained from oranges harvested near the city of Rosario (Argentina) and RH came from a rice mill located in San Javier (Argentina). Both, OP and RH were washed with water, dried at 40°C for 12 h, powdered and sieved to retain the fraction of particles in the size range of 0.3–1.2 mm (OP) or 0.3–0.5 mm (RH), and were stored at room temperature in sealed polyethylene bags.

The reference solid compounds: oxidation state of Cr(VI) as K_2CrO_4, Cr(V) as $Na[CrO(V)(ehba)_2]{\cdot}H_2O$, and Cr(III) as $Cr(NO_3)_3{\cdot}9H_2O$ and Cr_2O_3.

2.2. Chromium Analysis

The [Cr(VI)] was determined at 540 nm by using a double-beam UV-vis JASCO V-550 spectrophotometer after complexation with DPC [10]. $[Cr]_T$ = [Cr(VI)] + [Cr(III)] was determined by oxidizing Cr(III) to Cr(VI) using $K_2S_2O_8$ and $AgNO_3$ saturated solution as catalyst [11], prior to the DPC reaction. [Cr(III)] was calculated as the difference between $[Cr]_T$ and [Cr(VI)]. The amount of Cr sorbed by the OP and RH biomass exposed to Cr(III) and Cr(VI) solutions was calculated from the difference between the initial chromium concentration of the control solutions and the final total Cr concentration in the respective supernatant solutions.

2.3. Spectroscopic Analysis

Cr-laden solid biomaterial samples were examined by EPR, XPS and XAS spectroscopy. The EPR spectra were derived on a Bruker ESP 300 E spectrometer at room temperature. XPS analyses were done with a SPECS system equipped with a hemispherical energy analyzer, a nine channeltron detector System and a double anode X-ray source. XAS experiments at the Cr K-edge (5989 eV) were carried out at beamline BL-9A with a ring energy of 2.5 GeV and a ring current of 450 mA. A double-crystal Si(111) monochromator was used, and the beam was focused using a pair of bent conical mirrors coated with Rh [12]. XAFS measurements were performed in a transmission mode for Cr-laden OP samples (Cr loading 4.9 wt%) and in fluorescence a mode for Cr-laden RH samples (Cr loading 0.71 wt%), respectively. The spectra of Cr-laden OP samples were recorded in transmission mode, with N_2(30)-He(70) gas for the I_0 chamber and N_2 gas for the I chamber to monitor the incident and transmitted X-rays, respectively. On the other hand, the spectra of Cr-laden RH samples were collected in a fluorescence mode, using an argon-filled Lytle detector with a vanadium filter ($\mu t = 6$) for monitoring the fluorescent X-ray (I_f). The XANES spectra were measured with 0.35 eV steps and 1 s collecting time between 5980 and 6060 eV, while the EXAFS spectra were measured with 2.5 eV steps and 4 s (in transmission mode) or 8 s (in fluorescence mode) collecting time between 5500 and 7080 eV. XAFS data were analyzed with commercially available software (REX2000 program, Rigaku Co.). EXAFS analysis was performed as described in detail elsewhere [13]. The reference samples were used to compare their spectral shapes and to identify major Cr species on the biomaterial surface [14].

2.4. Batch Studies

2.4.1. Effect of pH, Contact Time and Biomass Dosage on Cr(III) Adsorption

Batch equilibrium sorption studies were carried out at 20.0 ± 1.0°C. Biomaterials were suspended in Erlenmeyer flasks with an appropriate volume of work under constant stirring. $[Cr(III)]_0$ was 0.77 mM and 0.44 mM for OP and RH respectively. pH ranged from 0.2 to 5.2; pH was constantly controlled using a pH controller. A total amount of 5.0 g and 1.25 g of RH and OP, respectively, was used in these experiments. Time-based sorption uptake studies (process dynamics, including mass transfer and reaction) were carried out at 20.0 ± 1°C, using a series of 150 mL Erlenmeyer flasks. For Cr(III) sorption by OP, 1.50 g was suspended in 75.0 mL of Cr(III) solution at pH 4.0. Cr(III) sorption by RH was performed using 5.0 g of sorbent suspended in 50.0 mL of Cr(III) solution at pH 3.0. Mixtures were magnetically stirred and samples withdrawn at different time intervals followed by centrifugal solids separation. Clear supernatants were analyzed for their Cr content. Separate controls were maintained for each period of time. All experiments were performed in triplicate for statistical purposes.

2.4.2. Adsorption Isotherms

Equilibrium sorption experiments were performed under optimum conditions derived using factorial design. The sorbent material (OP or RH) was exposed to varying concentrations of Cr(III) in Erlenmeyer flasks containing 75.0 mL or 50.0 mL of solution. The pH was adjusted to 4.4 or 3.0 for OP or RH, respectively. The biosorbent

dosage was 1.45 g and 5.65 g for OP and RH, respectively. The Cr(III) adsorption experiments were performed at 20.0 ± 0.1°C. Mixtures were stirred for 120 min to reach equilibrium and then centrifuged. The supernatants were analyzed for their Cr content. All experiments were performed in triplicate for statistical purposes.

3. Results and Discussion

3.1. Cr-laden Biomaterials Spectroscopic Characterization

Characterization of the Chromium oxidation state on the surface of the biomaterial would establish if Cr(VI) adsorption-reduction mechanism contributes to its removal from the aqueous solution. Grainless stalk of corn (GLSC), an agricultural waste, was tested as a reference biomass for sorption and reduction of Cr(VI) [8]. The reduction took place mainly in the presence of solid biomaterial. High-resolution XPS of Cr-laden GLSC showed the presence of Cr(V) and Cr(III) at short contact time (**Figure 1(a)**) and only Cr(III) at prolonged contact time (**Figure 1(b)**).

The present experimental results support the conclusion of Park *et al.* [16] that the mechanism of Cr(VI) removal by GLSC is Cr(VI) sorption-coupled reduction to Cr(III) and partial complexation of Cr(III).

Figure 2 shows XPS spectra of Cr-laden OP. As can be seen in the high-resolution XPS spectrum of long-exposure Cr-laden OP, it was Cr(III) that became bound to the sorbent. While at short contact time, the amount of Cr sorbed by OP was below the XPS detection limit giving thus no discernible spectrum, at long contact times the amount of Cr sorbed was sufficient to produce an XPS spectrum with a Cr signal. Similarly, no chromium signal could be detected in the XPS spectrum of Cr-laden RH where Cr was still below the apparatus detection limit. The detection of intermediate states of Chromium for short contact times could be improved employing a more sensitive spectroscopic technique such as EPR. The EPR spectra are shown in **Figures 3** and **4**.

EPR spectra of Cr-laden OP and Cr-laden RH for different contact-time samples exhibit a sharp signal at g_{iso} = 1.9788 and g_{iso} = 1.9785, respectively, characteristic of Cr(V), superimposed on a broad signal (~ 600 G) at g_{iso} ~ 2.00, typical of Cr(III). The intensity of this broad signal increased for longer-contact time samples while the sharp Cr(V) signal diminished and finally disappeared, indicating thus that Cr(V) in these biosorbents was further reduced to Cr(III). The g_{iso} value of the Cr(V) EPR signal provides useful information on the nature and number of donor groups bound to Cr(V). The g_{iso} values 1.9788 and 1.9785 correspond to oxo-Cr(V) bound to

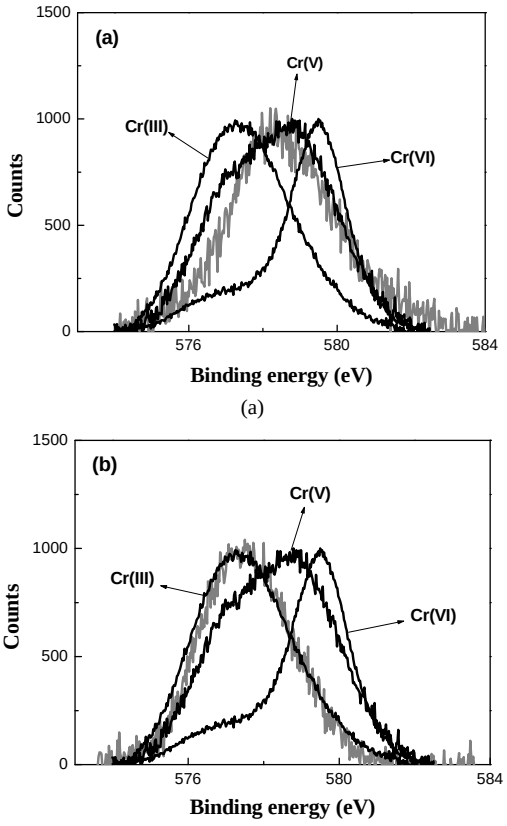

Figure 1. High-resolution XPS of Cr(VI)-laden GLSC. $Mass_{GLSC}$ = 0.3 g; V = 25.0 mL; pH = 0.9; [Cr(VI)] = 624 mg/L; contact time:(a) 12 h (b) 1 week.

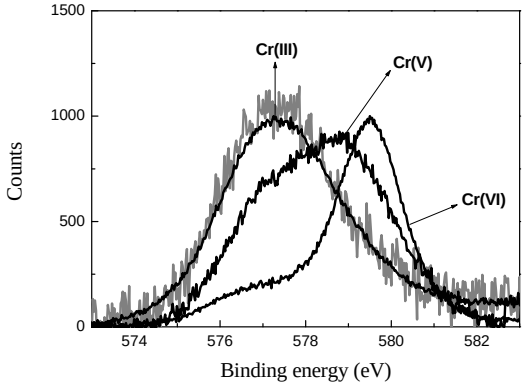

Figure 2. High-resolution XPS of Cr(VI)-laden OP. $Mass_{OP}$ = 0.3 g; V = 25 mL; pH = 2; [Cr(VI)] = 624 mg/L; contact time: 1 week.

carboxylate and alcohol groups [17]. The detection of Cr(V) bound by OP and RH biomaterials reinforces the sorption-reduction model hypothesis for the removal of Cr(VI) by these biosorbents. In both sorbents exposed to Cr(VI), Cr(III) was the final species as can be seen in the EPR and XPS spectra.

XPS spectroscopy was also employed for detection of

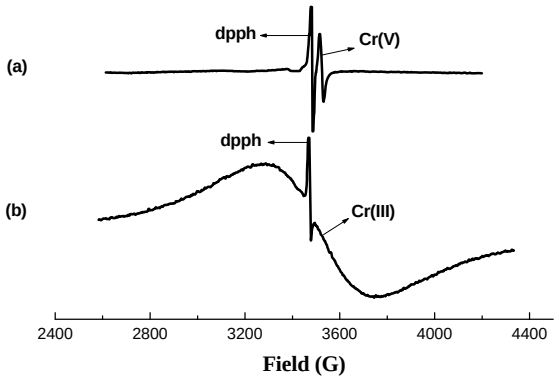

Figure 3. EPR spectra of Cr-laden OP at various contact time. $Mass_{OP}$ = 0.2 g; V = 75 mL; pH = 2.0; $[Cr(VI)]_0$ = 624 mg/L; contact time: (a) 12 hs; (b) 1 week.

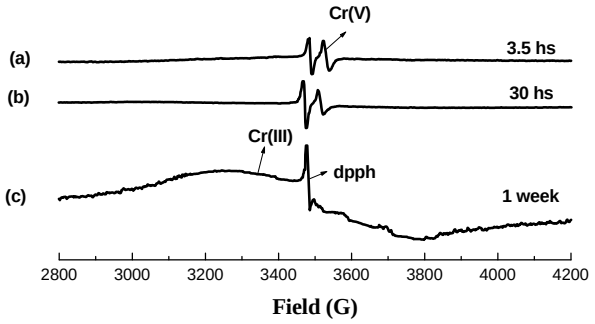

Figure 4. EPR spectra of Cr-laden RH at various contact time. $Mass_{RH}$ = 0.2 g; V = 50 mL; pH = 2.0; $[Cr(VI)]_0$ = 624 mg/L; contact time: (a) 3.5 hs; (b) 30 hs; (c) 1 week.

Cr(III) in metal-laden biomaterials and compared with a model complex Cr(III)-pectinate and Cr_2O_3.

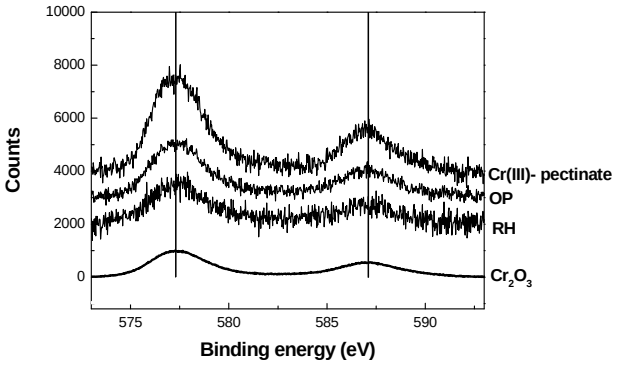

Figure 5. High-resolution XPS of Cr(III)-laden biomaterials. $Mass_{biomaterial}$ = 0.3 g; V = 25 mL; pH = 4; [Cr(III)] = 624 mg/L; contact time: 1 week.

High-resolution XPS spectra collected from the Cr2p core region indicated that there were significant contributions of the Cr bound to the biomaterials. **Figure 5** shows bands of Cr_2O_3 (576.8 and 586.7 eV). The spectra of all the Cr(III)-laden biomaterials (OP, RH) could well be matched with that of the Cr_2O_3, similarly as with Cr(III)-pectinate. This fact indicates that Cr(III) is bound to oxygen atoms in the solid structures of the biosorbent. The XANES data were used to verify the oxidation state of the Cr(VI)- or Cr(III)-laden biomass. **Figure 6** shows the normalized Cr K-edge XANES spectra of reference compounds. The XANES data for Cr(III) standards show a small peak at 5990.5 eV, while those for Cr(V) and Cr(VI) show a pre-edge peak at 5993.0 and 5993.3 eV, respectively. The edge energy and the intensity of pre-edge absorbance decrease in the following order:

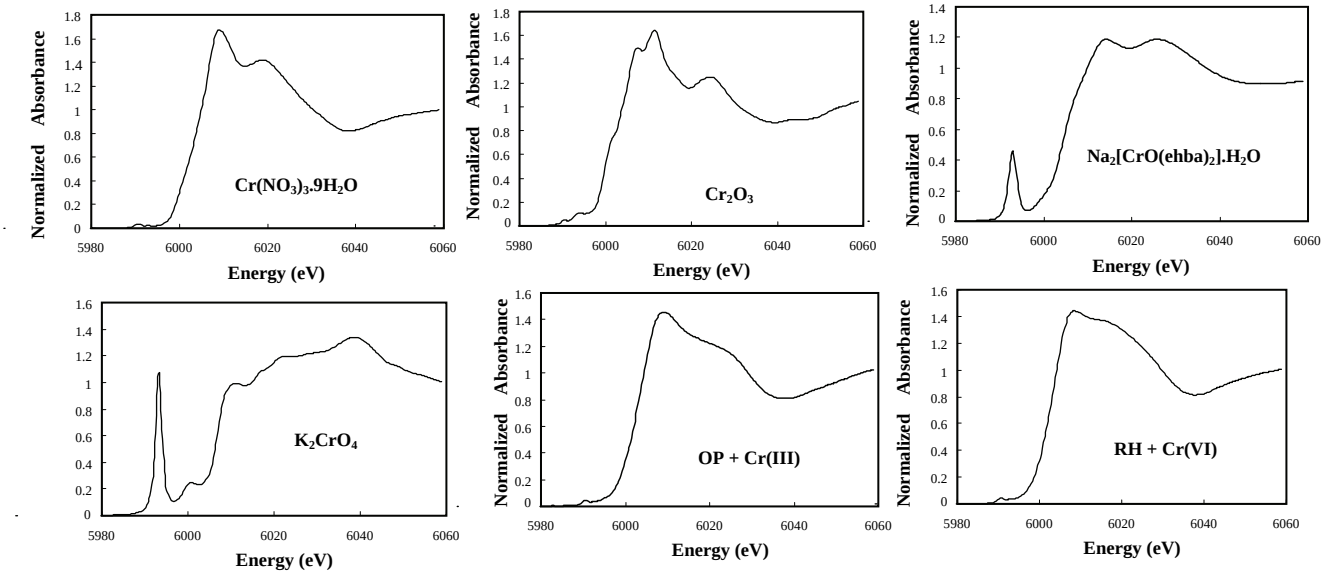

Figure 6. Cr K-edge XANES spectra of solid samples.

Cr(VI) > Cr(V) > Cr(III). The octahedral symmetry in XANES spectra of Cr(III) compounds is characterized by small resonances in the pre-edge region as signed to transitions of 1s electrons into antibonding orbitals with octahedral symmetry [18] whereas Cr(0) (body centered cubic) shows a broad pre-edge conduction band feature. The XANES data for K_2CrO_4 show the well-defined pre-edge peak from 5990 to 5997 eV [19], and for Na-[Cr(V)O(ehba)$_2$]·H_2O, the pre-edge peak position is consistent with that reported in the literature [20].

On the other hand, both Cr(III)-laden OP and Cr(VI)-laden RH samples do not show a pre-edge peak between 5990 and 5997 eV, and they have a small peak at 5990.5 eV, indicating the presence of Cr(III) binding in both biomaterials. It is also evident that Cr(III) is bound in the OP and Cr(VI) sorbed by the RH is completely reduced to Cr(III). This is quite consistent with the XPS and EPR results. EXAFS spectroscopy was employed to determine the local atomic structure of Cr in Cr(III)-laden OP and Cr(VI)-laden RH biomaterials. The experimental Fourier transform results are shown in **Figure 7** and the curve-fitted values are given in **Table 1**.

For $Cr(NO_3)_3$·$9H_2O$, the k^3-weighted FT function gave a main peak centered at 1.60 Å which arises from first-shell oxygen back-scattering and another smaller peak centered at ~ 3.15 Å (phase-uncorrected). Three main peaks at 1.60, 2.52, and 3.31 Å (phase-uncorrected) could also be observed for the Cr_2O_3 compound, assigned to the first, second, and third shell contributions of a Cr(III) in an octahedral symmetry, respectively. For Na[Cr(V)O(ehba)$_2$]·H_2O, a main peak is observed at 1.47 Å. The structure of the first coordination shell in the Cr(V) seems to be similar to that in the Cr(III). The Fourier transformed EXAFS spectra for the Cr(III)-laden OP and Cr(VI)-laden RH biomaterials were very similar to those for Cr(III) reference compound. This result means that the coordination environment of the chromium on the OP and RH biomaterials was also similar to that of Cr(III) compound, where Cr(III) is in an octahedral geometrical arrangement. The Cr-O bond distances were approximately the same lengths, which corresponds to the Cr-O bond lengths cited in the literature [18,21,22]. Cr(III)-laden OP sample showed the presence of the second and third peaks of Cr_2O_3 allowing thus a guess as to the formation of Chromium polynucleate species [23]. For the curve-fitting to determine the structural parameters, phase and amplitude functions for the absorbing and back-scatterer (Cr, O) pair were extracted from the filtering of the first peak of the EXAFS Fourier transform

Table 1. Cr K-edge EXAFS fitting results for reference samples and Cr-laden biomaterials.

Sample	Bond	CN	r (Å)	ΔE (eV)	σ (Å)	R (%)
Cr_2O_3	Cr-O	5.7	1.97	0.238	0.063	0.226
Na[CrO(ehba)$_2$]	Cr-O	2.4	1.91	−0.961	0.075	7.847
K_2CrO_4	Cr-O	3.8	1.66	1.089	0.066	1.931
OP + Cr(III)	Cr-O	6.1	1.97	−0.903	0.072	0.261
RH + Cr(VI)	Cr-O	5.2	1.96	−1.605	0.049	0.456

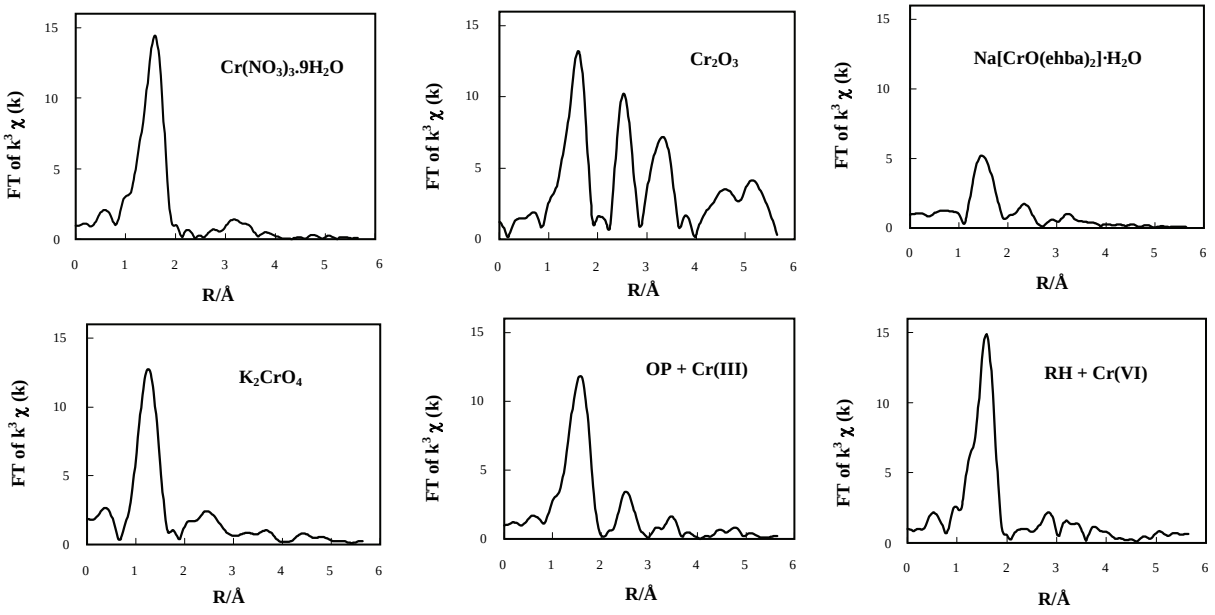

Figure 7. Fourier-transformed EXAFS spectra of solid samples.

of $Cr(NO_3)_3.9H_2O$, where the chromium absorbing atom is surrounded by 6 oxygen atoms at the bond distance of 1.96 Å [21].

3.2. Effect of pH

The effect of pH, on the removal of Cr(III) by OP and RH is shown in **Figure 8**. The uptake of Cr(III) ion increased with increasing pH and OP biomaterial was more efficient in the removal. At pH ≤ 1.0 there was a small adsorption, less than 7-25% for RH or OP respectively and Cr(III) removal yield increased up to 86-98% at pH 3.0-4.0 for OP. RH showed a capacity something smaller than OP for Cr(III) adsorption. In spite of employing four times biomass, only 78.0-85.0% was achieved at pH 3.0-4.0. At lower pH values, the higher $[H^+]$ effectively leads to fewer ligands being available for metal ions binding [24]. According to the pH dependence of this biosorption process, deprotonation of the carboxylic groups of uronic pectin moieties [4,5] might be involved. Increasing pH, surfaces becomes deprotonated, resulting in more ligand groups available for Cr(III) cations binding and electrostatic attraction available from carboxylate groups is likely enhanced. Thus, at high pH values where the $[H^+]$ is very low, carboxylic groups from OP and RH work as ion exchanger, where protons are released in the solution while metal ions are sorbed.

3.3. Sorption Process Dynamics

Reaction kinetics of the sorption process that is based on ion exchange is inherently very fast and studying it is experimentally difficult and inaccurate. With biosorbent particles involved that are "transparent" to ionic species, it is predominantly the intraparticle mass transfer that is observed externally and that represents the rate-limiting step. With easily accessible surface layers of the particles saturating first and fast, biosorption of Cr(III) onto OP and RH features two apparent steps, a fast initial sorption followed by a slower phase that reflects the penetration of sorbate into the particles. Correspondingly, the biosorption uptake increased sharply in the first 30 min, with more than 80% of Cr(III) taken up, and then continued increasing only at much slower rate. The sorption system equilibrium was reached in less than 120 min. A distinct two-step behavior has often been reported for metal ion biosorption. While Liu and Huang [25] attributed the two-step sorption characteristic to the heterogeneity of the surface binding sites on sorbents, Qin *et al.* [26] asserted that the fast initial sorption was the result of the fast transfer of metal ions to the surface of biomaterial, followed by a relatively slow uptake caused by the slow diffusion of metal ions into the intra-particle spaces of sorbents.

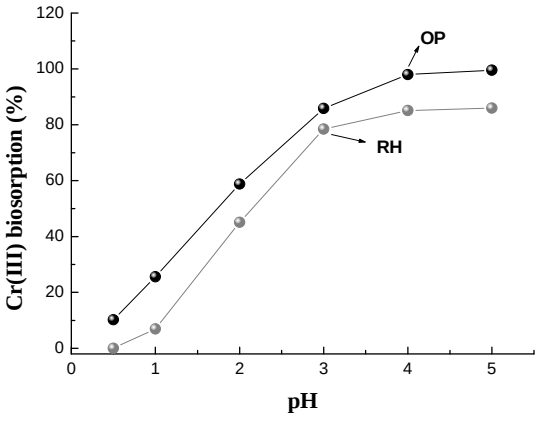

Figure 8. Effect of pH on the removal of Cr(III) by OP and RH. T = 20°C; V = 75.0 mL; $[Cr(III)]_0$ = 0.77 mM (OP) and 0.44 mM (RH); mass = 5.0 g (OP) and 1.25 g (RH).

We tested of three kinetic models approach in order to stablish the mechanism of Cr(III) adsorption onto OP/RH. Pseudo-first-order kinetic model (Lagergren [27]) is:

$$\frac{dq}{dt} = k_1 (q_e - q_t) \quad (1)$$

Pseudo-second-order kinetic expression (Ho [28]) is:

$$\frac{dq_t}{dt} = k_2 (q_e - q_t)^2 \quad (2)$$

k_1 (1/min) and k_2 (g/mg min) are the equilibrium rate constant of pseudo-first and pseudo-second order sorption respectively, and q_e and q_t are the amounts of solute sorbed per unit adsorbent at equilibrium (mg/g) and at time t, respectively.

Separating variables of (2), integrating and reordered one can obtain the following lineal expression:

$$\frac{t}{q_t} = \frac{1}{k_2 q_e^2} + \frac{t}{q_e} \quad (3)$$

The intraparticle diffusion model (Weber-Morris [29] is:

$$q_t = k_{dif} t^{0.5} + C \quad (4)$$

where k_{dif} is the intraparticle diffusion rate constant and C can be obtained from the slope and intercept of the plot q_t *vs.* $t^{0.5}$.

The correlation coefficient (R^2) of pseudo-first-order (1), are nearly 0.86 (OP) and 0.54 (RH), and q_e calculated with (1) are lower than the experimental q_e. Therefore, the pseudo-first-order equation is not a good fit for Cr(III) adsorption on OP and RH.

The kinetic adsorption data were further fitted by the pseudo-second-order kinetic model, using (3). **Table 2** shows the experimental q_e, k_2, R^2 values, and the calculated q_e values which agree perfectly with the experimental q_e values. Those results indicate that the rate-limiting step is a chemical sorption involving valance

Table 2. Kinetic parameters from pseudo-second-order for Cr(III) sorption.

Biomaterial	k_2 (g/mg min)	q_e (exp) (mg/g)	q_e (calc) (mg/g)	R^2
OP	0.14	0.83	0.88	0.9975
RH	2.26	0.40	0.42	0.9997

force through sharing between adsorbent and adsorbate.

The intraparticle diffusion kinetic model (4) provides information about the nature of the adsorption process [29]. A plot of q_t *vs.* $t^{0.5}$ for Cr(III) adsorption on OP and RH afforded two linear sections. A deviation of the straight line from the origin indicates that the intraparticle diffusion is not the only rate controlling step [30] and boundary layer diffusion controls the adsorption to some. If the regression of q_t *vs.* $t^{0.5}$ is linear and passes through the origin, intraparticle diffusion is the sole rate-controlling step [31]. The first straight portion was attributed to the fast mass transfer of sorbate molecules from the bulk solution to the sorbent surface and the second linear portion to the slower intraparticle diffusion into the biosorbent. Similar results were found for acid dye adsorption on activated palm ash [32].

Additionally, the kinetic model proposed by Boyd *et al.* [33] was applied to check that sorption proceeds via surface uptake followed by intra-particle diffusion:

$$F = 1 - \left(\frac{6}{\pi^2}\right) e^{-Bt} \quad (5)$$

where F is the fraction of solute adsorbed at different times t:

$$F = \left(\frac{q_t}{q_e}\right) \quad (6)$$

Bt, in (5), is a mathematical function of F which can be evaluated from each value of F as:

$$Bt = -0.4977 - \ln\left(1 - \frac{q_t}{q_e}\right) \quad (7)$$

Plot of Bt *vs.* t for both, OP and RH, are shown in Figure 9 which are straight lines with R^2 of 0.9970 and 0.9921, respectively. The results suggest that intraparticle diffusion is not the sole rate controlling step because the plot does not pass through the origin. This is in agreement with the results obtained by using intraparticle diffusion model and, at the same time, indicating that the mechanism of metal adsorption by OP and RH is complex and both, external mass transport as well as intraparticle diffusion contribute to the rate determining step, being the rate limiting step the intraparticle transfer.

Value of rate constant B was calculated from the slope in **Figure 9** and used to calculate the effective diffusion coefficient, D_i (cm^2/s) employing the relationship:

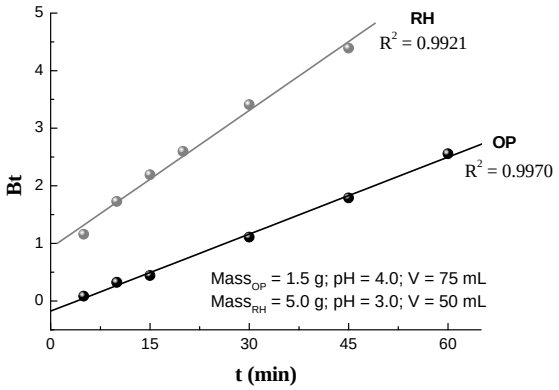

Figure 9. Boyd plot for Cr(III) sorption. T = 20°C; $[Cr(III)]_0$ = 0.385 mM (OP) and 0.77 mM (RH).

$$B = \pi^2 \frac{D_i}{r^2} \quad (8)$$

where r represents the radius of the assumed spherical particle. The calculated D_i values for OP and RH were 9.5×10^{-8} cm^2/s and 5.9×10^{-8} cm^2/s, respectively.

3.4. Adsorption Isotherms

Freundlich, Langmuir and Dubinin-Radushkevich (D-R) adsorption models were employed for describing the chromium biosorption behavior in the OP- and RH-Cr(III) systems.

Freundlich isotherm

$$q_e = K_f C_e^{1/n} \quad (9)$$

where C_e is equilibrium concentration of chromium in the bulk solution (mg/L), K_f and 1/n are Freundlich constants. Values of 1/n and K_f correspond to the adsorption intensity and maximum adsorption capacity, respectively. This empirical model can be applied to non-ideal adsorption on heterogeneous surfaces as well as multilayer adsorption. Relatively higher fractional values of 1/n ($0 < 1/n < 1$) indicate a fair validity of classical Freundlich isotherm over the entire concentration of Chromium [34].

Langmuir isotherm

$$q_e = \frac{q_m K_L C_e}{1 + K_L C_e} \quad (10)$$

where q_m is the monolayer adsorption capacity (mg/g) and K_L is the Langmuir constant related to the free energy of adsorption. High values of K_L are reflected by the step initial slope of a sorption isotherm and indicate a high affinity for the adsorbate.

The non-linear Freundlich and Langmuir isotherms for the uptake of Cr(III) on the OP and RH are presented in **Figures 10** and **11**. The solid curves represent the model fits in the wide range of concentrations. The corresponding Freundlich and Langmuir parameters together with

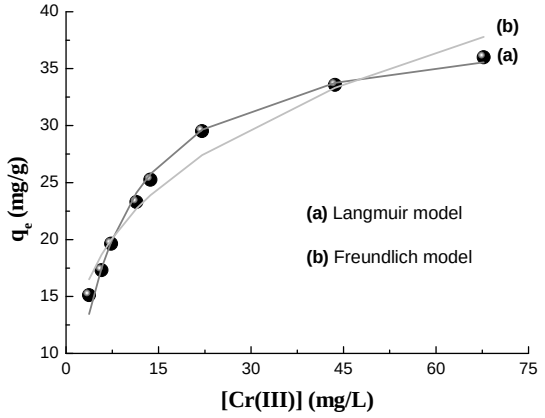

Figure 10. Adsorption isotherm for Cr(III) removal by OP. $Mass_{OP}$ = 1.45 g; T = 20°C; pH = 4.4; V = 75 mL; $[Cr(III)]_0$ = 76.96 - 769.60 mg/L; time contact = 120 min.

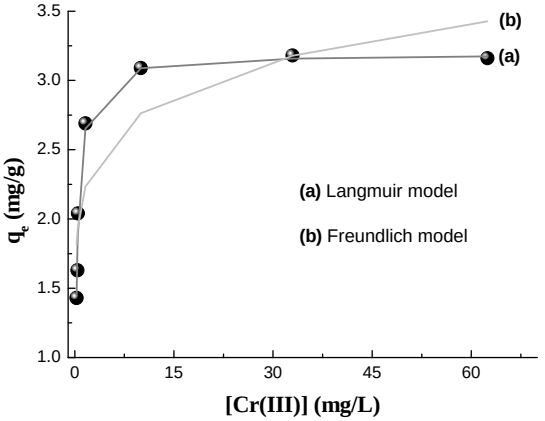

Figure 11. Adsorption isotherm for Cr(III) removal by RH. $Mass_{RH}$ = 5.65 g; pH = 3.0; T = 20°C; V = 50 mL; $[Cr(III)]_0$ = 23.09 - 461.76 mg/L; time contact = 120 min.

correlation coefficients are given in **Table 3**. In the given concentration range, the correlation coefficients showed that the Langmuir model fitted the experimental data better than the Freundlich model.

In previous studies [34,35], authors have suggested that using a dimensionless separation factor is suitable for evaluation of sorption data. For the Langmuir-type sorption process, the isotherm shape can be classified by a term R_L, dimensionless constant separation factor, which is defined as:

$$R_L = \frac{1}{1 + K_L C_0} \quad (11)$$

where C_0 is initial metal concentration. The parameter R_L indicates the shape of the isotherm accordingly: $R_L > 1$ unfavorable; $R_L = 1$ linear; $0 < R_L < 1$ favorable; $R_L = 0$ irreversible. The values of R_L were found to be less than 1 and greater than 0 for both biomaterials indicating a favorable adsorption for Cr(III) by the biomass.

Table 3. Langmuir and Freundlich constants and correlation coefficients for Cr(III) removal.

	Langmuir constants			Freundlich constants		
Biomaterial	q_m (mg/g)	K_L (L/mg)	R^2	K_f (mg/g)	1/n	R^2
OP	39.11	0.14	0.9902	11.30	0.29	0.9687
RH	3.20	2.98	0.9864	2.11	0.12	0.8173

D-R isotherm model [36]

$$\ln q_e = \ln q_M - \beta \varepsilon^2 \quad (12)$$

where q_M is maximum amount of ion that can be sorbed onto unit weight of sorbent (mol/g), β is a constant related to sorption energy (mol/kJ) and ε is the Polanyi potential:

$$\varepsilon = R T \ln\left(1+\frac{1}{C_e}\right) \quad (13)$$

where R is gas constant (8.314×10^{-3} kJ/mol K) and T is absolute temperature expressed in K. Constant β (-3.7×10^{-9} mol^2/J^2) and q_m (9.60×10^{-4} mol/g) values were obtained from slope and intercept of the plot of ln q_e *vs.* ε^2 (R^2 = 0.9891), (10) and **Figure 12**. The mean sorption energy, E, which is the free energy mean of transference for 1 mol of solute from infinity (in solution) to the surface of biomaterial, can be calculated from:

$$E = \frac{1}{\sqrt{-2\beta}} \quad (14)$$

The obtained value of E = 11.6 kJ/mol, is in the expected range of 8–16 kJ/mol for ion exchange phenomena [36]. The correlation coefficient for RH was lower than OP system (0.9136) using D-R model with an estimate value of E of 16 kJ/mol.

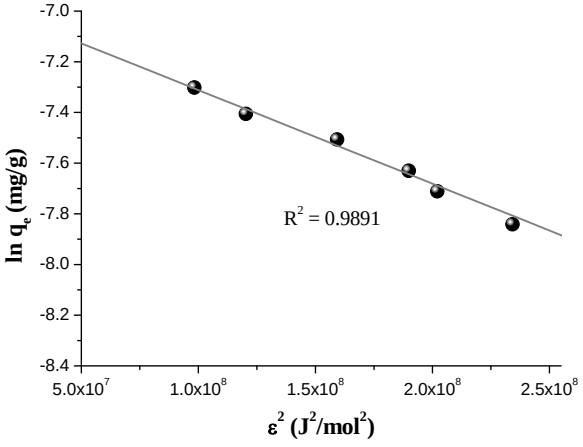

Figure 12. D-R isotherm plot for sorption Cr(III) onto OP. $Mass_{OP}$ = 1.45 g; T = 20°C; pH = 4.4; V = 75 mL; $[Cr(III)]_0$ = 76.96 - 769.60 mg/L; time contact = 120 min.

4. Conclusions

OP and RH agriculture biowaste materials were exam ined as possible low-cost sorbents for Cr(III) removal from aqueous solutions. Fitting of the intraparticle diffusion model indicated that intraparticle mass transfer resistance is likely the rate limiting phenomenon. The effective diffusion coefficient values for OP and RH were 9.5×10^{-8} cm^2/s and 5.9×10^{-8} cm^2/s. Sorption dynamics data indicated that the time required to reach sorption equilibrium was approximately 120 min. Langmuir, Freundlich and Dubinin-Radushkevich sorption isotherm models were fitted to the experimentally derived biosorption isotherms. The isotherm data most accurately conformed to the Langmuir equation. The values obtained for q_m were 39.11 and 3.20 mg/g for Cr(III) adsorption by OP and RH, respectively. The mean free energy of metal sorption process calculated from D-R parameter and the Polanyi potential was found to be in the range of 8-16 kJ/mol indicating that the main mechanism governing the sorption process is most likely ion exchange. Abiotic Cr(VI) reduction by the biomass was performed with various contact times, and characteristics of the Cr-laden biomass were determined by spectroscopic studies that demonstrated that the Cr(VI) bound to the biomass was reduced to Cr(III). Results indicated that OP and RH are biomaterials quite effective in removing Chromium from aqueous solutions to drinking water standards.

5. Acknowledgements

We thank the National Research Council of Argentina (CONICET) PIP 0075, National University of Rosario (UNR) PIP BIO145 for financial support. J. Ferrón thanks for a Grant PME 8 2003 for financing the purchase of a Multi Analysis System. L. F. Sala and M. Harada thank the Photon Factory Advisory Committee (PAC) at the High Energy Accelerator Research Organization (KEK) for approval to perform XAFS measurements (Proposal No. 2009G184). P. Blanes thanks the National Academy of Exact, Physic and Natural Sciences for grating a PhD fellowship.

6. References

[1] S. K. Sahu, P. Meshram, B. D. Pandey, V. Kumar and T. R. Mankhand, "Removal of Chromium(III) by Cation Exchange Resin, Indion 790 for Tannery Waste Treatment," *Hydrometallurgy*, Vol. 99, No. 3-4, November 2009, pp. 170-174.

[2] L. Yang and J. P. Chen, "Biosorption of Hexavalent Chromium onto Raw and Chemically Modified *Sargassum* sp.," *Bioresource Technology*, Vol. 99, No. 1, January 2008, pp. 297-307.

[3] M. Cieslak-Golonka, "Toxic and Mutagenic Effects of Chromium(VI),. A Review," *Polyhedron*, Vol. 15, No. 21, August 1996, pp. 3667-3675.

[4] J. C. González, S. I. García, S. Bellú, A. M. Atria, J. M. Salas Peregrín, A. Rockembauer, L. Korecz, S. Signorella and L. F. Sala, "Oligo and Polyuronic Acids Interactions with Hypervalent Chromium," *Polyhedron*, Vol. 28, No. 13, September 2009, pp. 2719-2729.

[5] S. E. Bellú, J. C. González, S. I. García, S. R. Signorella and L. F. Sala, "Kinetics and Mechanism of Oxidation of Apple Pectin by Cr^{VI} in Aqueous Acid Medium," *Journal of Physical Organic Chemistry*, Vol. 21, No. 12, December 2008, pp. 1059-1067.

[6] D. Mohan and C. U. Pittman Jr., "Activated Carbons and Low Cost Adsorbents for Remediation of Tri- and Hexavalent Chromium from Water," *Journal of Hazardous Materials*, Vol. 137, No. 2, September 2006, pp. 762-811.

[7] U. K. Garg, M. P. Kaur, V. K. Garg and D. Sud, "Removal of Hexavalent Chromium from Aqueous Solution by Agricultural Waste Biomass," *Journal of Hazardous Materials*, Vol. 140, No. 1-2, February 2007, pp. 60-68.

[8] S. Bellú, S. García, J. C. González, A. M. Atria, L. F. Sala and S. Signorella, "Removal of Chromium(VI) and Chromium(III) form Aqueous Solution by Grainless Stalk of Corn," *Separation Science and Technology*, Vol. 43, No. 11-12, August 2008, pp. 3200-3220.

[9] M. Krumpolc and J. Rocek, "Sodium bis[2-ethyl-2-hydroxybutyrato(2-)]-oxochromate(V)," *Inorganic Syntheses*, Vol. 20, 1980, pp. 63-65.

[10] L. Clesceri, A. Greenberg and A. Eaton, "Standard Methods for the Examination of Water and Wastewater," 20th Edition, American Public Health Association, American Water Work Association, and Water Environment Federation, Washington, D.C., 1998, p. 366.

[11] F. Burriel Martí, F. Lucena Conde, S. Arribas Jimeno and J. Hernández Méndez, "Qualitative Analytical Chemistry (Spanish)," 14th Edition, Paraninfo, Madrid, 1992, p. 600.

[12] M. Nomura and A. Koyama, "Performance of a Beamline with a Pair of Bent Conical Mirrors," *Nuclear Instruments and Methods in Physics Research Section A*, Vol. 467-468, July 2001, pp. 733-736.

[13] D. C. Koningsberger and R. Prins, "X-Ray Absorption: Principles, Applications, Techniques of EXAFS, SEXAFS, and XANES," John Wiley & Sons, New York, 1988.

[14] K. K. Kannan and M. A. Viswamitra, "Unit Cell, Space Group and Refractive Indices of $Al(NO_3)_3 \cdot 9H_2O$ and $Cr(NO_3)_3 \cdot 9H_2O$," *Acta Crystallographica*, Vol. 19, July 1965, pp. 151-152.

[15] H. Sakane, A. Munoz-Páez, S. Díaz-Moreno, J. M. Martínez, R. Pappalardo and E. Sánchez Marcos, "Second Hydration Shell Single Scattering versus First Hydration Shell Multiple Scattering in $M(H_2O)_6^{3+}$ EXAFS Spectra," *Journal of the American Chemical Society*, Vol. 120, No. 40, October 1998, pp. 10397-10401.

[16] D. Park, Y.-S. Yun and J. M. Park, "XAS and XPS Stud-

ies on Chromium-Binding Groups of Biomaterial during Cr(VI) Biosorption, " *Journal of Colloid and Interface Science*, Vol. 317, No. 1, January 2008, pp. 54-61.

[17] G. Barr-David, M. Charara, R. Codd, R. P. Farrell, J. A. Irwin, P. A. Lay, R. Bramley, S. Brumby, J.-Y. Ji and G. R. Hanson, "EPR Characterization of the Cr^{V} Intermediates in the $Cr^{VI/V}$ Oxidations of Organic Substrates and of Relevance to Cr-Induced Cancers," *Journal of the Chemical Society, Faraday Transactions*, Vol. 91, No. 8, April 1995, pp. 1207-1216.

[18] E. Groppo, C. Prestipino, F. Cesano, F. Bonino, S. Bordiga, C. Lamberti, P. C. Thüne, J. W. Niemantsverdriet and A. Zecchina, "In situ, Cr *K*-Edge XAS Study on the Phillips Catalyst: Activation and Ethylene Polymerization," *Journal of Catalysis*, Vol. 230, No. 1, February 2005, pp. 98-108.

[19] B. A. Manning, J. R. Kiser, H. Kwon and S. R. Kanel, "Spectroscopic Investigation of Cr(III)- and Cr(VI)-Treated Nanoscale Zerovalent Iron," *Environmental Science & Technology*, Vol. 41, No. 2, January 2007, pp. 586-592.

[20] A. Levina, R. Codd, G. J. Foran, T. W. Hambley, T. Maschmeyer, A. F. Masters and P. A. Lay, "X-Ray Absorption Spectroscopic Studies of Chromium(V/IV/III)−2-Ethyl-2-Hydroxybutanoato(2-/1-) Complexes," *Inorganic Chemistry*, Vol. 43, No. 3, February 2004, pp. 1046-1055.

[21] D. Lazar, B. Ribár, V. Divjakovic and Cs. Mészáros, "Structure of Hexaaquachromium(III) Nitrate Trihydrate," *Acta Crystallographica Section C*, Vol. 47, No. 5, May 1991, pp. 1060-1062.

[22] J. L. Gardea-Torresdey, K. J. Tiemann, V. Armendariz, L. Bess-Oberto, R. R. Chianelli, J. Rios, J. G. Parsons and G. Gamez, "Characterization of Cr(VI) Binding and Reduction to Cr(III) by the Agricultural Byproducts of *Avena Monida* (Oat) Biomass," *Journal of Hazardous Materials*, Vol. 80, No. 1, December 2000, pp. 175-188.

[23] H. Roussel, V. Briois, E. Elkaim, A. de Roy, J.-P. Besse and J.-P. Jolivet, "Study of the Formation of the Layered Double Hydroxide [Zn−Cr−Cl]," *Chemistry of Materials*, Vol. 13, No. 2, February 2001, pp. 329-337.

[24] P. X. Sheng, Y.-P. Ting, J. P. Chen and L. Hong, "Sorption of Lead, Copper, Cadmium, Zinc, and Nickel by Marine Algal Biomass: Characterization of Biosorptive Capacity and Investigation of Mechanisms," *Journal of Colloid and Interface Science*, Vol. 275, No. 1, July 2004, pp. 131-141.

[25] C. Liu and P. M. Huang, "Kinetics of Phosphate Adsorption on Iron Oxides Formed under Influence of Citrate," *Canadian Journal of Soil Science*, Vol. 80, No. 3, August 2000, pp. 445-454.

[26] F. Qin, B. Wen, X.-Q. Shan, Y.-N. Xie, T. Liu, S.-Z. Zhang and S. U. Khan, "Mechanism of Competitive Adsorption of Pb, Cu and Cd on Peat," *Environmental Pollution*, Vol. 144, No. 2, November 2006, pp. 669-680.

[27] S. Lagergren, "About the Theory of So-Called Adsorption of Soluble Substances, Zur Theorie der Sogenannten Adsorption Gelöster Stoffe," *Kungliga Svenska Vetenskapsakademiens, Handlingar*, Vol. 24, No. 4, 1898, pp. 1-39.

[28] Y. S. Ho, D. A. J. Wase and C. F. Forster, "Kinetic Studies of Competitive Heavy Metal Adsorption by Sphagnum Moss Peat," *Environmental Technology*, Vol. 17, No. 1, January 1996, pp. 71-77.

[29] W. J. Weber Jr. and J. C. Morris, "Kinetics of Adsorption on Carbon from Solution," *Journal of the Sanitary Engineering Division ASCE*, Vol. 89, No. (SA2), 1963, pp. 31-59.

[30] I. D. Mall, V. C. Srivastava and N. K. Agarwal, "Removal of Orange-G and Methyl Violet Dyes by Adsorption onto Bagasse Fly Ash-Kinetic Study and Equilibrium Isotherm Analyses," *Dyes and Pigments*, Vol. 69, No. 3, June 2006, pp. 210-223.

[31] W. H. Cheung, Y. S. Szeto and G. McKay, "Intraparticle Diffusion Processes during Acid Dye Adsorption onto Chitosan," *Bioresource Technology*, Vol. 98, No. 15, November 2007, pp. 2897-2904.

[32] B. H. Hameed, A. A. Ahmad and N. Aziz, "Isotherms, Kinetics and Thermodynamics of Acid Dye Adsorption on Activated Palm Ash," *Chemical Engineering Journal*, Vol. 133, No. 2, September 2007, pp. 195-203.

[33] G. E. Boyd, A. W. Adamson and L. S. Myers Jr., "The Exchange Adsorption of Ions from Aqueous Solutions by Organic Zeolites. II. Kinetics," *Journal of the American Chemical Society*, Vol. 69, No. 11, 1947, pp. 2836-2848.

[34] L. Khesami and R. Capart, "Removal of Chromium(VI) from Aqueous Solutions by Activated Carbons: Kinetic and Equilibrium Studies," *Journal of Hazardous Materials*, Vol. 123, No. 1-3, August 2005, pp. 223-231.

[35] Y. S. Ho and C. C. Wang, "Pseudo-Isotherms for the Sorption of Cadmium Ion onto Tree Fern," *Process Biochemistry*, Vol. 39, No. 6, February 2004, pp. 761-765.

[36] M. M. Dubinin, E. D. Zaverina and L. V. Radushkevich, "Sorption and Structure of Active Carbons. Adsorption of Organic Vapors," *Zhurnal Fizicheskoi Khimii*, Vol. 21, 1947, pp. 1351-1362.

J. Water Resource and Protection, **2010, 2, 898-906**
doi:10.4236/jwarp.2010.210107 Published Online October 2010 (http://www.SciRP.org/journal/jwarp)

Adsorption of Methyl Orange onto Chitosan from Aqueous Solution

Tapan Kumar Saha[1]*, Nikhil Chandra Bhoumik[1], Subarna Karmaker[1], Mahmooda Ghani Ahmed[1], Hideki Ichikawa[2], Yoshinobu Fukumori[2]
[1]*Department of Chemistry, Jahangirnagar University, Savar, Bangladesh*
[2]*Faculty of Pharmaceutical Sciences, Kobe Gakuin University, Chuo-ku, Japan*
E-mail: *tksaha_ju@yahoo.com*
Received August 8, 2010; *revised September* 7, 2010; *accepted September* 17, 2010

Abstract

Chitosan was utilized as adsorbent to remove methyl orange (MO) from aqueous solution by adsorption. Batch experiments were conducted to study the effects of pH, initial concentration of adsorbate and temperature on dye adsorption. The kinetic data obtained from different batch experiments were analyzed using both pseudo first-order and pseudo second-order equations. The equilibrium adsorption data were analyzed by using the Freundlich and Langmuir models. The best results were achieved with the pseudo second-order kinetic model and with the Langmuir isotherm equilibrium model. The equilibrium adsorption capacity (q_e) increases with increasing the initial concentration of dye and with decreasing pH. The values of q_e were found to be slightly increased with increasing solution temperatures. The activation energy (E_a) of sorption kinetics was found to be 10.41 kJ/mol. Thermodynamic parameters such as change in free energy (ΔG), enthalpy (ΔH) and entropy (ΔS) were also discussed.

Keywords: Adsorption, Kinetics, Chitosan, Anionic dyes, Wastewater

1. Introduction

With economic and technological development, water pollution is a common problem in worldwide. Water pollution has become more and more serious, especially regarding dye ions. Dye ions; mainly from dyeing industries have become serious threats to human beings and the aquatic ecosystem, due to their toxicity and persistence after being released into the natural water [1,2]. Therefore, discharge regulations are progressively becoming more stringent. Many recent studies have been focused on the development of efficient processes for the recovery of these organic contaminants from the effluents of textile industries [3-5]. Usually conventional techniques such as precipitation, coagulation and flocculation have been used in wastewater treatment although these techniques are not very efficient for removing several common dyes, especially from dilute solutions [3]. Photo-oxidation has also been proposed for the treatment of dye-containing effluents [4,5], however, this process is relatively expensive and not appropriate for the treatment of large flows. More recently, biological degradation has been cited as an alternative process for the decolorization of the reactive dye [6]. On the other hand, adsorption processes remain the most common useful techniques for the decontamination of the effluents of textile and dyeing industries. Many studies have been made on the possibility of adsorbents using mineral sorbents [7], activated carbons [8-10], peat [11,12], chitin [13-16], rice husk [17], soy meal hull [18] and agro wastes [19-21]. However, the adsorption capacity of the adsorbents is not very effective; to improve adsorption performance new adsorbents are still under development.

It is well known that chitosan (**Figure 1(a)**) has widely been used in the preparation of various biomedical products [22-24]. Chitosan is easily prepared from chitin by deacetylating its acetoamide groups with a strong alkaline solution. This is the most abundant biopolymer in nature after cellulose. The high proportions of amino functions in chitosan have been found to provide novel adsorption properties for many metal ions [25-27] and organic dyes [28-36]. The deacetylated amino groups in chitosan can be protonated and the polycationic properties of the polymer are expected to contribute to the charged interactions with a model dye, methyl orange (MO), which is an anionic azo dye (**Figure 1(b)**).

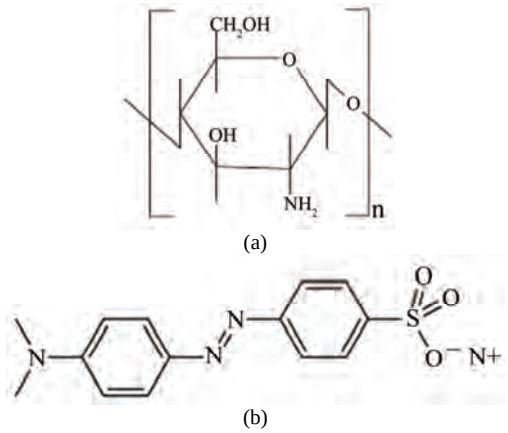

Figure 1. (a) The structures of chitosan 10B; (b) methyl orange (MO).

In this study, chitosan 10B (100% deacetylated) was used as an adsorbent to remove dye MO from aqueous solution. The investigation for dye removal was carried out through a series of batch adsorption experiments. The attention has been placed in an understanding of the kinetics; mechanisms and equilibrium processes involved in adsorption of MO onto the chitosan 10B. Treatment of the chitosan surface with a cross-linking agent was not utilized in this study since cross-linking may change the properties of chitosan. The effects of pH, initial concentration of MO and temperatures on the adsorption phenomena have been studied.

2. Materials and Methods

2.1. Chemicals and Preliminary Characterization of the Chitosan Sample

Chitosan 10B (100% deacetylated, Katokichi Bio Co., Ltd., Japan) was used without further purification. The mass median diameters of the chitosan flakes were estimated to be (228 ± 5) μm using a laser scattering particle size analyzer (LDSA-2400A, Tonichi Computer Applications, Japan) equipped with a dry dispersing apparatus (PD-10S, Tonichi Computer Applications, Japan).

The dye methyl orange (MO) was from Acros Organics (New Jersey, USA) and was used without further purification. The chemical structure of MO is shown in **Figure 1(b)**. The other reagents used in this study were of pure analytical grade. Deionized water was prepared by passing distilled water through a deionizing column (Barnstead, Syboron Corporation, Boston, USA).

2.2. Batch Adsorption Experiments

Batch adsorption experiments of MO were carried out in a 122 mL stoppered bottle at a constant temperature (33 ± 0.2°C) using a shaking thermostat machine at a speed of 120 r/min. The effect of pH on the adsorption of MO was examined by mixing 0.05 g of chitosan 10B with 25 mL of MO (100 μmol/L) solution with the pH ranging from 4.0 to 9.0. The pH of the samples was adjusted by adding micro liter quantities of 1 mol/L HCl or 1 mol/L NaOH. In kinetics studies, 0.05 g of chitosan 10B was mixed with 25 mL of MO solution with varied initial concentrations (15–100 μmol/L), and samples were withdrawn at desired time intervals. In isotherm experiments, 0.05 g of chitosan 10B was added to 25 mL of MO solution with varied initial concentrations (5–50 μmol/L).

After adsorption, the samples were centrifuged using a centrifuge machine (Labofuge 200, D-37520 Osterods, Germany) at a speed of 4000 r/min. The concentrations of MO in the supernatant liquor were determined by using standard curve. The absorbance of MO in aqueous solutions was measured with a Shimadzu UV-1601PC spectrophotometer at 465 nm, equipped with an electronically thermostatic cell holder (Shimadzu); the quartz cell had a path length of 1.0 cm. Before each measurement, the base line of spectrophotometer was calibrated against solvent. The standard curve was obtained by plotting absorbance versus concentration of MO.

The amount of MO adsorbed (q_e) was determined by using the following equation:

$$q_e = V(C_0 - C_e)/m \quad (1)$$

where C_0 and C_e represent the initial and equilibrium MO concentrations (μmol/L), respectively; V is the volume of the MO solution (L) and m is the amount (g) of chitosan 10B. The adsorption kinetics and equilibrium adsorption were also performed at different temperatures (27, 33, 40 and 45°C), respectively. The amount of adsorption was determined in the same way as described above.

3. Results and Discussion

3.1. Kinetics of Adsorption

3.1.1. Effect of pH

In order to avoid solubilization of the chitosan in aqueous solution at very low pH [37], adsorption experiments were conducted with the pH ranging from 4.0 to 9.0. The effect of pH on adsorption kinetics of MO onto chitosan 10B at 33°C is shown in **Figure 2**, where the initial dye concentration was 100 μmol/L. It indicates that the adsorption rate (dq/dt) and adsorption capacity (q_t) increase significantly with decrease in solution pH. After 240 min of adsorption, the equilibrium adsorption capacity (q_e) at pH 4.0 (30.14 μmol/g) is more than double of that at pH 9.0 (11.79 μmol/g) (**Table 1**). It can be seen that the pH

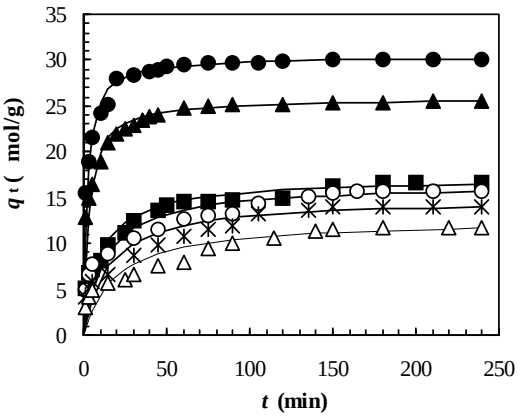

Figure 2. Adsorption kinetics of MO on chitosan 10B at different pH (initial concentration of MO: 100 μmol/L; solution volume: 25 mL; chitosan: 0.05 g; temperature: 33 °C; solution pHs: closed circles: pH 4; closed triangles: pH 5; closed squares: pH 6; opened circles: pH 7; stars: pH 8; opened triangles: pH 9). All solid lines are simulated adsorption kinetics of MO onto the chitosan at respective pHs. The simulated adsorption kinetic profiles were generated using the pseudo second-order model in Equation (3) and the values of equilibrium adsorption capacity ($q_{e(cal)}$) and the pseudo second-order rate constant (k_2) listed in Table 1.

of aqueous solution plays an important role in the adsorption kinetics of MO onto chitosan 10B and the most suitable pH is 4.0 among the observed pH ranging from 4.0 to 9.0. Similar results were also observed in the adsorption of reactive [32] and acid dyes [33] on cross-linked chitosan. **Figure 2** also shows that the time to reach equilibrium adsorption increases gradually with increase in pH of the aqueous solution. Our data show that the time to reach equilibrium adsorption is about 60 min for pH 4.0-5.0 and 120 min for pH 6.0-9.0, respectively.

3.1.2. Effect of Initial Dye Concentration

Figure 3 shows that the effect of initial MO concentration on the adsorption kinetics of the chitosan 10B at pH 4.0 and temperature 33°C. An increase in the initial dye concentration leads to an increase in the adsorption capacity of the dye on chitosan. This is due to the increase in the driving force of the concentration gradient, as an increase in the initial dye concentration [32]. **Figure 3** also shows that most of the dye is adsorbed to achieve equilibrium adsorption within 60 min, although the data were taken for 120 min. The equilibrium adsorption capacity (q_e) at an initial dye concentration of 100 μmol/L is nearly six times larger than that of 15 μmol/L (**Table 1**).

3.1.3. Effect of Temperature

The effect of temperature on adsorption kinetics of MO

Table 1. Comparison of the pseudo first- and second-order adsorption rate constants, and calculated and experimental q_e values for different pH, initial dye concentrations and temperatures.

Parameters	Experimental	First-order kinetic model			Second-order kinetic model		
pH	$q_{e(exp)}$ μmol/g	k_1 (per min)	$q_{e(cal)}$ μmol/g	R^2	k_2 (g/μmol per min)	$q_{e(cal)}$ μmol/g	R^2
4	30.14	0.0545	9.73	0.976	0.0164	30.39	0.999
5	25.52	0.0543	11.29	0.991	0.0127	25.84	0.999
6	16.58	0.0204	9.37	0.908	0.0059	17.09	0.996
7	15.75	0.3026	20.46	0.619	0.0049	16.47	0.994
8	14.02	0.0280	12.92	0.942	0.0046	14.84	0.990
9	11.79	0.0202	9.28	0.970	0.0042	12.58	0.993
Initial dye concentration (μmol/L) (pH 4.0)							
15	5.53	0.0764	2.71	0.986	0.0642	5.65	0.999
30	11.26	0.0893	4.61	0.982	0.0477	11.43	1.000
40	15.52	0.0693	4.99	0.942	0.0403	15.72	0.999
50	19.08	0.0736	6.85	0.973	0.0310	19.34	0.999
70	24.29	0.0741	10.09	0.994	0.0207	24.75	0.999
100	29.82	0.0545	9.72	0.976	0.0164	30.40	0.999
Temperature (°C) (pH 4.0)							
27	18.48	0.0771	7.83	0.927	0.0271	18.90	0.999
33	18.94	0.0755	6.92	0.973	0.0309	19.34	0.999
40	19.40	0.0755	6.65	0.974	0.0322	19.76	0.999
45	20.24	0.0810	6.63	0.971	0.0349	20.61	0.999

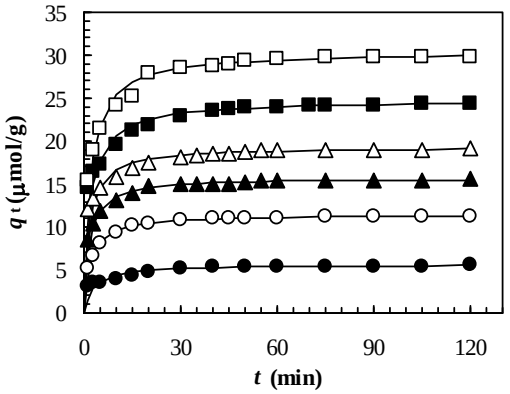

Figure 3. Adsorption kinetics of MO on chitosan 10B at different initial concentration. (solution volume: 25 mL; chitosan: 0.05 g; solution pH: 4; temperature: 33°C; initial concentrations of MO: closed circles: 15 μmol/L; opened circles: 30 μmol/L; closed triangles: 40 μmol/L; opened triangles: 50 μmol/L; closed squares: 70 μmol/L; opened circles: 100 μmol/L). All solid lines are simulated adsorption kinetics of MO onto the chitosan at respective initial concentrations of dye. The simulated adsorption kinetic profiles were generated using the pseudo second-order model in Equation (3) and the values of equilibrium adsorption capacity ($q_{e(cal)}$) and the pseudo second-order rate constant (k_2) listed in Table 1.

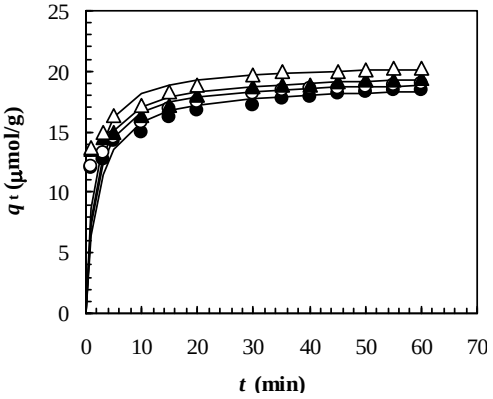

Figure 4. Adsorption kinetics of MO on chitosan 10B at different temperatures (initial concentration of MO: 50 μmol/L; solution volume: 25 mL; chitosan: 0.05 g; solution pH: 4; temperatures: closed circles: 27°C; opened circles: 33°C; closed triangles: 40°C; opened triangles: 45°C). All solid lines are simulated adsorption kinetics of MO onto the chitosan at respective temperature. The simulated adsorption kinetic profiles were generated using the pseudo second-order model in Equation (3) and the values of equilibrium adsorption capacity ($q_{e(cal)}$) and the pseudo second-order rate constant (k_2) listed in Table 1.

onto chitosan at pH 4.0 is shown in **Figure 4** where initial dye concentration was 50 μmol/L. Below and above the equilibrium time, an increase in the temperature leads to an increase in dye adsorption rate (dq/dt) and adsorption capacity (q_t), this indicates a kinetically controlling process. However, it can be seen from **Figure 4** that the temperature effects are insignificant. It has been reported that the variation of wastewater temperature does not significantly affect the overall decolorization performance [34]. However, a significant effect of temperature on the equilibrium isotherms was observed in the adsorption of trisodium 2-hydroxy-1,1'-azonaphthalene-3,4',6-trisulfonate onto chitosan [28] and of Acid Orange II (acid dye) onto the cross-linked chitosan [33].

3.2. Rate Constant Studies

In order to investigate the mechanism of adsorption kinetics, the pseudo first-order and pseudo second-order equations were used to test the experimental data of pH, initial concentration and temperature, respectively. The pseudo first-order rate expression of Lagergren and Annadurai and Krishnan [38,15] is given as:

$$\log(q_e - q_t) = \log q_e - (k_1/2.303)t \quad (2)$$

where q_e and q_t are the amounts of dye adsorbed on chitosan 10B at equilibrium and at time t, respectively (μmol/g), and k_1 is the rate constant of pseudo first-order adsorption (per min). A straight line of $\log(q_e - q_t)$ versus t suggests the applicability of this kinetic model to fit the experimental data. The equilibrium adsorption capacity (q_e) is required to fit the data, but in many cases q_e remains unknown due to slow adsorption processes. Also, in many cases, the pseudo first-order equation of Lagergren does not fit well to the whole range of contact time and is generally applicable over the initial stage of the adsorption processes [38,39].

The pseudo second-order kinetic model [39,40] is expressed as:

$$q_t = k_2 q_e^2 t/(1+ k_2 q_e t) \quad (3)$$

where k_2 (g/μmol per min) is the rate constant of pseudo second-order adsorption and can be determined from a linearized form of this equation, represented by Equation (4):

$$t/q_t = 1/k_2 q_e^2 + (1/q_e)t \quad (4)$$

If second-order kinetics is applicable, the plot of t/q_t versus t should show a linear relationship. There is no need to know any parameter beforehand and the equilibrium adsorption capacity (q_e) can be calculated from Equation (4). Contrary to the other model it predicts the behavior over the whole range of adsorption and is in agreement with an adsorption mechanism being the rate-controlling step [39,40], which may involve interactions between dye anions and adsorbent.

The slopes and y-intercepts of plots of $\log(q_e - q_t)$ versus t were used to determine the pseudo first-order rate constant (k_1) and equilibrium adsorption capacity

(q_e). These results are shown in **Table 1**. A comparison of results with the correlation coefficients (R^2) is also shown in **Table 1**. The values of R^2 for the pseudo first-order kinetics model were low. Also, the calculated q_e values obtained from the pseudo first-order kinetic model do not give reasonable values, which are too low compared with experimental q_e values (**Table 1**). These results suggest that the adsorption of dye MO onto the chitosan 10B is not a pseudo first-order reaction.

The slopes and *y*-intercepts of plots of t/q_t versus t were used to calculate the pseudo second-order rate constant k_2 and q_e. The straight lines in plot of t/q_t versus t (**Figure 5**) show a good agreement of experimental data with the pseudo second-order kinetic model for different initial dye concentrations. The similar straight-line agreements are also observed for data at different pH and temperature although their plots are not shown in this paper. The computed results obtained from the pseudo second-order kinetic model are shown in **Table 1**. The values of correlation coefficients (R^2) for the pseudo second-order kinetic model are ≥ 0.999 for almost all the cases. The values of calculated equilibrium adsorption capacity ($q_{e(cal)}$) also agree very well with experimental data (**Table 1**). Moreover, the experimental adsorption kinetic profiles (**Figures 2**, **3** and **4**) are perfectly reproduced in the simulated data (each solid line in **Figures 2**, **3** and **4**) obtained from numerical analysis on the basis of pseudo second-order kinetic model (Equation (3)) using the values of k_2 and $q_{e(cal)}$ listed in **Table 1**. These results indicate that the present adsorption system belongs to the pseudo second-order kinetic model. The similar phenomena were also observed in biosorption of reactive blue 2 (RB2), reactive yellow 2 (RY2) and Remazol black B on biomass [20,21]. According to the pseudo second-order model, the adsorption rate dq/dt is proportional to the second-order of ($q_e - q_t$). Since the chitosan 10B in our experiments have relatively high values of q_e (**Table 1**), the adsorption rates become very fast and the equilibrium times are short. Such short equilibrium times coupled with high adsorption capacity indicate a high degree of affinity between the dye MO and the chitosan 10B [20].

The rate constant k_2 at different temperatures listed in **Table 1** was used to estimate the activation energy of the MO adsorption onto chitosan 10B. Assume that the correlation among the rate constant (k_2), temperature (T) and activation energy (E_a) follows the Arrhenius equation, which induces the following expression:

$$\ln k_2 = - E_a/R\ (1/T) + \text{const} \qquad (5)$$

where R is the gas constant. The slope of plot of $\ln k_2$ versus $1/T$ was used to evaluate E_a. The value of E_a was estimated to be 10.41 kJ/mol. This value seems to be small and the adsorption rate is not very sensitive to temperature in the range (27−45°C) we studied.

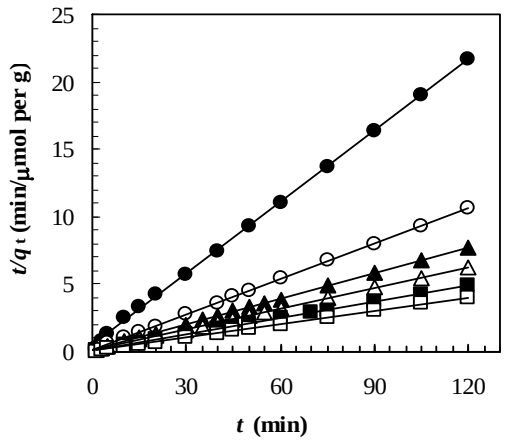

Figure 5. Plot of the pseudo second-order model (t/q_t versus t) at different initial dye concentration. (closed circles: 15 μmol/L; opened circles: 30 μmol/L; closed triangles: 40 μmol/L; opened triangles: 50 μmol/L; closed squares: 70 μmol/L; opened circles: 100 μmol/L).

3.3. Equilibrium Adsorption

Adsorption isotherms describe how adsorbates interact with adsorbents and so are critical in optimizing the use of adsorbents. Thus, the correlation of equilibrium data by either theoretical or empirical equations is essential to the practical design and operation of adsorption systems. A plot of the equilibrium adsorption capacity, q_e (μmol/g), versus the liquid phase MO equilibrium concentration, C_e (μmol/L), for various temperatures at pH 4 is shown in **Figure 6**. The adsorption capacities of the chitosan increased slightly when the solution temperature was increased from 27 to 45 °C. The isotherm constants obtained from the linearized plots of Freundlich and Langmuir equations and the values of correlation coefficients (R^2) are discussed in the following sections.

3.3.1. Freundlich Isotherm

The well-known Freundlich isotherm [41] used for isothermal adsorption is a special model for heterogeneous surface energy in which the energy term in the Langmuir equation varies as a function of surface coverage strictly due to variation of the sorption. The Freundlich equation is given as:

$$q_e = K_F C_e^{1/n} \qquad (6)$$

Equation (6) can be linearized by taking logarithms to find out the parameters K_F and $1/n$.

$$\ln(q_e) = (1/n)\ln C_e + \ln K_F \qquad (7)$$

where K_F is roughly an indicator of the adsorption capacity and $1/n$ of the adsorption intensity. K_F and $1/n$ can be determined from the linear plot of $\ln(q_e)$ versus $\ln(C_e)$. The calculated results are listed in **Table 2**. The magni

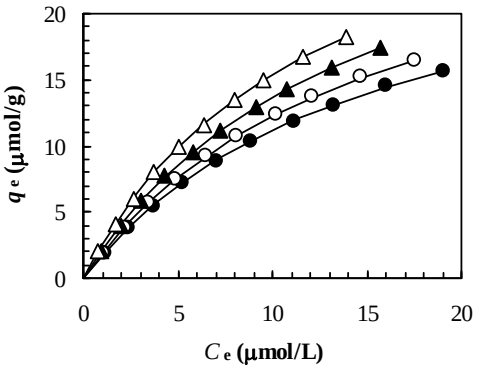

Figure 6. Equilibrium adsorption of MO on chitosan 10B at different temperatures (initial concentration of MO: 5-50 μmol/L; solution volume: 25 mL; chitosan: 0.05 g; solution pH: 4; temperatures: closed circles: 27°C; opened circles: 33°C; closed triangles: 40°C; opened triangles: 45°C). All solid lines are simulated equilibrium adsorption of MO onto the chitosan at respective temperature. The simulated equilibrium adsorption isotherms were generated using the Langmuir model in Equation (8) and the Langmuir isotherm constants listed in Table 2.

tude of the exponent 1/*n* gives an indication of the favorability of adsorption. From **Table 2**, the exponent *n* is larger than 1 for adsorption of MO onto the chitosan at different temperatures indicating favorable adsorption condition [14]. However, the low values correlation coefficients ($R^2 < 0.999$) show poor agreement of Freundlich isotherm with the experimental data.

3.3.2. Langmuir Isotherm

The widely used Langmuir isotherm [42] has found successful application in many real sorption processes and is expressed as:

$$q_e = K_L C_e/(1 + a_L C_e) \quad (8)$$

The constants K_L and a_L are the characteristics of the Langmuir equation and can be determined from a linearized form of this equation, represented by Equation (9):

$$C_e/q_e = 1/K_L + (a_L/K_L)C_e \quad (9)$$

Therefore, a plot of C_e/q_e versus C_e gives a straight line of slope a_L/K_L and *y*-intercept $1/K_L$. The constant K_L is the equilibrium constant and the ratio a_L/K_L gives the inverse of theoretical monolayer saturation capacity (q_m).

A linearized plot of (C_e/q_e) versus C_e is obtained from the model as shown in **Figure 7**. The values of K_L and a_L are computed from the slopes and *y*-intercepts of different straight lines representing at different temperatures. The calculated results are shown in **Table 2**. The fits are quite well for all the four different temperatures under the concentration range studied (correlation coefficient, $R^2 > 0.999$). From the results shown in **Table 2**, the capacities of the chitosan for dye adsorption are not significantly dependent on the solution temperature although the values of K_L and q_m slightly increase when the solution temperature was increased from about 27 to 45°C. These results also suggest that the dye-chitosan interaction must be an endothermic process.

In an effort to understand the equilibrium processes involved in MO adsorption onto the chitosan, a computer simulation of the adsorption isotherms has been performed numerically on the basis of the Langmuir model in Equation (8) and using the Langmuir isotherm constants listed in **Table 2**, and the results are compared with the experimental data (**Figure 6**). The observed curves were obtained from the plots of equilibrium adsorption capacity, q_e (μmol/g), versus the liquid phase MO equilibrium concentration, C_e (μmol/L), at different temperatures. The simulated curves (all solid lines) were obtained as described as stated. The adsorption capacities of the chitosan increased slightly when the solution tem-

Table 2. Freundlich and Langmuir isotherm constants at different temperatures, and thermodynamic parameters for the adsorption of dye MO onto chitosan from aqueous solution at pH 4.

Parameters	Freundlich			Langmuir			
Temperature (°C)	K_F (μmol/g)	n (g/L)	R^2	K_L (L/g)	a_L(L/μmol)	q_m (μmol/g)	R^2
27	1.9776	1.36	0.991	1.8386	0.0647	28.41	0.999
33	2.1338	1.33	0.991	2.0292	0.0657	30.86	0.999
40	2.3556	1.31	0.991	2.3031	0.0684	33.67	0.999
45	2.7385	1.32	0.991	2.7617	0.0793	34.83	0.999
Thermodynamic parameters							
Temperature (°C)	ΔG (kJ/mol)		ΔH (kJ/mol)		ΔS (J/K/mol)		R^2
27	–1.52						
33	–1.80		17.29		62.52		0.960
40	–2.17						
45	–2.68						

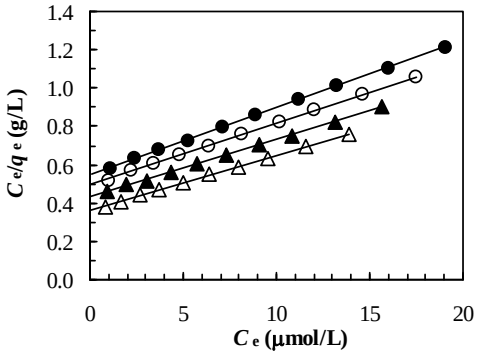

Figure 7. Plot of Langmuir model (C_e/q_e versus C_e) at different temperatures (closed circles: 27°C; opened circles: 33 °C; closed triangles: 40°C; opened triangles: 45°C).

perature was increased from 27 to 45°C. These features of the observed data are well reproduced in the simulated data as shown in **Figure 6**, supporting that the all isotherms data are described well by the Langmuir equation.

The thermodynamic parameters such as change in free energy (ΔG), enthalpy (ΔH) and entropy (ΔS) were determined using the following equations [35]:

$$\Delta G = -RT\ln K_L \quad (9)$$

$$\ln K_L = \Delta S/R - \Delta H/RT \quad (10)$$

where K_L is the equilibrium constant, T is the solution temperature (K) and R is the gas constant. ΔH and ΔS were calculated from the slope and y-intercept of van't Hoff plots of $\ln K_L$ vs. $1/T$. The results are presented in **Table 2**. The negative values of ΔG and positive value of ΔH indicate that the adsorption of MO on chitosan 10B is spontaneous and an endothermic process. These behaviors seem to be explained by the ionic-nature of the dye MO-chitosan interaction [16,36]. The positive value of ΔS suggests that entropy is responsible for making the ΔG negative for the adsorption process to be spontaneous.

4. Conclusions

The kinetics and adsorption mechanism of methyl orange (MO) onto chitosan 10B were studied in the present work. Batch experiments showed that both the initial dye concentration and the pH of aqueous solutions significantly affect the adsorption capacity of dye MO on the chitosan 10B. However, the adsorption kinetics of the dye on chitosan is slightly influenced by the temperature. The pseudo second-order kinetic model agrees very well with the dynamical behavior for the adsorption of dye MO on chitosan flakes under several different pHs, initial dye concentrations and temperatures in the whole ranges we studied. The q_e values calculated from this kinetic model are very similar to the experimental q_e values obtained from several experiments as shown in **Table 1**. Moreover, the experimental adsorption kinetic profiles are perfectly reproduced in the simulated data obtained from numerically on the basis of the pseudo second-order kinetic model in Equation (3) and using the isotherm constants listed in **Table 1**. On the contrary, the pseudo first-order kinetic model fits the experimental data poorly for the entire range under study. The Langmuir equation is the best-fit equilibrium isotherm for the sorption of dye MO onto chitosan based on a linearized correlation coefficient. The experimental adsorption isotherms also are perfectly reproduced in the simulated data obtained from numerical analysis on the basis of the Langmuir model in Equation (8) and using the Langmuir isotherm constants listed in **Table 2**. The Gibbs free energy (ΔG) demonstrated that the adsorption process is favorable for the interaction cited and the pronounced chitosan-dye interaction is reflected in the positive values of entropy (ΔS).

It may be concluded that chitosan may be used as a low-cost, natural and abundant source for the removal of anionic azo dyes from water and wastewater as an alternative to more costly materials such as activated carbon.

5. References

[1] M. S. Tsuboy, J. P. F. Angeli, M. S. Mantovani, S. Knasmueller, G. A. Umbuzeiro and L. R. Ribeiro, "Genotoxic, Mutagenic and Cytotoxic Effects of the Commercial Dye CI Disperse Blue 291 in the Human Hepatic Cell Line HepG2," *Toxicology in Vitro*, Vol. 21, No. 8, 2007, pp. 1650-1655.

[2] S. Vinitnantharat, W. Chartthe and A. Pinisakul, "Toxicity of Reactive Red 141 and Basic Red 14 to Algae and Waterfleas," *Water Science and Technology*, Vol. 58, No. 6, 2008, pp. 1193-1198.

[3] Z. Raïs, L. El Hassani, J. Maghnouje, M. Hadji, R. Ibnelkhayat, R. Nejjar, A. Kherbeche and A. Chaqroune, "Dyes' Removal from Textile Wastewater by Phosphogypsum Using Coagulation and Precipitation Method," *Physics and Chemistry News*, Vol. 7, 2002, pp. 100-109.

[4] A. Rezaee, M. T. Ghaneian, S. J. Hashemian, G. Moussavi, A. Khavanin and G. Ghanizadeh, "Decolorization of Reactive Blue 19 Dye from Textile Wastewater by the UV/H_2O_2 Process," *Journal of Applied Sciences*, Vol. 8, No. 6, 2008, pp. 1108-1112.

[5] J. Racyte, M. Rimeika and H. Bruning, "pH Effect on Decolorization of Raw Textile Wastewater Polluted with Reactive Dyes by Advanced Oxidation with UV/H_2O_2," *Environmental Protection Engineering*, Vol. 35, No. 3, 1999, pp. 167-178.

[6] R. Saraswathi and M. K. Saseetharan, "Investigation on Microorganisms and their Degradation Efficiency in Paper and Pulp Mill Effluent," *Journal of Water Resource and Protection*, Vol. 2, No. 7, 2010, pp. 660-664.

[7] C. Varlikli, V. Bekiari, M. Kus, N. Boduroglu, I. Oner, P. Lianos, G. Lyberatos and S. Icli, "Adsorption of Dyes on Sahara Desert Sand," *Journal of Hazardous Materials*,

Vol. 170, No. 1, 2009, pp. 27-34.

[8] A. Rodriguez, J. Garcia, G. Ovejero and M. Mestanza, "Adsorption of Anionic and Cationic Dyes on Activated Carbon from Aqueous Solutions: Equilibrium and Kinetics," *Journal of Hazardous Materials*, Vol. 172, No. 2-3, 2009, pp. 1311-1320.

[9] G. McKay, "The Adsorption of Dyestuffs from Aqueous Solution Using Activated Carbon: Analytical Solution for Batch Adsorption Based on External Mass Transfer and Pore Diffusion," *Chemical Engineering Journal*, Vol. 27, No. 3, 1983, pp. 187-196.

[10] K. C. L. N. Rao and K. K. Ashutosh, "Color Removal from a Dyestuff Industry Effluent using Activated Carbon," *Indian Journal of Chemical Technology*, Vol. 1, No. 1, 1994, pp. 13-19.

[11] A. N. Fernandes, C. A. P. Almeida, C. T. B. Menezes, N. A. Debacher and M. M. D. Sierra, "Removal of Methylene Blue from Aqueous Solution by Peat," *Journal of Hazardous Materials*, Vol. 144, No. 1-2, 2007, pp. 412-419.

[12] K. R. Ramakrishna and T. Viraraghavan, "Dye Removal using Low Cost Adsorbents," *Water Science and Technology*, Vol. 36, No. 2-3, 1997, pp. 189-196.

[13] R. Dolphen, N. Sakkayawong, P. Thiravetyan and W. Nakbanpote, "Adsorption of Reactive Red 141 from Wastewater onto Modified Chitin," *Journal of Hazardous Materials*, Vol. 145, No. 1-2, 2007, pp. 250-255.

[14] G. McKay, H. S. Blair and J. R. Gardner, "Adsorption of Dyes on Chitin. I. Equilibrium Studies," *Journal of Applied Polymer Science*, Vol. 27, No. 8, 1982, pp. 3043-3057.

[15] G. Annadurai and M. R. V. Krishnan, "Adsorption of Acid Dye from Aqueous Solution by Chitin: Batch Kinetic Studies," *Indian Journal of Chemical Technology*, Vol. 4, 1997, pp. 213-222.

[16] E. Longhinetti, F. Pozza, L. Furlan, M. D. N. D. Sanchez, M. Klug, M. C. M. Laranjeira and V. T. Favere, "Adsorption of Anionic Dyes on the Biopolymer Chitin," *Journal of Brazilian Chemical Society*, Vol. 9, No. 5, 1998, pp. 435-440.

[17] A. K. Chowdhury, A. D. Sarkar and A. Bandyopadhyay, "Rice Husk Ash as a Low Cost Adsorbent for the Removal of Methylene Blue and Congo Red in Aqueous Phases," *Clean*, Vol. 37, No. 7, 2009, pp. 581-591.

[18] M. Arami, N. Y. Limaee, N. M. Mahmoodi and N. S. Tabrizi, "Equilibrium and Kinetics Studies for the Adsorption of Direct and Acid Dyes from Aqueous Solution by Soy Meal Hull," *Journal of Hazardous Materials*, Vol. 135, No. 1-3, 2006, pp. 171-179.

[19] K. S. Mundhe, A. A. Bhave, R. C. Torane, N. R. Deshpande and R. V. Kashalkar, "Removal of Cationic Dye from Aqueous Solution using Raw Agro Wastes as Non–Conventional Low–Cost Adsorbent," *Oriental Journal of Chemistry*, Vol. 25, No. 4, 2009, pp. 953-959.

[20] Z. Aksu and S. Tezer, "Equilibrium and Kinetic Modeling of Biosorption of Remazol Black B by Rhizopus Arrhizus in a Batch System: Effect of Temperature," *Process Biochemistry*, Vol. 36, No. 5, 2000, pp. 431-439.

[21] Z. Aksu, "Biosorption of Reactive Dyes by Dried Activated Sludge: Equilibrium and Kinetic Modeling," *Biochemical Engineering Journal*, Vol. 7, No. 1, 2001, pp. 79-84.

[22] T. K. Saha, H. Ichikawa and Y. Fukumori, "Gadolinium Diethylenetriaminopetaacetic Acid-Loaded Chitosan Microspheres for Gadolinium Neutron-Capture Therapy," *Carbohydrate Research*, Vol. 341, No. 17, 2006, pp. 2835-2841.

[23] N. Bhattarai, J. Gunn and M. Zhang, "Chitosan-Based Hydrogels for Controlled, Localized Drug Delivery," *Advanced Drug Delivery Reviews*, Vol. 62, No. 1, 2010, pp. 83-99.

[24] M. Manconi, S. Mura, M. L. Manca, A. M. Fadda, M. Dolz, M. J. Hernandez, A. Casanovas and O. Díez-Sales, "Chitosomes as Drug Delivery Systems for C-Phycocyanin: Preparation and Characterization," *International Journal of Pharmaceutics*, Vol. 392, No. 1-2, 2010, pp. 92-100.

[25] K. H. Chu, "Removal of Copper from Aqueous Solution by Chitosan in Prawn Shell: Adsorption Equilibrium and Kinetics," *Journal of Hazardous Materials*, Vol. 90, No. 1, 2002, pp. 77-95.

[26] P. Miretzky and A. Fernandez Cirelli, "Hg(II) Removal from Water by Chitosan and Chitosan Derivatives: A Review," *Journal of Hazardous Materials*, Vol. 167, No. 1-3, 2009, pp. 10-23.

[27] J. R. Rangel-Mendez, R. Monroy-Zepeda, E. Leyva-Ramos, P. E. Diaz-Flores and K. Shirai, "Chitosan Selectivity for Removing Cadmium(II), Copper(II), and Lead(II) from Aqueous Phase: pH and Organic Matter Effect," *Journal of Hazardous Materials*, Vol. 162, No. 1, 2009, pp. 503-511.

[28] T. K. Saha, S. Karmaker, H. Ichikawa and Y. Fukumori, "Mechanisms and Kinetics of Trisodium 2-hydroxy-1, 1'-azonaphthalene-3,4',6-trisulfonate Adsorption onto Chitosan," *Journal of Colloid and Interface Science*, Vol. 286, No. 2, 2005, pp. 433-439.

[29] P. R. Modak, K. S. Singh and D. A. Connor, "Experimental Study on the Elimination of Colour and Organic Matter from Wastewater Using an Inexpensive Biomaterial, Chitosan," *Water Quality Research Journal of Canada*, Vol. 44, No. 3, 2009, pp. 295-306.

[30] A. H. Chen and Y. Y. Huang, "Adsorption of Remazol Black 5 from Aqueous Solution by the Templated Crosslinked-Chitosans," *Journal of Hazardous Materials*, Vol. 177, No. 1-3, 2010, pp. 668-675.

[31] N. K. Lazaridis, G. Z. Kyzas, A. A. Vassiliou and D. N. Bikiaris, "Chitosan Derivatives as Biosorbents for Basic Dyes," *Langmuir*, Vol. 23, No. 14, 2007, pp. 7634-7643.

[32] M.-S. Chiou and H.-Y. Li, "Equilibrium and Kinetic Modeling of Adsorption of Reactive Dye on Cross-Linked Chitosan Beads," *Journal of Hazardous Materials*, Vol. 93, No. 2, 2002, pp. 233-248.

[33] H. Yoshida, A. Okamoto and T. Kataoka, "Adsorption of Acid Dye on Cross-Linked Chitosan Fibers: Equilibria," *Chemical Engineering Science*, Vol. 48, No. 12, 1993, pp. 2267-2272.

[34] M. N. V. R. Kumar, "A Review of Chitin and Chitosan Applications," *Reactive and Functional Polymers*, Vol. 46, No. 1, 2000, pp. 1-27.

[35] M. S. Chiou and H. Y. Li, "Adsorption Behavior of Reactive Dye in Aqueous Solution on Chemical Cross-Linked Chitosan Beads," *Chemosphere*, Vol. 50, No. 8, 2003, pp. 1095-1105.

[36] F. S. C. dos Anjos, E. F. S. Vieira and A. R. Cestari, "Interaction of Indigo Carmine Dye with Chitosan Evaluated by Adsorption and Thermochemical Data," *Journal of Colloid and Interface Science*, Vol. 253, No. 2, 2002, pp. 243-246.

[37] R. A. A. Muzzarelli, "Natural Chelating Polymers: Alginic Acid, Chitin and Chitosan," Pergamon, Oxford, 1973.

[38] S. Lagergren, "Zur Theorie der Sogenannten Adsorption Geloster Stoffe," *K. Sven. Vetenskapsakad. Handl.*, Vol. 24, No. 4, 1898, pp. 1-39.

[39] G. McKay and Y. S. Ho, "The Sorption of Lead(II) on Peat," *Water Research* , Vol. 33, No. 2, 1999, pp. 578-584.

[40] G. McKay and Y. S. Ho, "Pseudo-Second Order Model for Sorption Processes," *Process Biochemistry*, Vol. 34, No. 5, 1999, pp. 451-465.

[41] H. Freundlich, "Adsorption Solution," *Zeitschrift für Physikalische Chemie*, Vol. 57, 1906, pp. 384-470.

[42] I. Langmuir, "Adsorption of Gases on Plain Surfaces of Glass Mica Platinum," *Journal of American Chemical Society*, Vol. 40, No. 9, 1918, pp. 1361-1403.

J. Water Resource and Protection, **2010, 2, 907-915**
doi:10.4236/jwarp.2010.210108 Published Online October 2010 (http://www.SciRP.org/journal/jwarp)

Water Quality Assessment, Trophic Classification and Water Resources Management

Arkadi Parparov[1*], Gideon Gal[1], David Hamilton[2], Peter Kasprzak[3], Alexandr Ostapenia[4]
[1]*Israel Oceanographic and Limnological Research, Kinneret Limnological Laboratory, Migdal, Israel*
[2]*Centre for Biodiversity and Ecology Research, University of Waikato, Waikato, New Zealand*
[3]*Leibniz-Institute of Freshwater Ecology & Inland Fisheries, Department of Stratified Lakes, Neuglobsow, Germany*
[4]*Belarus State University, Laboratory of Hydroecology, Minsk, Belarus*
E-mail: *parpar@ocean.org.il*
Received July 19, 2010; *revised August* 9, 2010; *accepted August* 18, 2010

Abstract

Quantification of water quality (WQ) is an integral part of scientifically based water resources management. The main objective of this study was comparative analysis of two approaches applied for quantitative assessment of WQ: the trophic level index (TLI) and the Delphi method (DM). We analyzed the following features of these conceptually different approaches: A. similarity of estimates of lake WQ; B. sensitivity to indicating disturbances in the aquatic ecosystem structure and functioning; C. capacity to reflect the impact of major management measures on the quality of water resources. We compared the DM and TLI based on results from a series of lakes covering varying productivity levels, mixing regimes and climatic zones. We assumed that the conservation of aquatic ecosystem in some predefined, "reference", state is a major objective of sustainable water resources management in the study lakes. The comparison between the two approaches was quantified as a relationship between the DM ranks and respective TLI values. We show that being a classification system, the TLI does not account for specific characteristics of aquatic ecosystems and the array of different potential uses of the water resource. It indirectly assumes that oligotrophication is identical to WQ improvement, and reduction of economic activity within the lake catchment area is the most effective way to improve WQ. WQ assessed with the TLI is more suitable for needs of natural water resources management if eutrophication is a major threat. The DM allows accounting for several water resource uses and therefore it may serve as a more robust and comprehensive tool for WQ quantification and thus for sustainable water resources management.

Keywords: Water Quality, Trophic Level Index, Delphi Method, Sustainable Management, Lakes

1. Introduction

The most challenging problem of modern theoretical and applied hydroecology is to understand the fundamental principles of ecology for its application in effective management of water resources for both hydrological availability and water quality [1]. Quality is not absolute; the terms "good" or "poor" water quality have meaning only in relation to the use of water and the assessment of the user. Quantification of water quality (WQ) aims at describing the condition of a water body with reference to human needs. Investigations of the eutrophication phenomenon in the 1960s and 1970s, resulted in quantification of a trophic classification system [2,3]. WQ has been considered synonymous with 'trophic status' in many cases [4-6]. Further progress in WQ assessment is associated with implementation of optimization approaches to establishment of the natural resource sustainable management policies contributing to conservation of aquatic ecosystems within some desired reference condition [1,7]. We analyze and compare two key approaches to WQ quantification in relation to the increasing need for natural water resources management. The approaches include:

1) Quantitative modification of the expert panel method developed by Horton [8] and Ott [9] and integrated into the Delphi method (DM [10]). In the DM, the WQ ranking is completely defined by the needs of the water

resources uses and management [11]. DM has been implemented to WQ assessment for several natural waterbodies in the USA [12,13], New Zealand [14], Belarus [15] and Israel [16];

2) The trophic classification method [2] and its modification, the Trophic Level Index [4] (hereafter termed 'TLI'). This approach involves ranking lakes according to their productivity and nutrient regimes and thereby evaluating WQ changes based solely on *trophic state* responses to various forcing factors (e.g., nutrient loading), the TLI in many cases serves as a monitoring tool [17-19].

Comparative studies of the Delphi and TLI approaches to WQ assessment for water resources management are not available in the literature. In this study, we compare the DM and TLI using a quantitative WQ assessment based on results from a series of lakes covering varying productivity levels, mixing regimes and climatic zones. The lakes include Kinneret (Israel), Stechlin (Germany), Naroch Lakes (Belarus) and Rotorua Lakes (New Zealand), all of which have extensive databases, are major focal points for regional lake management. We will search for a reply to the following questions: Do these conceptually different approaches provide similar estimates of lake WQ? Do these approaches successfully indicate disturbances in the aquatic ecosystem structure and functioning? How well do these approaches reflect the impact of major management measures on the quality of water resources?

2. Material and Methods

2.1. Water Quality Assessment for Water Resources Management Purposes

Quantitative assessment of WQ should be based on the following principles [11]:

1) WQ system consists of water quality indices (WQI), and their permissible ranges corresponding to acceptable WQ.

2) The following functional correspondences should be established: between the ecological values of the WQI (e.g. nutrient concentration or Secchi depth) and some numeric rating value (R): R = f(WQI); between WQI and the intensity of the management measures (MM. e.g., economic activity in the watershed and water supply): WQI = Φ(MM). These two relationships allow establishment of a direct relationship between WQ and the management measures: R = F(MM)

3) Any system of WQ is subjective, reflecting a compromise between different stake holders and partners in water resources use and management.

4) An established WQI system should serve as a common language for all partners using a water resource, and in this sense, it is a tool for water resources management. Quantified WQ should also serve as a management target.

2.2. Brief Description of Study Lakes

Lake Kinneret (Israel) is a subtropical meso-eutrophic lake located at about an altitude of -210 m (*i.e.*, below mean sea level). The lake water level depends on climatic inputs and withdrawal for water supply. Limnology of the lake is well documented [20]. The WQ system for conservation of L. Kinneret was assessed with the Delphi method [16]. The major environmental threat to the conservation of the lake ecosystem is the progressive lowering of its water level. The most critical issue for lake ecosystem stability and WQ is the progressively increasing proportion of cyanobacteria amongst the algal assemblage [21] and increase of water salinity above an assigned acceptable level of 240 mg Cl l^{-1}.

The Naroch Lakes (Belarus) consist of three connected lakes: Batorino (eutrophic), Miastro (meso-eutrophic) and Naroch (oligo-mesotrophic). The Naroch Lakes has been intensely studied [22]. The WQ system for the Naroch Lakes was also established based on the Delphi method [15].

Lakes Rotorua and Rotoiti are two lakes that form part of a complex of volcanic lakes known collectively as the Rotorua Lakes, in the North Island of New Zealand. A Trophic Level Index is assigned from routine monitoring conducted in the Rotorua Lakes [19] and is used as a basis for the implementation and assessment of management actions for the lakes [4]. An attempt to assess WQ has also been made using the Delphi method for Lakes Rotorua and Rotoiti (Hamilton and Parparov, unpublished data).

Lake Stechlin (Germany) is one of the few remaining oligotrophic clear-water lakes in Germany's South-Baltic Lake District. Long-term monitoring indicates significant changes in the structure and function of the lake ecosystem especially throughout the past two decades. The changes relate to a decrease in oxygen concentration in the deeper hypolimnion accompanied with substantial increase of hypolimnetic phosphorus concentration, and a trend of increasing of chlorophyll *a* concentration [23,24]. An attempt to assess WQ based on the Delphi method for Lake Stechlin has recently been completed (Kasprzak, unpublished data).

Relevant limnological properties of the study lakes are summarized in **Table 1**. In this study we use the following data sets: for Lake Kinneret - 1991 to 2008, Naroch

Table 1. Limnological variables for the study lakes. For the Naroch Lakes, the first value relates to the period from 1979 to 1982 and the second to the period from 1988 to 2000.

Parameters	Lakes						
	Kinneret₪	*Naroch Lakes*†			*Rotorua Lakes*£		*Stechlin*€
		Naroch	*Miastro*	*Batorino*	*Rotoiti*	*Rotorua*	
Surface area, km^2	160	79.6	13.1	6.3	33.5	80	4.3
Average depth, m	22-24*	8.9	5.3	2.8	31.5	10.5	22.8
Secchi depth, m	2.3	5.1/6.1	1.7/3.8	0.8/1.1	5.3	2.4	8.5
Total Nitrogen mg l^{-1}	0.6	0.9/0.4	1.1/0.7	1.6/0.9	0.3	0.3	0.45
Total Phosphorus μg l^{-1}	20	28/16	52/34	84/44	26	32	10
Chl *a*, μg l^{-1}	18.0	4.9/2.0	20.0/4.9	50/31	6.7	11.7	1.0-4.0
Primary production, g C m^{-2} yr^{-1}	650	78/81	142/218	140/200	431	800	110-205

*- depending on climate conditions; ₪ - [20,30]; † - [22]; £ - [31,32]; € - [23,24]

Lakes - 1979 to 2008, Rotorua Lakes - 1990 to 2005, and Lake Stechlin - 1992 to 2006.

2.3. Methodology of Trophic Level Index and Delphi Methods of Water Quality Assessment

In the DM, WQ has five grades: from "very bad" (Rating 0 to 20) to "excellent" (Rating 80 to 100) [10,14]. The correspondence between the ecological values of WQI (e.g., nutrient concentration or Secchi depth) and some numeric Rating value ($0 < R < 100$) was established in a form of a rating curve. Long-term monitoring data, including frequency distributions, means and standard deviations of limnological parameters in the studied lakes were provided to separate expert panels for each lake. The experts assessed the "reference state" for each lake as a set of variables corresponding to time periods when lake water resource was suitable for all purposes (e.g., domestic water supply, recreation, fisheries). The panels were asked to choose about 10 parameters most indicative of WQ in the studied lakes, and to construct rating curves for each parameter, spanning the entire range of values observed in the lake. "Acceptable ranges" for the separate water quality indices were restricted to the range 60-100. Rating curves from individual panel members were averaged for each index. Piece-wise approximations of ratings and parameter values were used to construct graphic presentations of the temporal dynamics of the WQIs [16].

In the TLI, lake trophic state is *classified* by seven *types*: from "ultramicrotrophic" (rank 1) to "hypertrophic" (rank 7) [2,4]. Traditionally, the users of the TLI establish a correspondence between *trophic status* and *water quality, i.e., by default* oligotrophic lakes are considered to be of "good" water quality, and eutrophic lakes of "bad" water quality. Initially, the TLI system included three indices: Secchi depth (SD), concentrations of total phosphorus (TP) and chlorophyll *a* (Chl) [2]. This system has subsequently been supplemented with total nitrogen (TN) concentration [4]. The correspondence between ecological and Trophic Level values for individual indices (TL_i) was established in the form of a logarithmic function connecting the TL to four "trophic" parameters [2,4]:

$$TL_i = a_i + b_i LOG(Par_i) \quad (1)$$

where 'i' varies from 1 to 4, Par_i means SD, TN, TP and Chl, and 'a' and 'b' are coefficients.

For the objectives of this study, the TL varies from a value of 2 (oligotrophic = "excellent") to 7 (hypertrophic = "very bad") (we omitted the grade of 1, 'ultramicrotrophic', as irrelevant for this study). A similar correspondence in the DM is described by the rating curve R = f(WQI), in which the values of the WQ rating vary from 100 ("excellent") to 0 ("very bad"). The comparison between two systems was quantified as a relationship between the DM ranks and respective TL values:

$$R[TL] = 140 - 20*TL \quad (2)$$

The permissible range of the WQI can then be defined from the following expression: $60 \le R[WQI] \le 100$

We assumed that the conservation of aquatic ecosystem in some predefined, "reference", state is a major objective of sustainable water resources management in the study lakes. For the objectives of this study we used an operational definition of "sustainable management" suggested earlier [15], where water resources management should allow use of water resources while maintaining the quality of the resource in question within defined permissible ranges, *i.e.*,

$$\{WQI_L < WQI < WQI_H\} \Leftrightarrow \{MM_L < MM < MM_H\} \quad (3)$$

where 'L' and 'H' correspond to the lower and upper permissible values of the WQ index and Management Measure, and $\Leftrightarrow$ means correspondence. The set of management measures corresponding to (3) forms the basis for a "sustainable management policy".

In the TLI, an aggregated WQ (TLI) is calculated as an arithmetic mean of four "trophic" indices [4]:

$$TLI = (TL_{Chl} + TL_{SD} + TL_{TP} + TL_{TN})/4 \quad (4)$$

Accounting for (2) and (4), the TLI was transformed into rating values as follows:

$$R[TLI] = 140 - 20*TLI \quad (5)$$

We also compared R[TLI] with a similar arithmetic mean value obtained for the same *trophic* indices assessed with the DM:

$$R[DM] = (R[Chl] + R[S] + R[TP] + R[TN])/4 \quad (6)$$

where R[Chl], R[S], R[TP] and R[TN] are the rating values of Chl, SD, TP and TN, respectively, assessed with the DM. For some of the studied lakes with suitable databases (Kinneret, Stechlin and Naroch Lakes), R[TLI] was also compared with the values of the composite water quality index (CWQI) calculated for entire set of WQIs established with the DM according to the formula [11]:

$$CWQI = \Sigma(R_i*(R_0-R_i)/\Sigma(R_0-R_k)) \quad (7)$$

where $R_0 = 100$, and $R_{i,k}$ are the rating values for WQI i or k ($i, k = 1, 2,\ldots n$) from the WQ system established with the DM.

3. Results

3.1. Effects of Water Resource Uses and Environmental Threats on Water Quality Assessment

The multiple-use nature of water resources and the wide range of environmental threats require significant expansion of the variables included in the conventional TLI system, even for the objective of diagnosing a change in the lake trophic state. Therefore, at the initial stage of WQ assessment, the expert panel, using the DM, supplemented the WQI systems in all of the study lakes with additional WQIs beyond the four "trophic" indices in the TLI system. These expanded systems allowed for indications of WQ changes due to specific major water resource uses and associated environmental threats. The additional variables could be categorized generally as

- *eutrophication*: given by the percentage of cyanobacteria in algal biomass (Lakes Kinneret and Rotorua and Naroch Lakes); percent of oxygen saturation in the near bottom water layer (Naroch Lakes and Lake Stechlin); total phosphorus at the end of stratification period in the deepest water layer (Lake Stechlin); percent of oxygen saturation in surface water (Naroch Lakes); volumetric hypolimnetic oxygen demand (L. Rotorua);

- *pollutants indicative of organic pollution or relevant to human health*: number of coliform bacteria (Lake Kinneret and Rotorua Lakes) and BOD_5 test (Naroch Lakes);

- *food supply for fishes*: zooplankton biomass (Naroch Lakes, Lake Kinneret, Lake Stechlin and Lake Rotorua);

- *increase in salinity above accepted drinking water supply standards* (240 *mg* l^{-1}): chloride concentration (Lake Kinneret);

- *recreation*: pH and area occupied by emergent vegetation (Naroch Lakes).

3.2. Rating Curves and Permissible Ranges of WQI in DM and TLI Methods

We illustrate the differences between DM and TLI by comparing the rating curves for Chl established for oligotrophic Lake Stechlin and meso-eutrophic Lake Kinneret (**Figure 1**). In the TLI, lowering of a lake trophic status (*i.e.*, decrease in Chl) is equivalent to gradual improvement of WQ. In contrast to this, the DM shows that both an increase and a decrease of chlorophyll outside of some 'permissible' range (which varies between lakes) should be interpreted as WQ deterioration. Similar distinctions could be revealed for other WQIs under consideration (TN, TP and Secchi depth). This basic difference may lead to contrasting values for the permissible ranges for individual WQIs and management measures.

In the DM, permissible ranges for ecological values of individual WQIs can be described by the following equation:

$$\{WQI_L \le WQIc \le WQI_H\} \Leftrightarrow 60 \le R[WQI] \le 100 \quad (8)$$

where WQI_C is the current value of the index; WQI_L and WQI_H are the lower and upper permissible value of the index, and $\Leftrightarrow$ means "correspondence".

The TLI provides a threshold value, which can be described for TN, TP and Chl as follows:

$$\{WQIc \le WQI_H\} \Leftrightarrow 60 \le R[WQI] \le 100 \quad (9)$$

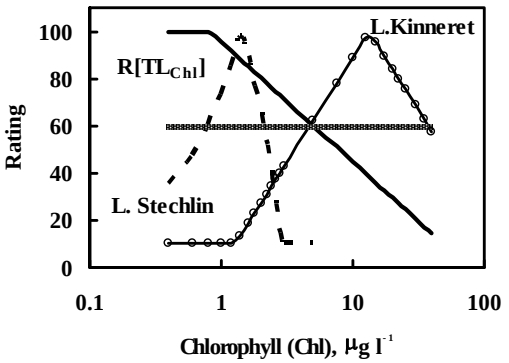

Figure 1. Rating curves of chlorophyll *a* assessed with the DM for Lakes Kinneret (round symbols) and Stechlin (dashed line), and calculated for the TLI (R[TL_{chl}], solid line) from ((4) and (8)). The horizontal line (R = 60) represents a boundary between acceptable and unacceptable WQ. Note logarithmic scale on *X*-axis.

For Secchi depth, this 'threshold' value is:

$$\{WQIc > WQI_L\} \Leftrightarrow 60 \le R[WQI] \le 100 \quad (10)$$

The main features of the two approaches can be illustrated using permissible ranges for chlorophyll (Chl) established for the study lakes (**Figure 2**). In the TLI, minimization of concentrations of TN, TP and Chl is indirectly considered as the desirable objective. An increase in Chl would therefore be taken as a sign of eutrophication, and therefore, of WQ 'deterioration'. According to this approach, the concentration limit of Chl for acceptable WQ (R[Chl] ≥ 60) is one-sided (dashed line in **Figure 2**), represented by the oligotrophic category of Chl ≤ 5.2 μg l^{-1} and is identical for all lakes. In the DM, one-sided rating curves are established only for pollution variables (e.g., densities of *fecal coliform* bacteria), or other components where

increases will always be undesirable (e.g., percentage of *cyanobacteria* in Lake Kinneret). For most WQIs, the DM gives a two-sided, lake-specific permissible range. For example, the desirable Chl ranges are 0.8 to 2.1 μg Chl l^{-1} for oligotrophic Lake Stechlin, 13.0 to 34.0 μg Chl l^{-1} for Lake Miastro, and 7.0 to 27.0 μg Chl l^{-1} for eutrophic Lake Batorino.

Similar distinctions between the TLI and DM exist in the case of use of total phosphorus (TP) as a WQI (*not shown*). The TLI gives a single-sided permissible limit of TP ≤ 20 g l^{-1} (identical for any lake), with concentrations higher than 20 g l^{-1} considered to represent deterioration in WQ. The DM defines a two-sided permissible range for TP: 7 < TP < 19 g l^{-1} for oligotrophic Lake Stechlin and 30 < TP < 100 g l^{-1} for eutrophic Lake Batorino.

3.3. Compatibility of Aggregated Estimates of WQ

Conceptual differences in approaches to WQ quantifica

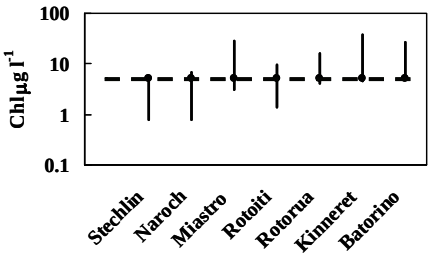

Figure 2. Comparison of permissible ranges for Chl *a* assessed with the DM (vertical lines) and TLI. The horizontal line represents the threshold values assessed with the TLI: 5.2 μg Chl l^{-1} The lakes on the X-axis are sorted according to their trophic state: from the lowest chlorophyll values in oligotrophic Lake Stechlin to the highest in eutrophic Lake Batorino.

tion cause distinctions in the aggregated WQ estimates obtained from the same sets of ecological values. The relationship between R[TLI] and R[DM] in all three Naroch lakes is non-linear (bell-shaped curve). The TLI qualifies as 'acceptable' WQ only for oligo-mesotrophic L.Naroch and a few values from L. Miastro, while WQ in eutrophic L. Batorino is ranked as 'unacceptable' (**Figure 3**). The DM qualifies most of the aggregated WQ values in all three Naroch lakes as 'acceptable'.

Monitoring of temporal dynamics of WQ is one of the tasks of WQ quantification [15]. Comparison of the dynamics of the calculated aggregated estimates (R[TL], R[DM] and CWQI; ((4) to (7)) indicates different sensitivities in their representation of change over time. For oligotrophic L.Stechlin, the dynamics of both R[TLI] and R[DM], calculated for the four 'trophic' indices ((5) and (6), respectively), do not indicate significant changes in WQ of these lakes over the last 15 years (**Figure 4**). In contrast, the aggregated WQ calculated as CWQI, from an expanded set of WQ variables (7), indicates clear-cut

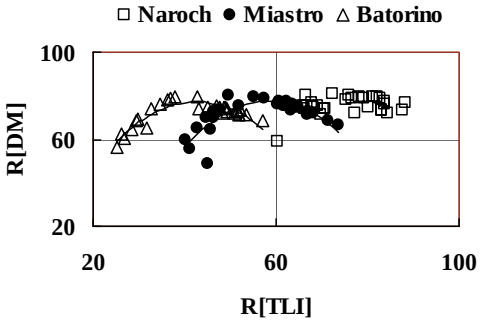

Figure 3. Scatter plots of the relationships between aggregated WQ estimates in the DMi and TLI (R[DM] and R[TLI]), respectively, for the Naroch Lakes (annual average values for 1978-2008). The lines represent best-fit regression lines. For the TLI, the acceptable WQ corresponds to areas to the right of the vertical line given by R[TLI] = 60. For the DM, acceptable WQ corresponds to areas above the horizontal line given by R[DM] = 60.

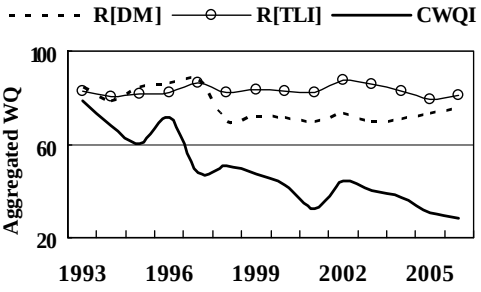

Figure 4. Time series of annual average estimates of aggregated WQ for L.Stechlin: R[TLI] (4&5), R[DM] (6) and CWQI (7).

trend in WQ deterioration. For L. Kinneret (*not shown*), the TLI indicates that WQ remains close to the boundary value that defines the difference between 'good' and 'intermediate' WQ. Conversely, the CWQI dynamics for L. Kinneret indicates gradual WQ deterioration from 'good' to 'intermediate'. Note that WQ deterioration in these lakes (as indicated by the CWQI dynamics) is associated primarily with the in-lake processes usually considered as signs of eutrophication: disruptions of phosphorus and oxygen regimes in hypolimnetic water (Lake Stechlin) and an increase in cyanobacteria abundance (L. Kinneret).

3.4. Relationships between WQ and Management Policy

Existing models (e.g., [25,26]) relate TP loading to TP concentrations in a lake. Here we applied the model of Rekhow [27] to L. Kinneret as this model specifically includes the potential addition of an internal P load associated with an anoxic hypolimnion. Assuming stability of the average lake depth and hydraulic turnover rate, for L. Kinneret, the following relationship can be established:

$$\text{Pload } [\text{g m}^{-2} \text{ yr}^{-1}] = 15.7 * \text{TP } [\text{mg l}^{-1}] \quad (11)$$

Permissible ranges for total phosphorus for L. Kinneret are as follows: TP $\leq$ 20 g l^{-1} (as obtained with the TLI from (8) and (10) and 7.5 $\leq$ TP $\leq$ 36 g l^{-1} (from the DM, [16]).

Substituting these values into (11) allows for an estimate of the permissible ranges of the external phosphorus load (Pload). The estimated maximum allowable Pload (based on TLI allowable TP values) is Pload $\leq$ 0.31 g m^{-2} yr^{-1} (**Figure 5**), which, given the TLI underlying assumptions, is universal for any lake, independent of its use as a water resource. In contrast, the permissible range of Pload into Lake Kinneret, based on the DM and its acceptable range of TP, is 0.12 to 0.58 g m^{-2} yr^{-1} (**Figure 5**). Management of Lake Kinneret due to Pload regulations within this established permissible range should allow sustaining and conserving the Lake Kinneret ecosystem.

For L. Kinneret, the relationship between aggregated WQ (as R[TLI] and CWQI) was established for the lake water level under the assumption that the water level is predominantly determined by the volume of water pumped from the lake and thus is a management decision . In a water level range of -210 to -214 m of, there was no significant relationship between R[TLI] and lake water level (**Figure 6**). Consideration of the aggregated WQ based on the expanded WQ system (CWQI) indicated a statistically significant (at $P < 0.05$) tendency for deterioration of the lake WQ with water level lowering (**Figure 6**). This dependence allowed estimation of a threshold water level value of approximately -213 m.

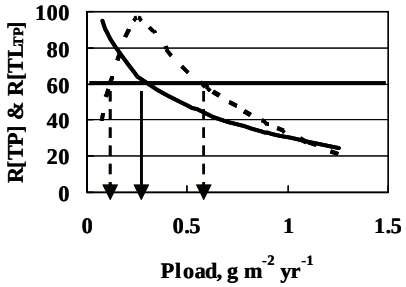

Figure 5. Relationship between management measure (phosphorus loading, Pload) and rating values of WQI (total phosphorus, TP): R[TL_{TP}] – obtained from (11) for L. Kinneret with the TLI (solid curve); R[TP] – obtained with the DM (dotted curve). The arrows indicate permissible ranges for Pload as regards to TP concentration (corresponding to R ≥ 60). Horizontal line corresponds to R = 60.

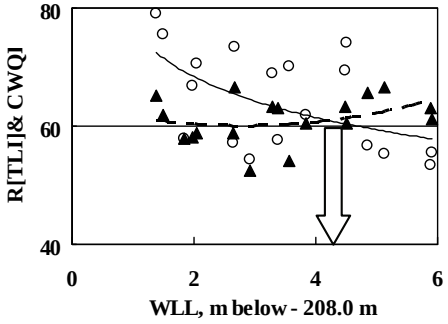

Figure 6. Scatter plots of the relationships between L. Kinneret water level lowering (WLL) as a management measure, and aggregated WQ: R[TLI] and CWQI (solid triangles and open circles, respectively). The best fit regression of R[TLI] vs WLL (dashed line) is not statistically significant (R^2 = 0.12, P>0.05), while the regression of CWQI vs WLL (solid line) is statistically significant (R^2 = 0.28, P<0.05). The block arrow indicates the permissible range of the lake water level lowering estimated with the DM.

4. Discussion

The problem of WQ quantification is equivalent to the quantitative solution of the task of "qualification", i.e., the terms like "good/bad", "improvement/deterioration" should be expressed in measurable units. This task is principally different from the task of "classification" (e. g., lake classification according to their mixing or trophic status). The developer of the quantitative trophic classification [28] warned: "An unfortunate misconception concerning trophic state is that the term is synonymous with the concept of water quality. Although the concepts are related, they should not be used interchangeably." Despite this warning, the trophic system of *classification*,

Table 2. WQ ranks in Delphi and TLI-system (modified from (4) and (14)).

Water Quality	Delphi		TLI	
	Rank	*Descriptor*	*Rank*	*Descriptor*
Excellent	80-100	Eminently usable for all purposes	2-3	Oligotrophic
Good	60-80	Suitable for all uses	3-4	Mesotrophic
Intermediate	40-60	Main use and/or some uses may be jeopardized	4-5	Meso-eutrophic
Bad	20-40	Unsuitable for main and/or several uses	5-6	Eutrophic
Very bad	0-20	Totally unsuitable for main and/or many uses	6-7	Hyper-eutrophic

under various forms, is widely used as a system of water *quality* [4-6,17,18].

Freshwater ecosystems are the objects of intense multipurpose use [29]. The use of the water resource in question is key to the DM (**Table 2**). In this study, we assumed that the objective of sustainable water resources management is *conservation* of the lake ecosystem in some predefined, "reference", state (3). The TLI approach does not consider the intended use (**Table 2**), and, therefore, the system of WQ indices assessed with this approach tends to be absolute, independent of the uses of the water resource in question, and associated hydroecological problems, Presumably, implementations of the TLI are based on an indirect assumption that eutrophication (caused by excessive entry of nitrogen and phosphorus) is the main hydroecological threat to waterbodies under WQ assessment. This is the underlying distinction between the DM and TLI as regards to WQ quantification, clearly illustrated in **Figures 1** and **2**. The respective rating curves of almost all WQIs in the DM are bell-shaped curves (**Figure 1**). As a consequence, the ecological values of parameters such as S, Chl, TN and TP should be sustained within limits, (permissible ranges, (8)); excessive increase and *decrease* of the respective variables should be ranked as WQ deterioration. Therefore, the WQ sets assessed with the Delphi method are more suitable for the needs of sustainable water resources management. Note that differences between permissible ranges assessed with the TLI and Delphi tend to increase with the lake trophic status, especially for Chl (**Figure 2**). In the TLI, the rating value is a monotone function of the concentration of Chl, TN and TP and S (1). It should be noted however, that monotone rating curves are possible also in the DM, usually assessed for pollutants (e.g., *E. coli* in the Rototua Lakes) or *cyanobacteria* (%Cyano) in L. Kinneret. However, in some cases, assessment of the monotone rating curves for basic ecosystem parameters may lead to paradoxical results resembling those based on the TLI. According to the monotone rating curves for TN and TP assessed with the TLI for transitional Mediterranean waters [6], the best WQ should correspond to TN, TP and Chl concentrations close to zero (**Figure 1** in [6]). This means that *complete distrophication* of transient water ecosystems is considered, at least formally, as WQ improvement. This, basic, distinction, is a direct reason for the discrepancies among the relationships between aggregated WQ and management measures. The differences in estimates of the permissible Pload values for L. Kinneret (**Figure 5**) have obvious consequences when translating them to management objectives and measures: the DM allows more intense economic activity in the lake watershed (expressed in terms of Pload), than possible according to the TLI, without unacceptable damage to the lake WQ. The discrepancies between the water level lowering effects on aggregated WQ have a significant impact on the entire process of decision-making in practical water resources management: acceptance of the TLI approach would mean that water level lowering of Lake Kinneret below −214.0 m does not affect lake WQ. In contrast to this, the DM indicates that the lake water level lowering below −213.0 m leads to unacceptable WQ deterioration (**Figure 6**). Similarly to WQ sets, we may conclude that the permissible ranges for management measures assessed with the DM better correspond to contributions of the sustainable water resources management. Respective "threshold" values of the management measures assessed with the TLI (or similar) approach are more suitable for the needs of a management which main objective is preventing of undesirable hydroecological consequences of the anthropogenic effects (e.g., eutrophication) without accounting for the needs of water resource management.

Comparison of the aggregated WQ dynamics obtained with the TLI and DM shows that the simplest average estimates (as R[DM] and R[TLI]) may lead to contrasting values of lake WQ (**Figure 3**). In some cases, a WQ system based on the TLI is not suitable for diagnostics of the eutrophication processes. The TLI approach does not indicate WQ deterioration (as shown by the CWQI dynamics, **Figure 4**) associated with the in-lake processes usually considered as signs of eutrophication: disruptions of the phosphorus and oxygen regimes in hypolimnetic water (L. Stechlin) and an increase in cyanobacteria abundance (L. Kinneret).

Decades of struggle against eutrophication have been expressed in the form of a paradigm linking between lake

trophic status and water quality. This misconception can result in a direct threat to the ecosystems of naturally eutrophic waterbodies, while producing a misleading understanding of the possibility of managing water quality based only on regulating activities according to the lake's trophic state. Accounting for the eutrophication problem only, and neglecting of requirements for water resources management prevents the trophic classification system from serving as a "common language" for communication between partners in management

5. Conclusions

In this study, we evaluated the suitability of the different water quality systems for the needs of sustainable water resources management. We compared two approaches used for quantitative assessment of water quality in natural waterbodies: the trophic level index and the Delphi method.

Comparative analysis of the assessed water quality systems allows us to draw the following conclusions:

1) The basic distinction between the Delphi and Trophic Level based approaches to quantification of water quality lies in the form of correspondence between the ecological and rating/trophic index values of the water quality index. In the trophic based system, the rating value is a strictly decreasing function of the concentration of Chl, TN and TP (increasing function of S). The respective rating curves of almost all water quality indices in the Delphi method account for the needs of sustainable management. Therefore they are bell-shaped curves, *i.e.*, the ecological values of such parameters as S, Chl, TN and TP should be sustained within limits (permissible ranges) that otherwise could result in WQ deterioration. In the trophic state based system, the acceptable limits for all water quality indices are one-sided and are taken by default to be applicable to all lakes. The Delphi method gives a two-sided, lake-specific limit within which sustainable water resources management will be possible.

2) The aggregated estimates of WQ with the Delphi and TLI approaches give comparable estimates for oligo- to mesotrophic lakes only. The differences between the two approaches increase with lake trophic state: the trophic status based system always valuate WQ in eutrophic lakes as "bad", independently on water resource uses.

3) The trophic state based system is a classification system, and therefore its implementation does not account for specific characteristics of aquatic ecosystems and the array of different potential uses as a water resource. The trophic state based system assumes reduction of economic activities in catchment areas as the most expedient mean to improve water quality. Therefore, water quality systems assessed with the trophic state based system are more suitable for needs of natural water resources management if eutrophication is a major threat. The Delphi method allows accounting for several water resource uses and therefore it may serve as a more robust and comprehensive tool for WQ quantification.

6. Acknowledgements

The authors thank the anonymous Reviewer whose comments improved the manuscript. We also thank Prof. P. Nöges for a valuable discussion which significantly improved this manuscript and Mrs M. Fridman for valuable help in editing of the manuscript. This research was supported by grants from the Ministry of Science and Technology Israel, and the Federal Ministry of Education and Research, Germany (BMBF), and the New Zealand Foundation of Research, Science and Technology (Contract UOWX0505) and Environment Bay of Plenty.

7. References

[1] R. G. Wetzel, "Limnology Lake and River Ecosystems," 3rd Edition, Academic Press, San Diego, 2001.

[2] R. E. Carlson, "A trophic State Index for Lakes," *Limnology and Oceanography*, Vol. 22, No. 2, 1977, pp. 361-369.

[3] OECD, "Eutrophication of Waters," Monitoring, Assessment and Control, Paris, 1982.

[4] N. Burns, J. McIntosh and P. Scholes, "Strategies for Managing the Lakes of the Rotorua District, New Zealand," *Lake and Reservoir Management*, Vol. 21, No. 11, 2005, pp. 61-72.

[5] C. Kaiblinger, O. Anneville, R. Tadonleke, *et al.*, "Central European Water Quality Indices Applied to Long-Term Data from Pre-Alpine Lakes: Test and Possible Improvements," *Hydrobiologia*, Vol. 633, No. 1, 2009, pp. 67-74.

[6] G. Giordani, J. M. Zaldivar and P. Viaroli, "Simple Tools for Assessing Water Quality and Trophic Status in Transitional Water Ecosystems," *Ecological Indicators*, Vol. 9, No. 5, 2009, pp. 982-991.

[7] S. E. Jorgensen and R. A. Vollenweider, "General introduction," In: S. E. Jorgensen and R. A. Vollenweider, Eds., *Guidelines of Lake Management*, International Lake Environment Committee, Shiga, Vol. 1, 1989, pp. 13-18.

[8] R. K. Horton, "An Index-Number System for Rating Water Quality," *Journal of Water Pollution Control Federation*, Vol. 37, No. 3, 1965, pp. 300-306.

[9] W. Ott, "Water Quality Indices: A Survey of Indices Used in the United States," Environmental Monitoring Series, EPA-600/4-78-005, 1978, p. 128.

[10] P. M. Brown, N. I. McClelland, R. A. Deninger and R. G. Tozer, "A Water Quality Index - Do we Dare?" Water Sewage World, 1970, pp. 339-343.

[11] A. Parparov and K. D. Hambright, "Composite Water

Quality: Evaluation and Management Feedbacks," *Water Quality Research Journal of Canada*, Vol. 42, No. 1, 2007, pp. 20-25.

[12] C. G. Cude, "Oregon Water Quality Index: A Tool for Evaluating Water Quality Management Effectiveness," *Journal of American Water Research Association*, Vol. 37, No. 1, 2001, pp. 125-137.

[13] M. A. House, "Water Quality Indices as Indicators of Ecosystem Change," *Environmental Monitoring and Assessment*, Vol. 15, 1990, pp. 255-263.

[14] D. G. Smith, "A Better Water Quality Indexing System for Rivers and Streams," *Water Research*, Vol. 24, No. 10, 1990, pp. 1237-1244.

[15] A. Parparov, K. D. Hambright, L. Hakanson and A. P. Ostapenia, "Water Quality Quantification: Basics and Implementation," *Hydrobiologia*, Vol. 560, No. 1, 2006, pp. 227-237.

[16] K. D. Hambright, A. Parparov and T. Berman, "Indices of Water Quality for Sustainable Management and Conservation of an Arid Region Lake, L. Kinneret (Sea of Galilee), Kinneret," *Aquatic Conservation*: *Marine and Freshwater Ecosystems*, Vol. 10, No. 6, 2000. pp. 393-406.

[17] USGS, "Water-Quality and Lake-Stage Data for Wisconsin Lakes, Water Year 2000," U.S Geological Survey, Open-File Report 01-86, Middleton, Wisconsin, 2001, p. 128.

[18] U. S. Environmental Protection Agency, "An Approach to a Relative Trophic Index System for Classifying Lakes and Reservoirs," National Eutrophication Survey, Working Paper No. 24, 1974.

[19] P. Scholes and M. Bloxham, "Rotorua lakes water quality 2006 Report. Environmental Bay of Plenty," Environmental Publication 2007/12, Whakatane, New Zealand, 2006, p. 86.

[20] C. Serruya, Ed., "Lake Kinneret," Dr. Junk Publishers, The Hague, 1978.

[21] T. Zohary, "Changes to the Phytoplankton Assemblage of L. Kinneret after Decades of a Predictable, Repetitive Pattern," *Freshwater Biology*, Vol. 49, No. 10, 2004, pp. 1355-1371.

[22] G. G. Winberg, Ed., "The Ecological System of the Naroch Lakes," Universitetskoye Press, Minsk, 1985.

[23] R. Koschel and D. D. Adams, "An Approach to Understanding a Temperate Oligotrophic Lowland Lake (Lake Stechlin, Germany)," *Archiv fur Hydrobiologie, Special Issues Advanced Limnology*, Vol. 58, 2003, pp. 1-9.

[24] T. Gonsiorczyk, P. Casper and R. Koschel, "Long-Term Development of the Phosphorus Accumulation and Oxygen-Consumption in the Hypolimnion of Oligotrophic Lake Stechlin and Seasonal Variations in the Pore Water Chemistry of the Profundal Sediments," *Archiv fur Hydrobiologie, Special Issues Advanced Limnology*, Vol. 58, 2003, pp. 73-86.

[25] R. A. Vollenweider, "Advances in Defining Critical Loading Levels for Phosphorus in Lake Eutrophication," *Memorie dell' Istituto Italiano di Idrobiologia*, Vol. 33, 1976, pp. 53-83.

[26] D. W. Schindler, "Evolution of Phosphorus Limitation in Lakes," *Science*, Vol. 195, No. 4275, 1977, pp. 260-262.

[27] K. H. Rekhow, "Empirical Lake Models for Phosphorus: Development, Applications, Limitations and Uncertainty," pp. 193-121, In: D. Scavia and A. Robertson, Eds., *Perspectives on Lake Ecosystem Modeling*, Ann Arbor Sciences, Ann Arbor, 1979.

[28] R. E. Carlson and J. Simpson, "A Coordinator's Guide to Volunteer Lake Monitoring Methods," North American Lake Management Society, Oklahoma, 1996.

[29] "Directive 2000/60/EC of the European Parliament and of the Council of 23 October 2000 Establishing a Framework for Community Action in the Field of Water Policy," Official Journal of the European Communities.

[30] Y. Z. Yacobi, "Temporal and Vertical Variation of Chlorophyll a Concentration, Phytoplankton Photosynthetic Activity and Light Attenuation in Lake Kinneret: Possibilities and Limitations for Simulation by Remote Sensing," *Journal of Plankton Research*, Vol. 28, No. 8, 2006, pp. 725-736.

[31] W. F. Vincent, M. M. Gibbs and S. J. Dryden, "Accelerated Eutrophication in a New Zealand Lake: Lake Rotoiti, New Zealand," *New Zealand Journal of Marine and Freshwater Research*, Vol. 18, 1984, pp. 431-440.

[32] N. M. Burns, J. Deely, J. Hall and K. Safi, "Comparing Past and Present Trophic States of Seven Central Volcanic Plateau Lakes, New Zealand," *New Zealand Journal of Marine and Freshwater Research*, Vol. 31, 1997, pp. 71-87.

J. Water Resource and Protection, **2010, 2, 916-922**
doi:10.4236/jwarp.2010.210109 Published Online October 2010 (http://www.SciRP.org/journal/jwarp)

Planning for Sustainable Water Supply through Partnership Approach in Wukari Town, Taraba State of Nigeria

Hassan Tsenbeya Ishaku[1], Mohammed Abubakar Husain[2], Fabian Mazawuje Dama[2], Ambrose Audu Zemba[3], Ajayi Abayomi Peters[2]
[1]*Department of Urban and Regional Planning, Universiti Teknologi Malaysia, Johor, Malaysia*
[2]*Department of Urban and Regional Planning, Federal University of Technology, Yola, Nigeria*
[3]*Department of Geography, Federal University of Technology, Yola, Nigeria*
E-mail: *htishaku*123@gmail.com
Received July 28, 2010; *revised August* 18, 2010; *accepted August* 25, 2010

Abstract

It has been observed that government resources and interventions towards sustaining water supply in Wukari town have been insufficient. The result has been constant water crisis and shortages over the years. The objective of this paper is to explore the possibility of partnering for sustainable water provision, to identify potential partners and to propose an appropriate partnership framework. Two hundred and seventy-five (275) questionnaires were administered in the three (3) wards of the town from where respondents were drawn at random. Findings revealed that the centralized system of water management, the location of Wukari on a basement rock and the scarcity of state financial resources are some of the greatest obstacles to sustainable water supply. However, about (90%) of the respondents are willing to collaborate with other stakeholders while the community members are ready to provide land and labor for the partnership arrangement. This study recommends a paradigm shift from the centralized water management to a partnership approach between service providers, recipients of services and other related stakeholders

Keywords: Planning, Sustainable Water Supply, Water Scarcity, Partnership Approach

1. Introduction

The World Health Organization [1] reported that the provision of potable water to an estimated one billion population who lack access to it remains one of the foremost challenges of human development today. For close to two decades, donors and leaders in developing countries have devoted public resources and leveraged private funds to construct improved water systems for urban and rural areas. While coverage rates is said to have improved over the years, growth in rural service has lagged behind compared to higher percentage of urban residents in developing countries who have gained access to better services. Currently, 1.2 billion people lack access to safe water sources. Nearly 2 billion people live with water scarcity, and this number is expected to rise to 4 billion by 2025, unless radical reforms emerge. Reports from development agencies, governments, water commissions, and research institutes continually point to an impending water crisis. These agencies also point to the water crisis arising from mismanagement not an absolute scarcity problem. Thus, improving current water provisions and avoiding a crisis of availability with the entire human suffering is possible. The message highlighted by various international efforts is that sub-optimal management of water is not an option if sustainable development is to be achieved.

M. Jacqueline [2] stated that in most developing countries, the dramatic pace of demographic, economic and social changes severely overburdens the capacity of the local authorities to provide urgently needed infrastructure services. The challenge of providing adequate services can not be met through investment in technical facilities alone; and the needs and problems themselves are evolving too rapidly. In these circumstances, service provision depends very much on efficient organization of service delivery processes and the best possible use of available material and human resources. This involves

mainly the issue of management which calls for cooperation between government agencies and infrastructure users as well as private sector actors.

Government must have the capacity to collaborate with recipients of service and related stakeholder to manage water infrastructure effectively and in a sustainable manner. Proponents of partnerships have often appealed to financial gains, cost reduction, efficiency gains, environmental compliance, human resource development and increased services which have followed private sector engagement. While opponents of partnerships have appealed to price increase, imbalance of power, labor disputes, inequalities environmental damage, and increased risks associated with private sector participation in water services. The aim of the partnership is to demonstrate how the private sector and the government can work together to deliver real and sustainable benefits of development for all. This approach argues that no government can afford to work in isolation. This means that partnerships can only complement and do not supplement governmental commitments. One of the ideals principles is the need to designate specific roles to individual or groups of potential partners based on previous similar projects or estimated financial potentialities.

P. Schubeler [3] argued that the partnership approach consists of a number of general principles that are designed to overcome the limitations of the traditional urban administration and the management of service delivery. It widens the scope of the actors involved in the provision of services to include urban infrastructure services. The stakeholders involved in the process include those whose interests are affected, those who posses relevant information and expertise and those who control and allocate resources. The partnership approach calls for an appropriate organizational basis for partners. It calls for a clear division of task in line with the interest and capabilities of each partner. The real benefits of participation derive not only from cost reduction and from resource mobilization during implementation of projects, but also from a more effective targeting of projects that measures the real needs of the people.

Although partnership is widely advocated for urban service delivery both in developed and developing countries, the concept has not been prominent in Nigeria. Most of the urban services are directly or indirectly planned and implemented by government through its various agencies. C. Shaw [4] stated that partnership aim at demonstrating how the private sector, civil society and the government can work together and to deliver real and sustainable benefits of development for all. This approach recognizes the strength and capabilities of different organization and to build partnership and network accordingly at the local level. The important element of this approach is that all partners act upon their different strengths-complementary resources, knowledge and skills to jointly address the complexities surrounding social, environmental and economic development.

Providing safe drinking water is a task so complex that neither the public nor the private sector can achieve it alone. The fact lies in large scale private sector participation in the provision of a much needed urban service such as water. Applying the principles of partnership will increase the potentials for both domestic and international private finance. To adequately understand the conceptual issues raised in this paper, partnership as applied in legal terms refers to an organization of two or more persons who have agreed to combine their labor, property and skill or some or all of them for the purpose of engaging in a lawful business and sharing the profits and loses between them. The parties forming such an association are known as partners.

1.1. Problem Investigated

Various studies [5-7] attributed water scarcity to distribution systems, technical problems and lack of adequate financial commitment from the part of the government. Other studies, A. Faniran and Y. Abdul [8,9] noted that water scarcity is due to inadequate knowledge about available water resources at all levels of planning and climatic changes. There is a growing realization in many developing countries that government provision of water services has been inadequate as publicly operated water supplies exposes residents to disease attacks despite the substantial efforts to improve the quality and coverage of service; one quarter of the urban population is not connected to public water system. However, private sector participation in water supply services was advocated as a way out of the water predicament. But the rural communities can not afford the high rates of water services charged by the private sector due to their low income as peasant farmers.

J. Saghir [10] stated that during the 1990s there was a wide spread expectations that the private sector would have a critical role to play in improving access to water services because of its know how, efficiency and investment capitals. However, in recent years many international operators have been disengaging rather than increasing their involvement in most developing countries. Various factors are responsible for this such as political opposition from civil society, contractual disputes between government and private operators and unclear legal, policy and institutional framework. The international private operators perceive their involvement in water sector as carrying increased risk and have become more cautious in entering any contractual arrangement, particularly if it involves financial commitment. This historical governance structures range from fully privatized

systems to public-private arrangements to public systems. In the light the problems in the water sector, public-private partnerships have been increasingly advocated and adopted in most parts of the world.

2. Methods

The objectives of this study are two folds: 1) to identify the partners and assess their roles in Wukari water supply, and 2) to propose an appropriate framework for effective water delivery in Wukari town. While the research questions which this study seeks to provide answers to include a) what is the percentage of households with or without access to safe water supply, b) what is the capacity of involvement of resident in water service delivery and c) is partnership the right way to improve water supply?

Primary data on the accessibility to water supply by households and willingness to pay for water bills were collected. For the households' (water users), discussion centered on their water supply sources, adequacy, how water was obtained, time spent in obtaining water, distance of water source from home, water storage facilities in use. Secondary data includes the data from published and unpublished literature on water supply was obtained from Federal Ministry of Water Resources. FMWR [11] and the Nigeria Population Commission NPC Official Result [12] etc. The secondary data from these agencies included budgetary allocations for urban water supply, the costs of various water facilities provided and cost recovery process, the actual population of each area delineated.

A structured questionnaire containing multi-choice answers was used as a guide for the interviews. This tool was used because of the possibility of its wide coverage as it helped to obtain data at a relatively short-term period. During the survey, questions attempted to elicit the following data on various sources of water supply, potential partners, socio-economic characteristics of respondents and willingness to pay for water bills among others.

A total of 275 persons were interviewed using the stratified random sampling. Wukari town was divided into three (3) wards from which respondent were drawn. These wards include Avyi ward (75) Hospital ward and (100) Puje ward (100). The population of Wukari in 2006 was put at 73,955 based on 3.0% growth rate; the estimated population for 2010 is expected to be 82,829 persons. This study utilized both descriptive and inferential statistics in data analysis. The descriptive statistic was used in summarizing the set of raw data into meaningful and concise information using percentages while inferential statistics enable generalization concerning the sampled population.

3. Discussion of Results

The variables used in this study are the factors that influence and determine water supply in Wukari town. These factors include existing and potential sources of water supply, household size, occupation of respondents and monthly income. Others include water per capita use, adequacy and willingness to pay for improved water services. **Table 1** below shows the various sources of water supply in Wukari town.

At present the existing and reliable source of water supply is the well accounting for 46.6%., although most of the wells do not yield water during the dry season. Water vending account for 37% it provides a wider coverage than well water. The water vendors either purchase water from borehole operators or fetch directly from the stream which is vulnerable to water borne diseases. The implication is that the partners will have to rely mostly on borehole using appropriate technology to get the required amount of water needed for the entire population.

Table 2 below shows that respondents within the household size of 6-10 account for 53.8%. This can be used as basis for calculating the water per capita use based on the current population which can be also projected for future demand.

Table 3 shows that respondents whose monthly income falls between 11,000-N15, 000 accounts for 38.90 and those whose monthly income exceeds 16,000-N20, 000 accounts for 26.30% indicating that a larger percentage of the population earn above the government prescribed minimum wage for civil servants. Given the amount spent on water daily (N400-500), a subsidized water bill for the residents will strengthen participation in the water business.

Table1. Sources of water supply in Wukari.

Source of water supply	Wards			Total	Percentage
	Avyi	Hospital	Puje		
Borehole	13	18	10	41	14.6
Well	37	45	45	127	46.6
Stream	1	2	2	5	1.80
Water vending	24	35	43	102	37.0
Total	75	100	100	275	100

Source: Fieldwork 2005

Table 2. Household size.

Household size	Wards			Total	Percentage
	Avyi	Hospital	Puje		
1-5	2	4	3	9	3.27
6-10	33	49	66	148	53.82
11-15	27	37	16	80	29.09
Over 15	13	10	15	38	13.82
Total	75	100	100	275	100

Source: Fieldwork 2005

Table 3. Monthly income.

Monthly income(Naira)	Wards			Total	Percentage
	Avyi	Hospital	Puje		
5,000-10,000	10	10	8	28	10.18
11000-15,000	28	57	22	107	38.90
16,000-20000	32	6	37	75	27.30
21,000-25000	2	4	13	19	6.90
Over 25,000	3	23	20	46	16.72
Total	75	100	100	275	100

Source: Fieldwork 2005

Table 4. Occupation of respondents.

Occupation	Wards			Total	Percentage
	Avyi	Hospital	Puje		
Civil servants	22	68	52	142	51.00
Businessmen	30	23	21	74	26.00
Farmers	23	9	27	59	23.00
Total	75	100	100	275	100

Source: Fieldwork 2005

Figure 1 below shows the monthly income of respondents. It is observed that respondents whose monthly income is 11, 000-N15, 000 account for 38.90%. This is above the government approved minimum wage of N7, 500 for the civil servants in the state.

Table 4 revealed that the civil servants accounts for 51% of the sampled population, while the businessmen and farmers accounts for 26 and 23% respectively. The implication of this is that the civil servants will be able to pay for improved service with ease as most of the farmers live in the villages. This means that cost recovery system will be effective as they are willing to pay for improved services.

Figure 2 shows the graphical representation of occupation status of respondents and the civil servants accounts for 51% of the total respondents while farmers represents 23% and mostly reside in the villages but commutes to the town at different times.

Table 5 above gives the per capita water use by ward, it worthy to note that daily water requirements are not evenly distributed due to differences in occupational status and water per capita use by respondents. Thus, on the average 20 liters of water is needed by each person on daily basis for proper hygiene and wellbeing of individuals World Bank Group [13].

Table 6 shows the water adequacy level of respondents. About 71.63% of the respondents are of the view that their daily water supply is inadequate. This is attributed to the fact that the centralized system of water management by government has not been effective. On

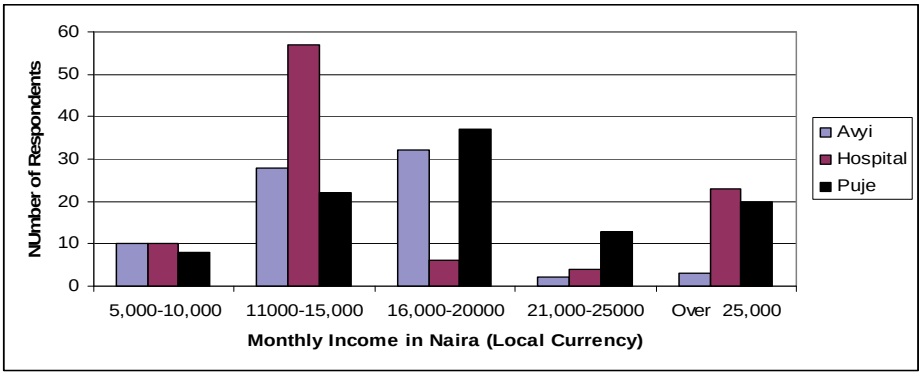

Note: 1.000 NGN = 154 USD

Figure 1. Monthly income of respondent in each ward.

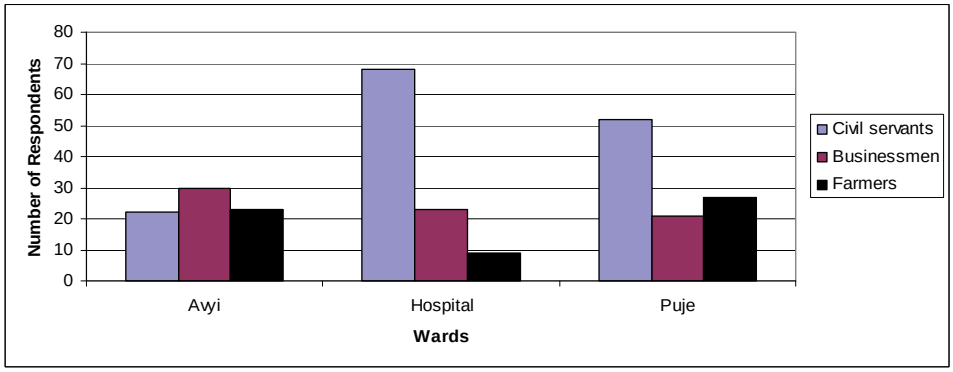

Figure 2. Occupation of respondents in each ward.

Table 5. Water per capita use (Water per capita use in liters (1 jerry can =20 liters).

Wter/person/day	Wards			Total	Percentage
	Avyi	Hospital	Puje		
20 liters	17	48	32	97	35.27
21-30 liters	37	34	59	130	47.27
Above 30 liters	21	18	9	48	17.46
Total	75	100	100	275	100

Source: Fieldwork 2005

Table 6. Adequacy water supply in Wukari.

Level of adequacy	Wards			Total	Percentage
	Avyi	Hospital	Puje		
Yes	12	39	27	78	28.36
No	63	61	73	195	71.64
Total	75	100	100	275	100

Table 7. Willingness to pay water for improved service.

willingness	Wards			Total	Percentage
	Avyi	Hospital	Puje		
Willing	71	93	86	250	90.90
Not willing	-	7	8	15	5.45
Undecided	4	-	6	10	3.65
Total	75	100	100	275	100

the other hand, 28.36% agreed that their daily water requirement is adequate which may be attributed to the low household size or proximity to alternative water source.

Responses on the willingness to pay for improved water services were also collected. **Table 7** below revealed that over 90% of the respondents are willing to pay for the water bills. This does not automatically mean that partnership will flourish 100 % but it will encourage the partners as they are most likely to benefit from their investment.

Figure 3 above shows a graphical representation **Table 7** willingness of respondents to pay for improved water service across the wards.

4. Partnership Frame Work for Wukari Water Supply

The important aspect of this study is to propose an effective partnership framework and machinery for the implementation that will translate these proposals for water supply into a reality. In view of the current state government dwindling financial resources which is reflected in its inability to tackle the water crisis for over 2 decades as well as growing demands for safe water supply, there is the need for an efficient arrangement which should reflect the participation of various consumers and service provider such as government agencies, private organizations, non-governmental organizations and community based organizations.

The responsibility of ensuring the enabling environment for the partnership to operate rest squarely with the government which need to provide the legal, fiscal and policy framework. However, role assignment becomes very necessary on the basis of previous similar projects or financial potentialities. Potential partners in Wukari water supply will involve the following stakeholders as shown in **Figure 4** below.

4.1. Taraba State Government

The Taraba state government is to play a supervisory role involving institutional, fiscal and legal framework. The state government is to also install water facilities, undertake rehabilitation works, provide technical advice and above all provide funds.

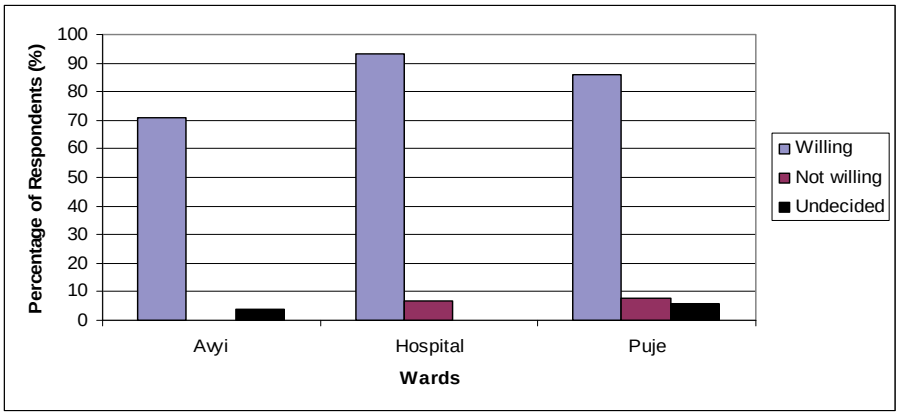

Figure 3. Percentage of willingness of Respondents per ward.

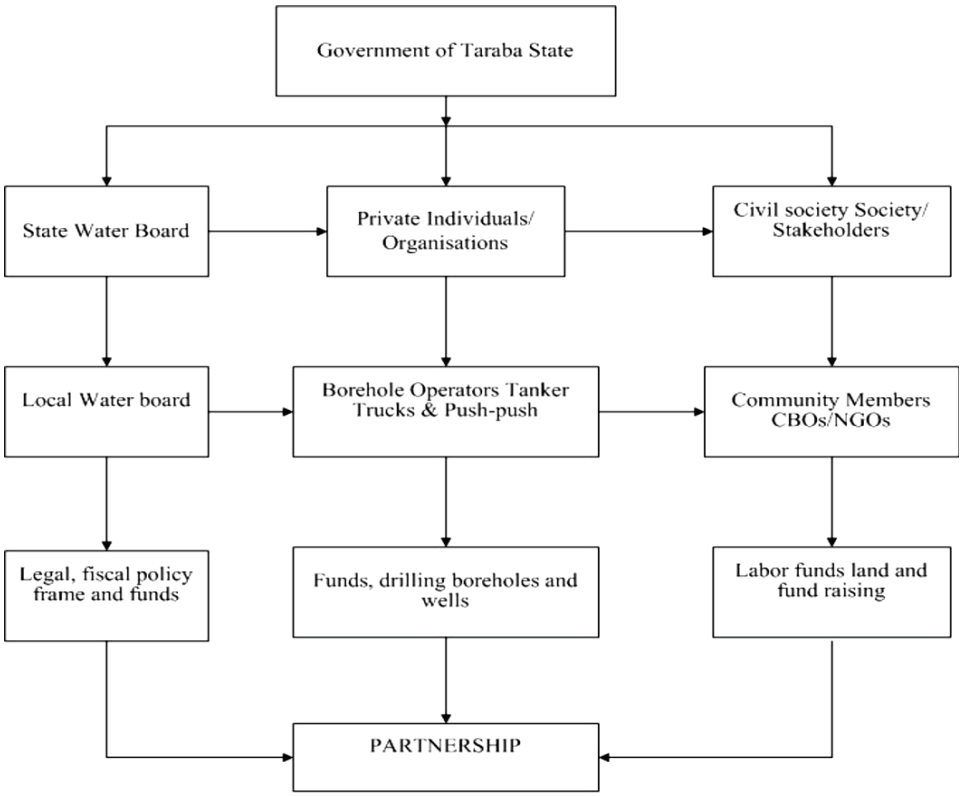

Figure 4. Partnership framework.

4.2. Wukari Local Government Council

The local government council is commonly referred to as the third tier of government will be responsible for operation and maintenance of water facilities, embark on awareness campaign, digging of additional sanitary wells and provide funds.

4.3. Non-Governmental Organizations (NGO's)

The non-governmental organizations though very few are potentially important in the partnership arrangement. They play a crucial role in facilitating communities in infrastructure development. They will provide free labor, technical advice, awareness campaign and raise funds

4.4. Community Based Organizations (CBOs)

The main objective is to support the local development of infrastructure services and to enhance the community capacity to manage services. Because of this bottom-up approach, the local partners have a sense of ownership of development project and strongly committed to seeing through a successful conclusion. They are to provide labor, land and food during constructional works, drill well and borehole, raise funds and embark on awareness campaign in the various communities

4.5. Private Sector

The private sector refers to institutions, firms and individuals who may be active in many different aspects of infrastructure management but whose objective is to generate profit from their investment. These groups shall provide funds, drill boreholes, offer technical advice and the maintenance of water facilities

At this point, partnership requires the establishment and strengthening of participating mechanisms which will ensure that all voices are heard in identifying problems and priorities, setting goals and exercising legal rights in determining service standard, mobilizing resources and implementing policies and programs of water supply in Wukari. This cooperation will result in organization of specific forms of coordinating committees by the state government through the local government.

5. Conclusions

The water supply plant for Wukari town is located in Tsokundi about 25 km away from Wukari town. This plant was meant to generate 3400 cubic meter (0.75 million gallons) of water per day, although the water de-

mand for the town was put at 7000 cubic meters (1.5 million gallons) per day. Dar-Alhandasah Consultant [14], this figure is far from being adequate for the estimated 59,955 people in 1996 and 73,955 in 2006 and estimated 82,829 persons in 2010 when compared with the national average per water supply of 63 and 21 liters per person per day for both urban and rural areas respectively.

The location of Wukari on a basement rock coupled with lack of funds and the centralized system of water management has significantly affected service delivery to the residents. This is evident in the fact that most taps have not had water for years. There is the need to undertake the geological survey to determine the aquifer and underground water recharge.

The treatment plant located in Tsokundi is usually heavily silted during the rainy season which adds to the total cost of treatment and hence the absence of tap water in the area. It is suggested that this plant be moved to river Ibi about 34 km which is not heavily silted and relatively maintains a higher volume of water during the dry season.

Another implication of the findings is that water vending constitutes the bulk of water source. This source has health related problems since the water is not usually treated before being sold to public.

6. References

[1] World Health Organization, Global Water Supply and Sanitation Assessment Joint Monitoring Program for Water Supply and Sanitation Series, 2000. www.who.int/water_sanitaion_health/monitoring/global/ assess/en/

[2] M. Jacqueline, "Water Governance," In: J. C. Cutler, Ed. *Encyclopedia of Earth*, Washington D.C. Environmental Information Coalition, National Council for Science and Environment, 2008. http://www.eoearth.org/article/water_governance27June2009.

[3] P. Schubeler, "Participation and Partnership in Urban Infrastructure Management," The World Bank, 1996. www.worldbank.org/wbi/sourcebook/sba/htm_cached.

[4] C. Shaw, "Tri-sector partnerships: How they work?" The Department for International Development Magazine Issue 18 Second Quarter, The Lime house Group, 2003. www.developments.org.uk/search?Searchabletext=improved

[5] A. Akintola and B. Areola, "The Perennial Incidence of Water Scarcity in Ibadan Nigeria; the Way Forward," Spectrum Books Ltd, Ibadan, 1980.

[6] A. Aliyu, "Water scarcity in Maiduguri Metropolis Problems and Prospects for Nigeria," Sabon-Dale Press, Awolowo Way, 1996.

[7] S. Lakhan, "Domestic Water in Northern Trinidad: Access, Collection and Quality," Florida, 2007. www.scribd.com/doc/19551153/Case-Study-Guide

[8] A. Faniran, "Strategies for Water supply Design in Developing Countries. An Appropriate Technology," University Press, Benin, 1992.

[9] Y. Abdul, "Water Shortages in Damaturu. The Way forward for Solving Water Crisis in Desert Areas of Nigeria," Unpublished, 1997.

[10] J. Saghir, "Public –Private Partnerships in Water Supply and Sanitation," The World Bank OECD Global Forum on Sustainable Development, Paris Press Information/Paper Presentations, Recent Trends and Opportunities, 29-30 November 2006. www.oecd.org/.../html

[11] Federal Ministry of Water Resources, Federal Republic of Nigeria, Old Federal Secretariat Garki, Abuja, 2000. http://www.uneca.org/awich/Nigerian%20Report. pdf.

[12] Nigeria Population Commission Official Result, "House and Population Census Figures," Bureau for National Statistics, Abuja, 2006. http://www.nigerianstat.gov.ng

[13] The World Bank Group, Annual Report on Access to Safe Water Supply in Developing Countries, 2004. http://www.worldbank.org/depweb/

[14] Dar-Alhandasah Consultant, "Wukari Master Plan 1977-2007," Shairs and Partners, London, 1977.

J. Water Resource and Protection, 2010, 2, 849-922
Published Online October 2010 in SciRes (http://www.SciRP.org/journal/jwarp/)

TABLE OF CONTENTS

Volume 2 Number 10 October 2010

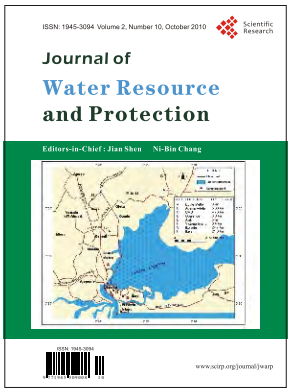

Call for Papers

Journal of Water Resource and Protection (JWARP)

http://www.scirp.org/journal/jwarp
ISSN:1945-3094 (Print), 1945-3108 (Online)

JWARP is an international refereed journal dedicated to the latest advancement of water resource and protection. The goal of this journal is to keep a record of the state-of-the-art research and promote the research work in these fast moving areas.

Editors-in-Chief

Editorial Board

Subject Coverage

This journal invites original research and review papers that address the following issues in water resource and protection. Topics of interest include, but are not limited to:

- Water resources and quality assessment
- Rivers, lakes and estuary systems
- Wastewater treatment and sludge biotreatment
- Water purification and water supply
- Water source protection and sustainable use
- Modeling, measuring and prediction of water pollution
- Ground water pollution control
- Reactions and degradation of wastewater contaminants
- Other topics about water pollution

We are also interested in short papers (letters) that clearly address a specific problem, and short survey or position papers that sketch the results or problems on a specific topic. Authors of selected short papers would be invited to write a regular paper on the same topic for future issues of the *JWARP.*

Notes for Intending Authors

Submitted papers should not have been previously published nor be currently under consideration for publication elsewhere. Paper submission will be handled electronically through the website. All papers are refereed through a peer review process. For more details about the submissions, please access the website.

Website and E-Mail

http://www.scirp.org/journal/jwarp Email: jwarp@scirp.org

J. Water Resource and Protection, 2010, 2, 849-922.
Published Online October 2010 in SciRes (http://www.SciRP.org/journal/jwarp).

TABLE OF CONTENTS

Volume 2 Number 10 **October 2010**

